HOLOGRAPHIC LENS FOR PILOT'S HEAD-UP DISPLAY

D. H. Close, et al

Hughes Research Laboratories

Prepared for:

Naval Air Development Center

1 August 1974

UNCLASSIFIED

SECURITY CLASSIFICATION OF THIS PAGE (When Data Entered)

REPORT DOCUMENTATION PAGE		READ INSTRUCTIONS BEFORE COMPLETING FORM
1. REPORT NUMBER N62269-73-C-0388	2. GOVT ACCESSION NO.	3. RECIPIENT'S CATALOG NUMBER
4. TITLE (and Subtitle) HOLOGRAPHIC LENS FOR PILOT'S HEAD-UP DISPLAY		5. TYPE OF REPORT & PERIOD COVERED Final Technical Report 1 Apr 1973 - 1 Apr 1974 6. PERFORMING ORG. REPORT NUMBER
7. AUTHOR(s) D.H. Close, A. Au, and A. Graube		8. CONTRACT OR GRANT NUMBER(s)
9. PERFORMING ORGANIZATION NAME AND ADDRESS Hughes Research Laboratories 3011 Malibu Canyon Road Malibu, CA 90265		10. PROGRAM ELEMENT, PROJECT, TASK AREA & WORK UNIT NUMBERS
11. CONTROLLING OFFICE NAME AND ADDRESS Naval Air Development Center Warminster, PA 18974		12. REPORT DATE August 1974 13. NUMBER OF PAGES
14 MONITORING AGENCY NAME & ADDRESS(if different from Controlling Office)		15. SECURITY CLASS. (of this report) Unclassified 15a. DECLASSIFICATION/DOWNGRADING SCHEDULE

16. DISTRIBUTION STATEMENT (of this Report)

Approved for public release, distribution unlimited.

17. DISTRIBUTION STATEMENT (of the abstract entered in Block 20, if different from Report)

18. SUPPLEMENTARY NOTES

19. KEY WORDS (Continue on reverse side if necessary and identify by block number)

Head-Up Display, Hologram Optics, Dichromated Gelatin, Dye Sensitization, Diffraction Efficiency, Ray Tracing, Hologram Recording Material

20 ABSTRACT (Continue on reverse side if necessary and identify by block number)

This report describes work on the development of a hologram lens system for a Head-Up Display (HUD) System having a 25° field of view, a 25-in. eye relief, and a 3-in. high by 5-in. wide exit pupil. The work includes a parametric analysis study, preliminary system design, development of a red-sensitive hologram recording material, and experimental work on a hologram lens element. The parametric analysis study is based on the Hughes continuous hologram lens design

DD FORM 1 JAN 73 1473 EDITION OF 1 NOV 65 IS OBSOLETE

UNCLASSIFIED

SECURITY CLASSIFICATION OF THIS PAGE (When Data Entered)

approach, applied to displays. Ray tracing, with efficiency calculations, is used to determine and compare focal surfaces, image distortions, aberrations and pupil errors, for several reflection and transmission hologram lenses. We conclude that a magnifying relay lens is required in order to meet the desired performance specifications. The preliminary system design shows how paraxial lens relationships constrain the overall system configuration, provide a relay lens design approach, and determine the degree of compensation of distortion at nonaxial field points. This work leads to the recommendation of a transmission hologram lens with a focal length of 13.5 in. for emphasis in the next stage of technology development. In the materials work, dichromated gelatin, sensitized to red light with methylene green dye, is chosen for the HUD lens recording material. After optimization of several procedures involved in its use, we obtain first order diffraction efficiency of over 80% from 12-μm thick films, with less than 5% scattering, using red light exposures of 600 mJ/cm^2. With 1.3 mW/cm^2 exposing power, the exposure time was about 8 min. The experimental lens is a symmetric transmission hologram, with a 40° off-axis angle and a 15.5 in. focal length. This experimental lens was recorded on conventional silver halide plates (Kodak 120), with the developed plate being bleached to provide a phase hologram. With a 7 mW laser (Spectra-Physics 123), the exposure time for the 8 x 9 in. hologram was about 45 s. The experimentally measured and calculated imaging characteristics are in excellent quantitative agreement. The excellent image quality predicted by the calculations and measurements is achieved in an operating demonstrator, using the experimental hologram lens.

TABLE OF CONTENTS

LIST OF ILLUSTRATIONS

I. Introduction and Summary

1. INTRODUCTION

This final technical report contains a detailed discussion of the tasks, objectives, approach, and results of the Phase 1 NADC program to develop a Holographic Lens for Pilot's Head-Up Display.

This is the final technical report on Contract N62269-73-C-0388, which consistutes Phase 1 of the Naval Air Development Center (NADC) program to develop a Holographic Lens for Pilot's Head-Up Display (HUD). The report covers work during the period 1 April 1973 to 1 April 1974; this work was performed at Hughes Research Laboratories, Malibu, California.

The optical system parameters and performance goals were given in the NADC "Specification for Hologram Lens System." The basic system parameters are a 25° diam field of view (FOV), an exit pupil size of 3 in. high by 5 in. wide, and eye relief of 25 in. In this study we have required that all points in the FOV be visible from any point within the exit pupil, so that a hologram element about 16 in. in diam is required.

The basic system, therefore consitutes a high quality, off-axis eye piece, covering a FOV of 25°. The use of hologram optics places highest priority on obtaining high optical efficiency, and our design approach takes this into account. The resulting lens element has aberrations and therefore introduces systems errors. It is not surprising that a single optical element is unable to perform this difficult task and still provide the desired performance characteristics, i.e., that auxiliary, correcting optical elements are required. We assume in this program that the correction will take place in a relay lens that produces a magnified, aerial image of the scanner output diffuser plate.

Table 1 provides a brief outline of the Tasks, Objectives, Approach, and Results of the Phase 1 program. It will also direct the reader to the appropriate section for a detailed discussion (or summary) of this information. The results of the program are highly favorable, and point to the successful development of a high quality HUD system, based on hologram optics. We recommend a transmission hologram configuration, with an off-axis angle of about 50°, for the next phase of technology development, although the final system may not have the same configuration.

TABLE 1

Outline of the Phase 1 Program

Task	Objectives	Approach	Results	Location (Summary)
1 Parametric Analysis	Understand hologram imaging characteristics; recommendations	Computer-based ray tracing, with efficiency calculations.	System feasible; requires auxiliary optics; emphasize transmission configurations in next phase.	Section II (I-3)
2 Preliminary System Design	Establish basic system trade-offs; estimate performance; recommend system	Paraxial optics; relay lens of magnification m	$1.25 < m < 1.6$; expect good performance and low distortion; $\phi = 50^{\circ}$ transmission with m 1 5	Section III (I-4)
3 Optimize Recording Material	Provide a red-sensitive recording material, suitable for large-aperture hologram optical elements.	Dye-sensitized dichromated gelatin	Over 80% efficiency in 12 μm film with 600 mJ/cm^2 exposure at 632.8 nm; exposure time ~8 min.	Section IV (I-5)
4 Experiments and Demonstrator	Confirm analysis; demonstrate holographic HUD imagery	Bleached silver halide; half-size hologram element; $\phi = 40^{\circ}$ transmission; experimental ray trace.	Excellent agreement between experiment and theory; high quality HUD image demonstrated; low-dispersion element preferred.	Section V (I-6)

T1372

1. Introduction and Summary

2. SPECIFIED SYSTEM PARAMETERS AND PERFORMANCE GOALS

The optical characteristics of the system were set by the NADC "Specification for Hologram Lens System," which specifies a 25° field of view, a 25 in. eye relief, a 3 in. high by 5 in. wide exit pupil, and high quality imagery.

The basic optical characteristics of the HUD system were set by the NADC "Specification for Hologram Lens Systems" (see Reference 8). These characteristics are summarized in Table 2. The major parameters specified are: a 25° diam FOV, a 25 in. eye relief, and exit pupil size of 3 in. high by 5 in. wide, and an operating wavelength of 632.8 nm (He-Ne laser). The input to the display system is the 4 in. square diffusing screen of an acousto-optical laser scanning system. In order to provide a 25° FOV from this source, the system focal length must be

$$f_o = \frac{4 \text{ in.}}{2 \tan 12.5^\circ} = 9.0 \text{ in.}$$

For the purposes of this study, we assume that the entire FOV must be visible from any point in the exit pupil. This is not a standard HUD design practice, because the combiner plate becomes quite large. For the 25° FOV system with a 3 in. by 5 in. exit pupil, the size of the hologram/combiner plate, projected on a plane perpendicular to the optical axis, is 2 x 25 x tan 12.5° + 5 in. = 16.1 in. horizontal by 14.1 in. vertical. When the vertical tilt is taken into account, the actual hologram must be about 16 in. in diam. The thin-film (low weight) nature of hologram optical elements allows us to consider making a HUD lens of this size, although it would be quite impractical with conventional optics.

The desired performance goals are also summarized in Table 2. The optical efficiency of 80% is high for a HUD system, and is in the range achievable with hologram optical elements with low scattering losses. The resolution of 1 mrad is easy to achieve for ray bundles the size of the pupil of the eye. Accuracy is considered to be the ability to put an image point at particular field angles; errors could arise from three sources: (1) mechanical stability, (2) errors and stability in the scanner, and (3) variation of image position with eye location in the exit pupil. Of these, only (3) is of concern to the present study, and this variation is called "collimation error," because if the light from an object point is perfectly collimated by the optical system, there will be no variation of image position with eye location. The collimation error and binocular disparity are discussed in detail in Section II.

TABLE 2

25° Field of View System

Given Parameters	
Field of View	25° circular
Eye Relief	25 in.
Exit Pupil Size	3 in. high x 5 in. wide
Operating Wavelength	632.8 nm (monochromatic)
Calculated Parameters	
Hologram Size	16 in. x 16 in.
System Focal Length	9.0 in.
Performance Goals	
Optical Efficiency	80% min
Resolution	1.0 mrad
Accuracy	1.0 mrad, central 12° 2.0 mrad, to 25°
Binocular Disparity	
Vertical	Less than 1.0 mrad
Horizontal divergent	Less than 1.0 mrad
Horizontal convergent	Less than 2.5 mrad

T1373

I. Introduction and Summary

3. SUMMARY OF PARAMETRIC ANALYSIS

The parametric analysis study is based on the Hughes continuous hologram lens design approach applied to displays, and it uses ray tracing with efficiency calculations to determine focal surfaces, distortion, aberrations, and pupil errors; comparison of the imaging characteristics for different configurations leads to the recommendation of a transmission hologram configuration for the next stage of technology development.

The parametric analysis is based on a general design approach that was invented at Hughes Research Laboratories. We call this the "continuous lens" technique. The aim of the continuous lens approach, as applied to displays, is to produce a lens element with a single holographic exposure, that provides high optical efficiency across the angular FOV, and has correctable aberrations that are uniform across the FOV. A particular design approach that implements the continuous lens technique for display elements, and is convenient for further system design and optimization, as well as the parametric analysis, utilizes two point sources, one of which is located at the center of the system exit pupil. This design approach and its development are described in Section II-A.

The scope of the parametric study and the techniques used in the study are the subjects of Section II-B. The study is primarily devoted to reflection and transmission of continuous lens geometries that are inherently off axis and used in configurations that provide both the collimating and combining functions. The basic system geometry is given by six parameters that specify a particular configuration and determine the imaging characteristics. Recognizing the need for auxiliary correcting optics, usually in the form of a relay lens that forms a magnified, intermediate, aerial image of the scanner output plane, we specify ten basic configurations for analysis. These configurations include five reflection systems, four transmission systems, and one pseudo-inline transmission system, with the off-axis angle chosen at the most significant independent variable.

The analysis techniques are based on ray tracing. The first step is to determine the characteristics of the intermediate image, i.e., the astigmatism, tilts and curvatures of the hologram focal surfaces. The second step is unique to hologram optics, but is extremely important; this is to determine the optical efficiency variation across the FOV and across the exit pupil. For the basic continuous lens design, the efficiency remains high for chief rays across the entire angular FOV, but tends to limit the exit pupil size, depending primarily on the thickness of the film of recording material.

The third step in the analysis is to study the distortion characteristics. Of primary concern is the anamorphic distortion. This is measured by the ratio of horizontal magnification to vertical magnification, required by a relay lens to optimally compensate for the hologram lens distortion.

The final step in the analysis is to calculate the aberrations in the hologram imaging transformation, and determine the resulting system pupil errors. For this purpose we use ray intercept curves, which plot ray intercepts with the image surface relative to the chief ray intercept, as a function of ray position in the system exit pupil. The two important pupil errors are the collimation error and binocular disparity, which are defined and analyzed in terms of the differential ray intercepts.

The results of applying these four analysis steps to the ten basic configurations are given in Section II-C. The tilts of the hologram focal surfaces are toward being parallel with the hologram surface, but are usually different for horizontal and vertical ray fans. The radii of curvature of these surfaces are usually different in horizontal and vertical sections, making a structure of two intersecting spheroids.

The optical efficiency characteristics can be estimated from a simple formula. In order to maintain desirable efficiency characteristics, the hologram should have minimum asymmetry and should be fabricated with point source construction beams, with one point source in the center of the pupil.

The relationship between intermediate image and angular field coordinates is nearly linear for reflection systems, but increases from 2.7% at $\phi = 30^{\circ}$ to 16.7% at $\phi = 60^{\circ}$ for transmission systems. The vertical/horizontal difference includes both constant anamorphic and keystone distortion, increasing with off-axis angle, mostly anamorphic in reflection systems and mostly keystone in transmission systems.

The ray intercept curves typically show a combination of coma and spherical aberration, with coma dominating. The magnitude of the aberrations is approximately in the ratio of 1:2 for transmission and reflection systems, and 1:4 for pseudo-inline and reflection systems. These aberrations, and therefore the binocular disparity and collimation error, increase with off-axis angle and are in all cases large enough to require correcting elements in the final system. Although transmission systems have from 1.5 to 2.5 times less coma than reflection systems with the same off-axis angle, their coma variation across the FOV is larger, making it possibly easier to correct the reflection systems, using tilted surfaces in the relay lens.

Based on an overall consideration of the results of the parametric analysis study, and on the current state of the art of hologram lens design and fabrication, we recommend a transmission configuration for the next phase of technology development. Furthermore, we specify a symmetric transmission configuration, with an off-axis angle of 50°, for the preliminary system design study task of this program.

4. SUMMARY OF PRELIMINARY SYSTEM DESIGN

Paraxial relay lens relationships constrain the overall system configuration, provide a relay lens design approach, and determine the degree of compensation of distortion at nonaxial field points; this leads to the recommendation of a minimum-distortion focal length of 13.5 in. for the transmission hologram that is recommended for the next stage of technology development.

The objective of the preliminary system design task is to establish the relationships involving the relay lens that constrain the configuration of the overall holographic HUD system. These constraints are of two types: the first type is the paraxial relationships of the relay lens characteristics to the system parameters, and the other type is the paraxial relationships between tilted object and image, and the extent to which the relay tilted object/image situation corrects for the distortion inherent in the hologram image. The result of the preliminary system design is a specific configuration recommendation for the next phase of technology development.

In order to maintain brightness across the FOV, the relay lens exit pupil must be located at a hologram construction point source. Through this, the hologram focal length determines the relay lens focal length and the overall length of the optical system. The system exit pupil size places a requirement on the relay lens exit pupil size, and therefore sets the relay lens f/number. These fundamental system requirements restrict the practical range of hologram focal length to the range $11.25 \text{ in.} < f_H < 14.4 \text{ in.}$ Equivalently, the basic relay lens magnification is restricted to the range $1.25 < m < 1.6$.

Tilted object/image planes are used in the holographic HUD system to compensate for the intrinsic difference in hologram image magnification in the horizontal and vertical directions. In order to calculate the degree of distortion compensation that is achieved, we provide the paraxial imaging relationships for the tilted object/image situation, relating the object and image tilt angles to the relay lens magnification, and the tilted image height to the tilted object height.

The system paraxial relationships and the axial anamorphic distortion determine the relay lens axial magnification, focal length and f/number in both vertical and horizontal sections. Furthermore, the image tilt angle and the axial vertical magnification determine the object tilt angle. This completely specifies the relay lens optical system.

The relay lens optical system is, therefore, designed to provide an intermediate image that is in focus and exactly compensates, on axis, for the hologram anamorphic distortion. Using the tilted object/image relationships, the degree of distortion compensation achieved across

the FOV can be calculated. For a 50° off-axis angle, symmetric transmission configuration, excellent distortion compensation is achieved across the entire FOV for a hologram focal length of about 13.5 in. This system is recommended for the next phase of technology development, but not necessarily for the final system.

I. Introduction and Summary

5. SUMMARY OF MATERIALS WORK

Dichromated gelatin, sensitized with methylene green dye, was chosen for the final HUD lens recording material, and after extensive optimization of the several procedures involved in its use, we obtained first order diffraction efficiency of over 80% with less than 5% scattering, using red light exposures of 600 mJ/cm^2 and exposure times of about 8 min.

The objective of the materials work was to develop a red-sensitive recording material with the properties required for fabricating practical holographic lens elements for HUD systems. Dye-sensitized dichromated gelatin was selected as the best material candidate, based on the requirements of high index modulation, low scattering noise, practical exposure requirements and environmental stability.

Dichromated gelatin has been investigated and used for several decades as a basis for numerous printing techniques involving physical etching of the gelatin layer. Since the hologram recording material is based on a bulk refractive index change process, these old investigations are not directly applicable.

The spectral response of dichromated gelatin is high in the blue region of the spectrum, but negligible for red light. The response can be extended to the red by the addition of photo-reducible dyes. Our survey of over 120 dyes revealed that the thiazine and triphenylmethane dyes are the best red spectral sensitizers for dye-sensitized dichromated gelatin. The primary factors involved in the selection of a dye are the dye-dichromate solubility product and the efficiency of conversion of red light to reduced dichromate by the dye. We discovered that the amount of useful dye in the sensitizing solution can be increased, in the unique case of methylene green dye, by adding the dye to the dichromate solution in the solid state. A sensitizing solution prepared in this way produces 12-μm thick gelatin layers that are very efficient, absorbing over 60% of the incident red light.

Using the methylene green dye, we optimized the dye sensitized dichromated gelatin over the several processing steps. We found that the film sensitivity is maximized when both ammonium dichromate and ammonium nitrate are used in high concentrations in the sensitizing solution. We explored several previously-reported methods for etched dichromated gelatin film sensitivity improvement, but the sensitivity of the dye sensitized dichromated gelatin used for hologram recording was not improved. The drying time for best dye-sensitized dichromated gelatin film sensitivity was empirically determined to be about 15 min.

In the optimization of post exposure processing techniques, our goal was to achieve high diffraction efficiency and low noise, and also to develop a process that would be amenable to fabricating large holograms. With extensive experimentation, we arrived at techniques that result in first order diffraction efficiencies of over 80%, with 600 mJ/cm^2 exposures at 632.8 nm, while maintaining scattering levels below 5%. The exposure times in these experiments were about 8 min. The same results should hold for Krypton laser exposures at 647.1 mm. Specific procedures are given that should be directly applicable to the 18-in. square plates required for full-size hologram fabrication.

I. Introduction and Summary

6. SUMMARY OF EXPERIMENTAL WORK

The experimental work, on a 40° off-axis angle, symmetric transmission configuration, showed that the measured and calculated imaging characteristics are in excellent quantitative agreement, and that the excellent image quality predicted by the calculations and measurements is in fact achieved in an operating demonstrator, using the experimental hologram lens.

The objectives of the experimental work were, first, to quantitatively compare the experimentally observed imaging characteristics with those derived from the theoretical ray tracing techniques used in the parametric analysis study of different configurations, and second, to provide a simple, operating holographic HUD system to demonstrate the performance characteristics obtainable with the holographic lens approach. An experimental demonstration and study of a holographic HUD lens was accomplished, using a symmetric transmission continuous lens configuration, similar to the configuration that was recommended for the next phase of technology development. The experimental hologram lens is approximately one-half size, with an off-axis angle of 40° and a focal length of 15.5 in.

An optical system, including a 14-in. diameter spherical mirror, was built up on a vibration isolated table, along with a He-Ne laser, to provide the required hologram construction beams. This apparatus was used to expose a 6 μm thick, silver halide emulsion, resulting in amplitude holograms, which were converted to volume phase holograms, using the high quality bromine vapor bleach process that was developed on this program.

Analysis of the experimental hologram lens was accomplished by comparing theoretical and experimental ray trace data on the system and image quality characteristics. The results of this comparison show that:

a. Computed and measured focal surface characteristics agree on focal length, astigmatism versus field, and tilt angles.

b. Deviations between predicted and observed optical efficiency are accounted for by a systematic loss of fringe stability during recording, which can be avoided with an improved recording apparatus.

c. The calculated and measured distortion characteristics of the experimental hologram are the same, within experimental errors, being 1.5% anamorphic and 5% keystone, calculated, and 2.5% anamorphic and 4.95% keystone, measured.

d. Theoretical and experimental ray intercepts, used to calculate collimation error and binocular disparity, are in excellent agreement for two different horizontal eye locations in the pupil, giving about 5 mrad maximum pupil errors.

The experimental hologram lens thus confirms our analysis and design techniques. This lens was incorporated in a HUD demonstrator that shows excellent image quality.

II. Parametric Analysis

A. Choice of Approach

1. BACKGROUND

The Head-Up Display system is ideally suited to the continuous lens hologram optical element, which was invented and successfully developed at the Hughes Aircraft Company

Hughes Research Labortories proposal to NADC for a Holographic Lens for Pilot's Head-Up Display (HUD) was based on a finite-element array approach.[1] The array is designed to overcome the loss of optical efficiency and buildup of image errors observed as the FOV is increased in a single hologram that is recorded with object and reference point sources having an object/image relationship.[2,3] The array overcomes these limitations of the "single hologram" approach, and demonstrates much smaller efficiency loss and pupil errors for the HUD application.[1] However, the array suffers from localized image discontinuities associated with unaligned intersections between elements of the array. By the time the present NADC HUD program began on 1 April, 1973, it was known that the only effective measures for correcting these discontinuities required increasing the number of array elements, with a corresponding decrease in element size. Also by this time, Mr. Gaylord Moss of Hughes Research Laboratories had invented the "continuous lens" approach to the design of holographic optical elements.[3] For a display system, the continuous lens is, in effect, an array with a very large number of infinitesimally small elements, recorded with a single holographic exposure. In the continuous lens, the image discontinuities of the array are smoothed into distributed image errors or aberrations, which can be corrected with usual optical design techniques. This evaluation of hologram optical elements is summarized in Table 3.

Since the continuous lens approach is ideally suited to the HUD-type system having an exit pupil that is small compared to the system aperture, the analytical effort of the present program has been spent in studying this approach, and remarkably good performance has been calculated and observed. The optical efficiency remains high across the FOV, and the pupil errors remain small compared to the "single hologram" approach. Furthermore, the pupil errors are correctable by a suitably designed relay lens.

A major confirmation of the continuous lens design approach was the successful development of a 30° FOV helmet mounted display (HMD) system,[4] in parallel with the HUD studies. In order to allow this development, major advances were made in hologram optical system design and in the tools necessary to carry out the design process. Much has been learned about the types of refractive elements needed in the hologram recording and playback stages to effectively correct residual

aberrations in a display system. The ray tracing programs that allow this type of system to be analyzed and designed, as well as the experience gained with the HMD system, are available for the HUD system design. Furthermore, the HUD system allows greatly reduced geometrical asymmetry, and there is thus greatly reduced astigmatism and a considerably simplified design task.

In this subsection we describe the different types of hologram optical element. This description requires explicit consideration of optical efficiency, as well as image quality, because hologram optical elements, in contrast to refractive and reflective elements, do not inherently provide high optical efficiency.

The array approach to a holographic eyepiece for an infinity display system has been discussed in detail in references 1 and 5, and those details will not be repeated here. Briefly, the array is a contiguous assembly of "single hologram" elements arranged to cover an extended FOV. A "single hologram" element is a hologram lens recorded so that the object and reference point sources occupy the same locations as the central object and image points in the display system. In order to explain the continuous lens concept as the limit of an array with infinitesimal elements, we will begin with the single hologram, then briefly discuss the finite-element array and finally describe the continuous lens. The explicit example of two-dimensional, off-axis transmission hologram elements will be used; however, the ideas apply equally well to three-dimensional geometries and reflection or pseudo-inline transmission configurations.

TABLE 3

Evolution of Holographic Display Elements

Type of Element	Characteristics
1. Single lens	Good axial image Small field of view Large pupil errors
2. Array lens	Large field of view Small pupil errors Local image errors
3. Continuous lens	Large field of view Small pupil errors Correctable aberrations

T1374

II. Parametric Analysis

A. Choice of Approach

2. THE SINGLE HOLOGRAM

The single hologram element is capable of a large pupil size, but a rapid buildup of image errors and loss of optical efficiency combine to strongly limit the achievable FOV.

As an introduction to the characteristics of the "continuous lens" type of hologram optical element, which has been analyzed in the present program, we briefly describe here the characteristics of the "single hologram" element.

The single hologram optical element is a hologram lens recorded so that the object and reference point sources occupy the same positions, relative to the hologram aperture, as the central object and image points in the display system. Figure 1 indicates the construction and use of a single hologram element. The construction geometry shown in Fig. 1(a), utilizes a point source P, located at the center of the source in the display system, and a collimated beam (point source at infinity), incident along the central viewing direction of the display. During reconstruction, indicated in Fig. 1(b), the central source point P illuminates the hologram with a wave that duplicates the diverging construction beam. The hologram, therefore, recreates the collimated construction beam, and a viewer in the exit pupil of the system observes a virtual image of point P, projected to infinity with zero aberration. As seen in Fig. 1(c), another source point, P', also illuminates the hologram with a diverging wave, but from a different angle. The P' wave is not identical to the diverging construction wave, and the new reconstructed wave is not a collimated beam. There are errors across the system pupil, and the viewer observes an aberrated image of P'. The angular shift of the P' wave also leads to a loss of diffraction, or optical efficiency.[6] This loss of image brightness and the size of the image errors both increase rapidly as the P' point moves away from the construction point P, strongly limiting the useful FOV of the system.[1] Note, however, that the single hologram element is capable of a large pupil size, limited only by the aperture of the element.

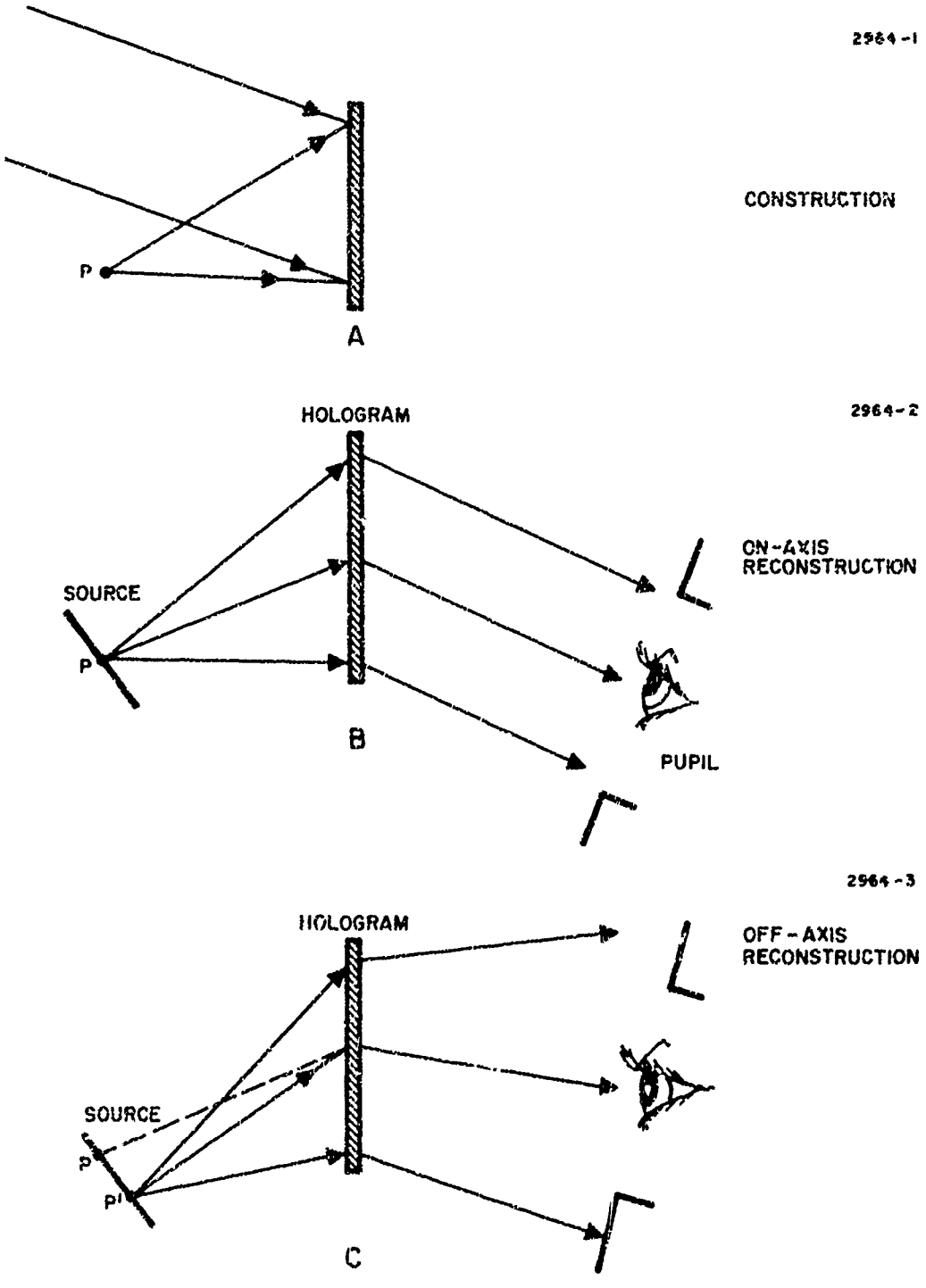

Fig. 1. A single hologram transmission display element. (a) Beam configuration during construction; (b) beam configuration during on-axis reconstruction; (c) beam configuration during off-axis reconstruction.

II. Parametric Analysis

A. Choice of Approach

3. THE FINITE-ELEMENT ARRAY

The finite-element array, which provides high optical efficiency across an extended field of view, has local discontinuities in the image, which merge gradually into a continuous image error as the element size is reduced.

The finite-element array, which was proposed for the NADC HUD system,[1] is briefly described here as an introduction to the characteristics of the "continuous lens" type of hologram optical element which has been analyzed in the present program.

The finite-element array approach is illustrated in Fig. 2. This approach utilizes the fact that the exit pupil is much smaller than the system aperture, therefore different parts of the aperture correspond to different parts of the angular FOV. Therefore, if multiple "single hologram" elements are properly aligned in the aperture, high brightness and good image quality can be maintained across an extended FOV. Figure 2 illustrates a one-dimensional array with three single hologram elements recorded in the aperture, using three point sources, P_1, P_2 and P_3, distributed in the source, and three, corresponding, collimated reference beams. Each element covers a small enough FOV to maintain high efficiency and image quality. The requirements and techniques for alignment of the array elements at their common boundaries have been discussed before.[1,5] Also described were the local image errors arising from necessarily unaligned element intersections in a two-dimensional array.

Although the array shows good brightness uniformity and much smaller pupil errors than the single hologram element, the localized image errors do substantially degrade the overall image quality.[1,5] Several techniques were suggested for controlling these localized errors,[1,5] but the only practical method is to reduce the size of the single hologram elements of the array and to correspondingly increase their number. This situation is illustrated in Fig. 3, where the array elements are smaller than the system pupil. In this case, several of the local image discontinuities, associated with unaligned intersections, may be observed simultaneously by the viewer. Since these discontinuities are smaller than for the array of Fig. 2, the effect is to produce a less distinct but more uniform overall image. The total amount of image error is approximately conserved. In the limit of infinitesimal element size, the image becomes continuous, with a continuous error, or aberration, degrading the image quality. This last case is one form of continuous lens element, and the aberration can be corrected with appropriate auxiliary elements, providing a high-quality, bright image across an extended FOV.

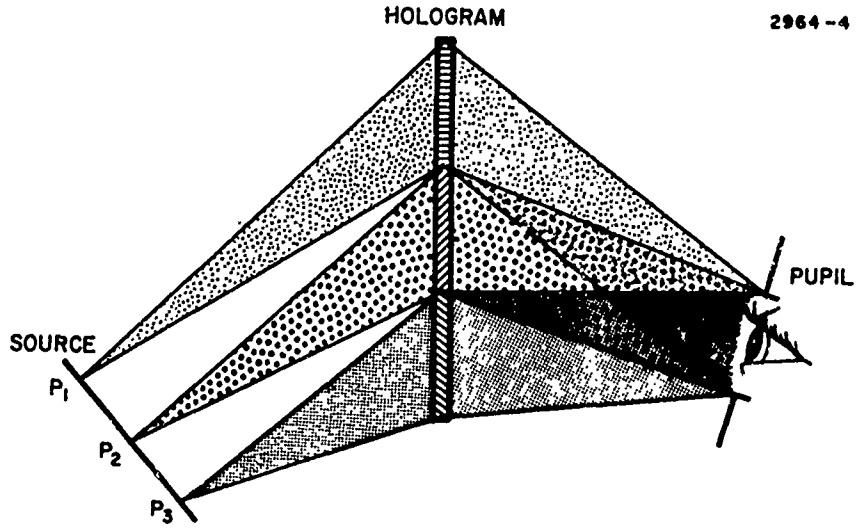

Fig. 2. A three-element linear array, showing the on-axis reconstruction from the three construction point sources, P_1, P_2, and P_3.

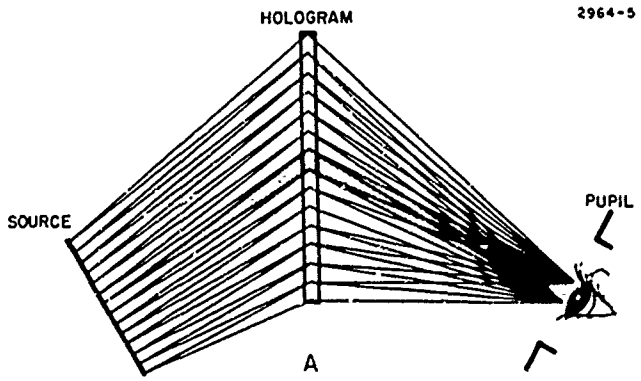

Fig. 3.
A linear array with element size small compared to the system pupil size, showing on-axis reconstruction from the three construction point sources. One of the construction beam paths is shaded.

II. Parametric Analysis

A. Choice of Approach

4. THE CONTINUOUS LENS

In the limit of infinitesimal element size, the array becomes a continuous element that can be constructed with a single holographic exposure, provides high optical efficiency across the FOV, and has uniform, correctable aberrations.

The type of continuous lens element studied in the present program can be described as the limit of infinitesimal element size in an array. Figure 4 illustrates an array with the element size smaller than the size of the system pupil. This case provides smaller local image discontinuities, with multiple discontinuities evident because several elements in the array are projecting light from any particular object point through the system pupil. Also, the optical efficiency of this projection tends to be less near the edges of the system pupil, because the corresponding array elements are being used at angles other than those occurring in their construction geometry.

In the limit of infinitesimally small array element size, only the chief rays of the system (the rays going through the center of the pupil) are recorded. In this limit, the image error is continuous, and the optical efficiency varies uniformly across the pupil. This limiting case is indicated in Fig. 5 by a few of the chief rays. Taken together, the chief rays define a beam that produces a point source located in the center of the pupil and appears to come from a source located behind the source distribution. The limiting case can therefore be achieved in practice by recording a hologram as a single exposure with two construction beams whose rays duplicate the chief ray geometry. One of the construction beams, therefore, forms a point source in the center of the exit pupil. The other beam can often be approximated by a point souurce, as indicated by the dashed lines in Fig. 5. This example of a "continuous lens" element has pupil errors (the limit of the local image discontinuities in the array) that are nearly constant across the FOV, and can be corrected by auxiliary optics in the display system. The price for obtaining uniform brightness across the FOV is that the fall-off in diffraction efficiency, associated with reconstruction rays differing in direction from the construction rays, limits the effective size of the exit pupil. Obtaining a desirable exit pupil size requires a recording material film thickness that is small enough to supply the required angular response; the proper characteristics seem to be available in practice. The continuous lens is therefore ideal for a display system with a large FOV and a small exit pupil, while the single hologram approach is ideal for a system with a small FOV and large exit pupil.

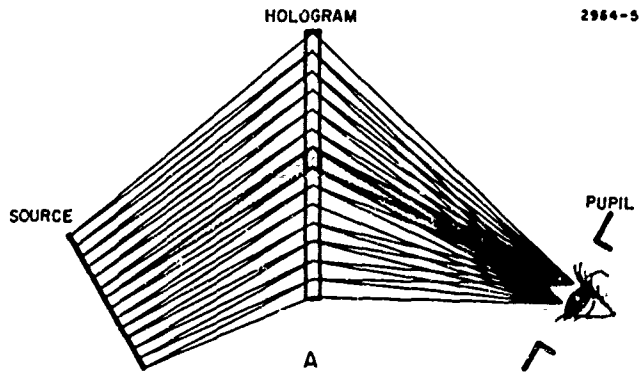

Fig. 4.
A linear array with element size small compared to the system pupil size, showing on-axis reconstruction from the three construction point sources. One of the construction beam paths is shaded.

Fig. 5.
A linear array in the ideal limit of infinitesimal element size. A small number of reconstruction beam paths show the chief ray geometry. Often the chief rays can be traced backwards from the source to locate an approximate point source, as indicated by the dashed lines.

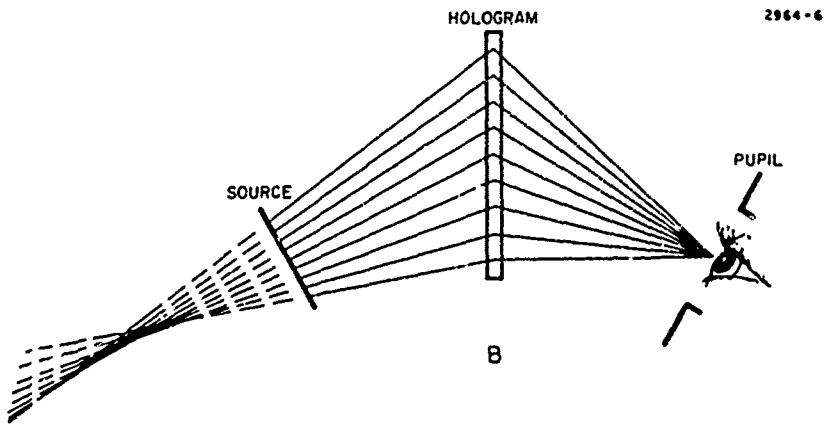

II. Parametric Analysis

A. Choice of Approach

5. A CONTINUOUS LENS DESIGN APPROACH

A continuous hologram lens design approach that is convenient for both parametric analysis and further system design, specifies the hologram focal length and places one of the two construction source points at the center of the system exit pupil.

A convenient and useful type of continuous lens to use in practice is one made using beams generated by two point sources. Such an element is indicated in Fig. 6, and the steps in its design are outlined in Table 4. This element can be described in conventional terms as having a focal length, f, related to the distances, d_1 and d_2, of the two point sources, P_1 and P_2, from the hologram by the equation

$$\frac{1}{f} = \frac{1}{d_1} + \frac{1}{d_2} \quad . \tag{1}$$

This focal length is directly related to the display parameters. In fact, if the auxiliary optics used to correct the pupil errors are placed in a relay lens that forms an intermediate image of the actual source at the "source location" of Fig. 6, then the focal length, f, of eq. (1) satisfies the relationship

$$f = mf_o \quad . \tag{2}$$

In eq. (2), m is the magnification of the intermediate image, relative to the actual source, and f_o is the overall system focal length, defined by the equation

$$\tan \theta = \frac{s}{2f_o} \quad , \tag{3}$$

where θ is the half-angular FOV and s is the size of the actual source. For the 25° FOV system, $\theta = 12.5^\circ$ and s = 4 in., giving a system focal length $f_o = 9.0$ in. Therefore, if point P_2 of Fig. 6 is placed at the center of the exit pupil then distance d_1 is chosen, along with the relay lens magnification, m, to provide the desired system parameters. Furthermore, since the hologram forms an image of the system exit pupil, at P_1, that point should also be the location of the relay lens exit pupil.

It should be noted that the location of the construction point sources P_1 and P_2, i.e., the construction wavefront centers of curvature, are shown in Fig. 6 for a vertical section through the display system. If we consider instead a horizontal section through the system, the construction wavefront centers of curvature may be located at distances different from d_1

and d_2; i.e., the construction waves may have substantial astigmatism. The use of such astigmatic construction beams is only one of several possible modifications that can be made in the construction waves; however, it is the only one that was used in the present parametric analysis. The amount of astigmatism in a particular construction beam is taken to be the axial separation of the horizontal and vertical centers of curvature.

The above steps totally specify the continuous lenses studied in this program. With this basic design, ray tracing techniques[9] are used to analyze the system and evaluate the image quality. This analysis considers the characteristics of the hologram and its imaging properties; it does not consider the effects on image quality of adding a correcting lens. In the preliminary system design (Section III), we have considered the paraxial specifications of the relay lens, and the effects on overall system distortion of a paraxial relay lens.

The final system design is a very complex task, requiring consideration and balancing of all parts of the system: hologram geometry, construction beam characteristics, and properties of a nonparaxial, thick, compensating relay lens. This final design task is presently scheduled for the proposed Phase 3 program.

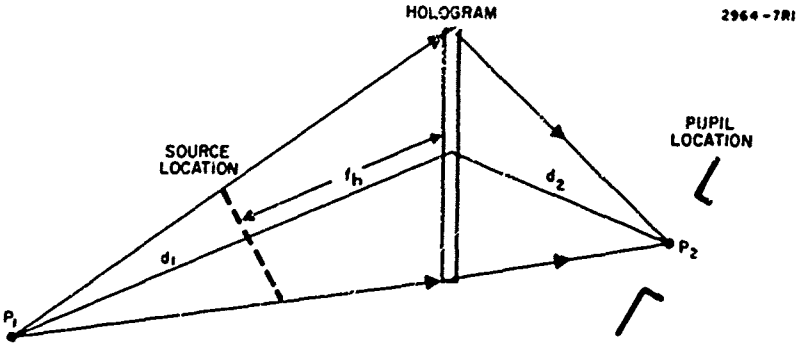

Fig. 6.
Point source locations for a continuous lens element that provides high chief ray optical efficiency across the entire field of view.

TABLE 4

Steps in HUD Continuous Hologram Lens Design

1.	Choose a hologram configuration and focal length.
2.	Locate one construction beam source in the center of the system exit pupil.
3.	Locate the second construction beam source to give the desired hologram focal length.
4.	Provide a relay lens with the proper magnification ($m = f_h/f_o$), and with its exist pupil located at the construction beam source, P_1.
5.	Adjust the construction beam and relay lens properties, by adding and/or modifying optical elements, until the optimum image quality is obtained.

T1375

II. Parametric Analysis

B. Scope of the Parametric Study

1. SYSTEM GEOMETRY

The system geometry for reflection and transmission continuous hologram lenses is given by six basic parameters that specify a particular configuration and determine the corresponding imaging characteristics.

In this topic we define and describe the parameters that specify the hologram system geometry for the purpose of a parametric performance analysis. For this purpose, we restrict the discussion to the continuous lens geometries that are inherently off axis and are used in configurations that provide both the combining and collimating functions. The reflection continuous hologram lens system is indicated in Fig. 7(a), and the transmission continuous lens system is indicated in Fig. 7(b). These drawings represent vertical sections of the systems through the optical axis. The systems are very similar and the same parameters apply to both.

The system exit pupil, of size P, is indicated at the left side of the drawings, displaced from the hologram aperture by the eye relief distance, D, along the optical axis. The viewer's eyes are located within the exit pupil, and the projected image is viewed through the hologram aperture, in the general direction of the optical axis. The data to be projected by the display appears at the "intermediate image" location, which is separated from the hologram by the hologram focal length, f. The eye relief and the focal length meet at an angle ϕ, the off-axis angle of the system. The hologram is on a flat substrate and the normal to the hologram surface makes an angle Ψ with the bisector of the off-axis angle ϕ. This asymmetry angle is taken to be positive when the hologram is tilted toward being perpendicular to the optical axis. The intermediate image may be tilted away from being normal to the focal length, and the tilt angle Ω is taken to be positive when the normal to the image surface is tending toward being parallel with the optical axis.

The intermediate image structure is generally more complex than indicated in Fig. 7. The detailed imaging properties of the hologram, which are discussed in Section II-B-4, generally require two image surfaces, corresponding to horizontal and vertical fans of rays. These two surfaces may have different tilt angles, Ω_h and Ω_v, and may also be curved. The average curvature or radius of curvature is taken to be positive when the surface is convex toward the hologram.

The system specifications[6] require a system exit pupil P = 3 in. high by 5 in. wide. and eye relief D = 25 in., a circular FOV 25° in diam and centered on the optical axis, and a system focal length f_o = 9 in.

With a relay lens of magnification, m, providing the intermediate image, the hologram focal length $f = mf_o$. We require that the entire FOV be visible from any location within the system exit pupil, and this requirement fixes the overall size of the hologram aperture and the extent of the "viewing volume," the latter being indicated in Fig. 7 by lines at $\pm 12.5^{\circ}$ to the optical axis, from the pupil to the hologram aperture.

The procedure followed in performing the parametric analysis is to choose ϕ, Ψ and m, and then use ray tracing[9] to establish the image surface characteristics, the optical efficiency, and the system errors. This procedure is described in detail in the remainder of Section II-B. We should note here that the significance of the asymmetry angle Ψ is that when $\Psi = 0$ there is zero axial astigmatism in the intermediate image for spherical construction wavefronts. In some of the analyses, we assume astigmatic construction wavefronts in order to cancel axial image astigmatism associated with $\Psi \neq 0$, or to modify the astigmatism across the image surfaces. Otherwise, since we are mainly concerned with the inherent hologram imaging characteristics, we neglect the possible control of imaging characteristics available through modification of the hologram construction wavefronts. However, this type of image control should be studied thoroughly as an important part of any later system design effort.

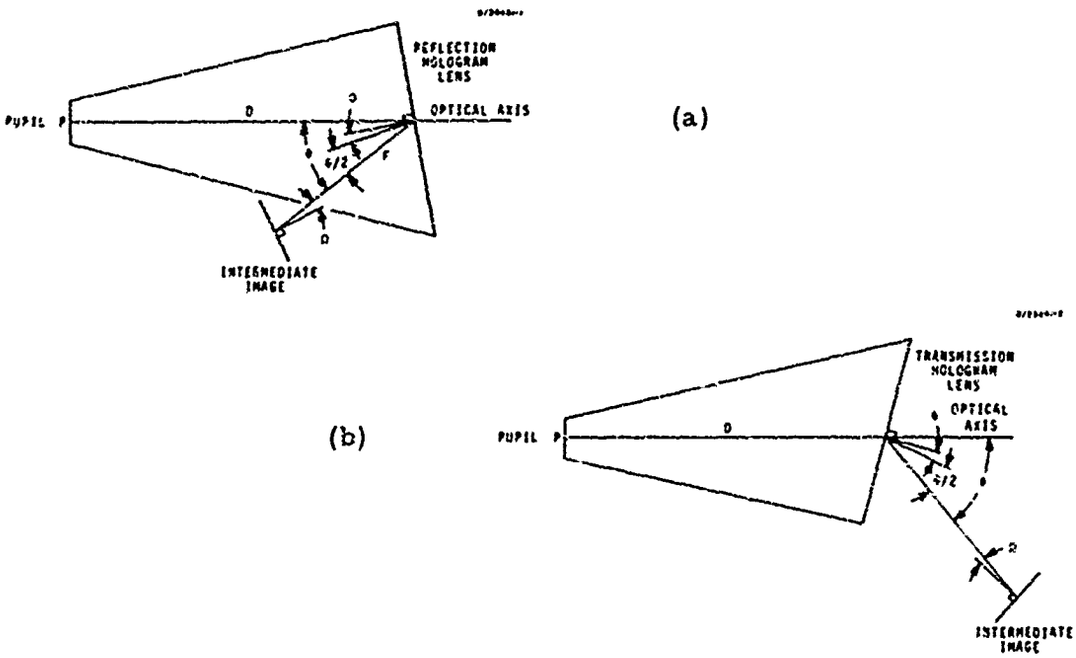

Fig. 7. Geometry of continuous hologram lenses used as HUD collimator/combiner elements: (a) Reflection continuous lens; (b) transmission continuous lens.

II. Parametric Analysis

B. Scope of the Parametric Study

2. THE NEED FOR A RELAY LENS

The holographic HUD system requires auxiliary optics, usually in the form of a magnifying relay lens, to increase the range of available configurations, reduce system distortion, and provide adequately small system errors.

The system focal length of 9 in. limits the range of configurations available for the holographic HUD system in two ways: First, if no relay lens is used, the off-axis angle ϕ must be large in order to keep the source diffuser out of the viewing volume, and second, for large ϕ and f = 9 in., the distortion inherent in the holographic imaging process becomes quite large. For example, Fig. 8(a) indicates a vertical section (to scale) through a reflection system with f = 9 in. and $\phi = 90^{\circ}$. The dotted lines show the chief ray directions at the edges of the FOV, and the asymmetry of these lines is an indication of the large amount of distortion inherent in this configuration. Figure 8(b) shows that for a $\phi = 45^{\circ}$, transmission hologram system, the source intrudes into the viewing volume, obstructing part of the FOV. These difficulties are strongly mitigated by the addition of a relay lens to the system, providing an aerial, intermediate image to be projected by the holographic collimator. Figure 8(c) indicates a transmission hologram system utilizing a relay lens with magnification m = 1.3. In this case the hologram focal length is $f = m f_o = 11.7$ in., and the amount of distortion is substantially reduced, as indicated by the more symmetric extreme chief rays (dashed lines).

Another advantage of the relay lens that is not apparent from these geometrical considerations is that it can be used to correct residual aberrations in the HUD system. This is an extremely important point, because the hologram configuration must be chosen to provide high optical efficiency across the FOV, and configurations that do so introduce errors that are considerably larger than the system specification allows.[8] These errors are such that they can be effectively controlled by a properly designed relay lens, which therefore becomes essential to the system. In fact, it can be stated that any holographic HUD system that maintains optical efficiency across an extended FOV will require auxiliary optics, in the form of field lenses and/or a relay lens, to provide suitable performance.

In order to extend the range of available configurations, correct distortion, and decrease system errors, we will generally assume that a relay lens is included in the system.

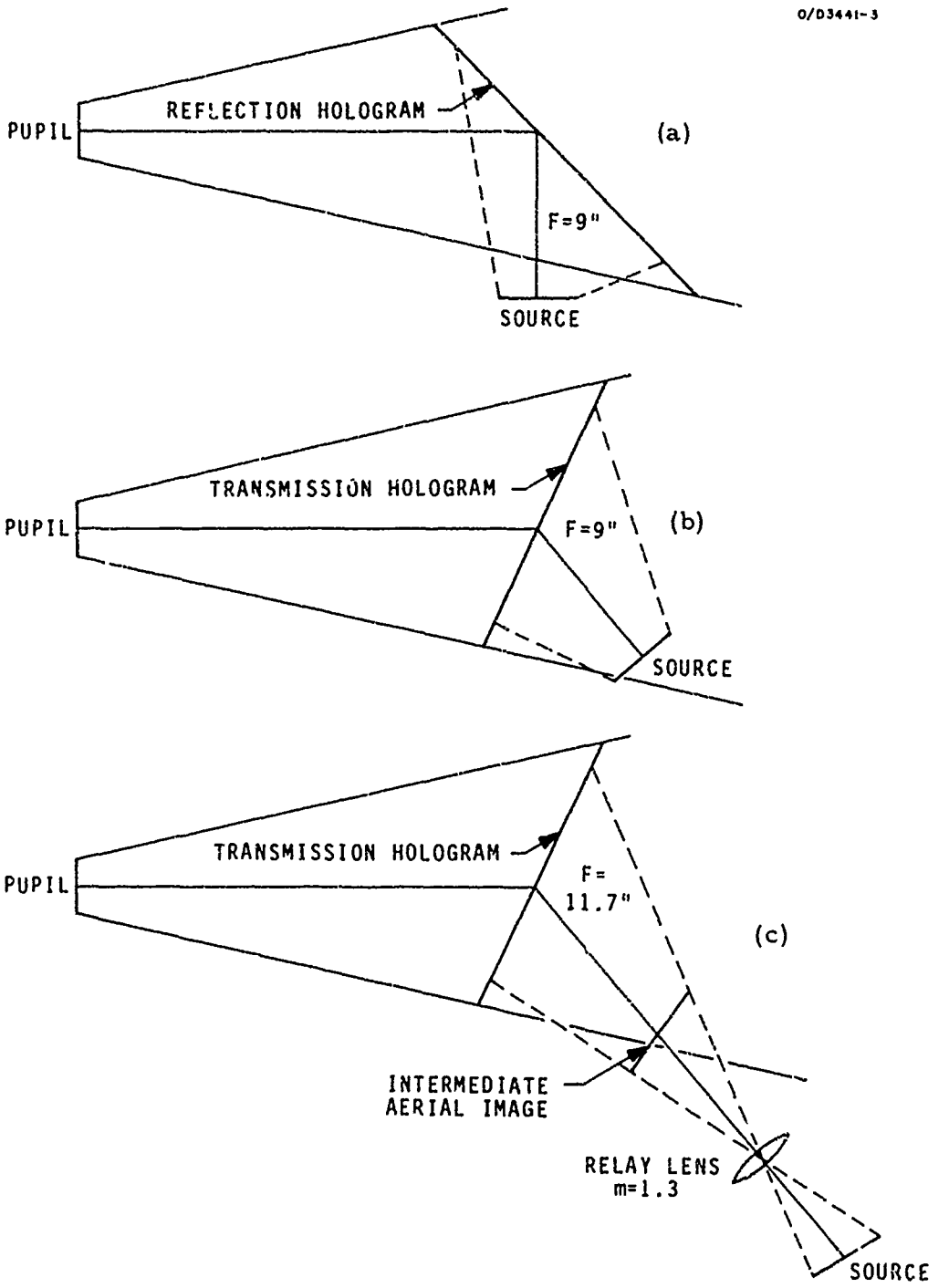

Fig. 8. Vertical sections of holographic HUD systems. (a) Reflection system without a relay lens; (b) transmission system without a relay lens; (c) transmission system with a relay lens.

II. Parametric Analysis

B. Scope of the Parametric Study

3. SUMMARY OF SYSTEMS STUDIED

The parametric study included reflection, transmission, and pseudo-inline transmission systems, having approximately the same focal length, with the off-axis angle chosen as the most significant variable.

In order to provide an overview of the systems studied, we provide here a summary of the range of parameters covered. The systems that have been considered are of three basic configurations, indicated in Fig. 9. Figure 9(a) is a reflection continuous lens system, Fig. 9(b) is a transmission continuous lens system, and Fig. 9(c) is a pseudo-inline transmission continuous lens system.[1,9] The total possible range of configurations had to be limited in order to make the parametric study of manageable size. The major goal was taken to be a study of the imaging properties of holograms having a range of off-axis angles in systems with a dual-function holographic element (i.e., providing both the collimating and combining functions). Therefore, most of the systems studied used either a reflection continuous lens or a transmission continuous lens, as shown in Figs. 9(a) and 9(b). The pseudo-inline transmission (PILT) continuous lens configuration of Fig. 9(c) is of relatively little interest, but was also included in the study for completeness. The focal length of the hologram was held approximately constant at about f = 14 in; corresponding to a relay lens magnification $m \approx 1.5$, which was shown in the preliminary system design to be approximately optimum (see Section III).

A secondary variable was the asymmetry angle Ψ. The main effect of this variable is to introduce axial astigmatism when $\Psi \neq 0$.

Table 5 lists the major systems that were analyzed in the parametric study. Five asymmetric reflection configurations, with $\phi = 20^\circ$ to 60°; one symmetric reflection configuration, with $\phi = 40^\circ$, four symmetric transmission configurations, with $\phi = 30^\circ$ to 60°; and one pseudo-inline configuration were included. All of the systems studied have the specified eye relief of 25 in., a 25° circular FOV and a 3 in. high by 5 in. wide system exit pupil. All holograms were assumed to be constructed at $\lambda = 632.8$ nm and operated at the same wavelength. With reference to Table 5, systems 1 to 5 and 7 to 10 were studied with astigmatic construction wavefronts, chosen to minimize astigmatism across the intermediate image surface; systems 6 to 11 were studied with spherical construction wavefronts.

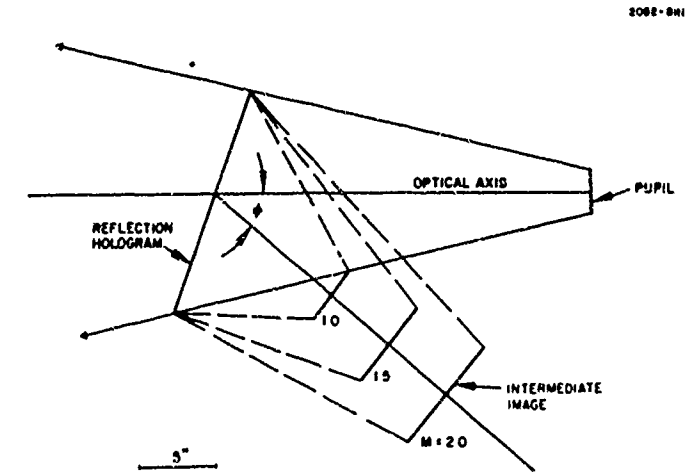

(a)

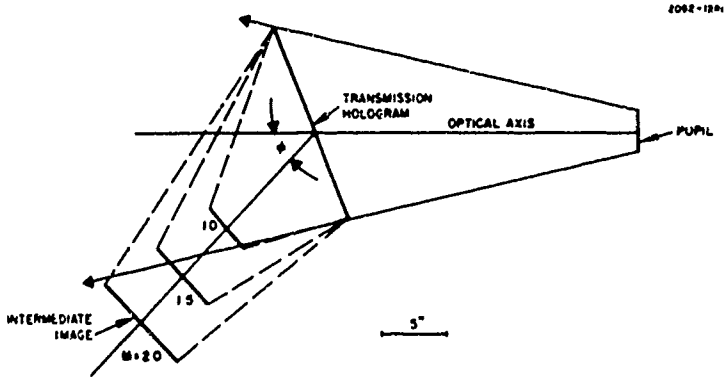

(b)

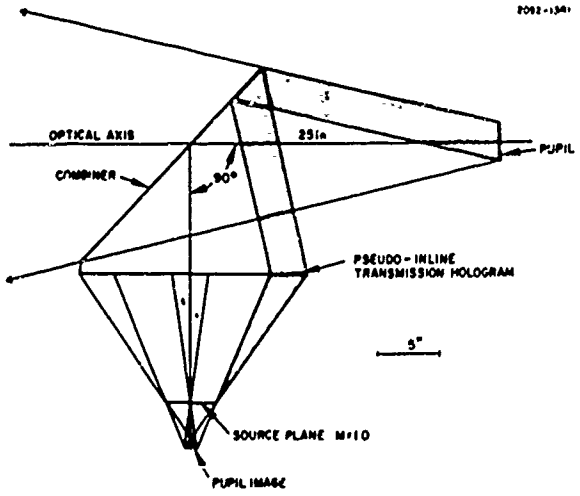

(c)

System
1
2
3
4
5
6
7
8
9
10
11

Fig. 9.
Three possible holographic HUD configurations with different magnifications, shown as vertical sections. (a) Reflection hologram collimator/combiner; (b) transmission hologram collimator/combiner; (c) pseudo-inline transmission collimator, with a separate combiner.

TABLE 5

Systems Analyzed in Parametric Study

System	Type	ϕ (deg)	f (in.)	m	Ψ (deg)
1	R	20	14.1	1.57	5
2	R	30	14.2	1.58	5
3	R	40	14.2	1.57	5
4	R	50	13.1	1.45	4
5	R	60	13.2	1.46	3
6	R	40	14.1	1.57	0
7	T	30	14.4	1.59	0
8	T	40	14.4	1.59	0
9	T	50	14.4	1.59	0
10	T	60	14.4	1.59	0
11	PILT	—	14.2	1.57	—

T1376

Fig. 9.
Three possible holographic HUD configurations with different magnifications, shown as vertical sections. (a) Reflection hologram collimator/combiner; (b) transmission hologram collimator/combiner; (c) pseudo-inline transmission collimator, with a separate combiner.

II. Parametric Analysis

B. Scope of the Parametric Study

4. ASTIGMATISM AND FIELD TILTS AND CURVATURES

The characteristics of the intermediate image, i.e., astigmatism, tilts and curvatures, are determined by tracing bundles of parallel rays through the system, and are dependent on the hologram construction wavefront curvatures as well as the geometrical configuration of the system.

The first step in the analysis of a particular configuration is to determine the location, orientation, and curvature of the intermediate image surfaces. These surfaces are defined as the collection of points such that rays from these points produce a set of parallel rays at the center region of the pupil (i.e., an image at infinity). In general these points are different for rays in a vertical section of the system than for rays in a horizontal section of the system, and the separation of these two image surfaces is the astigmatism. The two image surfaces are indicated in Fig. 10, which shows vertical and "horizontal" sections through a transmission type system. The "horizontal" section is taken perpendicular to the vertical section, but along the folded optical axis.

A rectangular coordinate system is set up near the image surfaces, with its z-axis along the optical axis, as shown in Fig. 10. The y-z plane is taken to be in the vertical section, and the x-z plane is therefore in the horizontal section. The hologram image is in general two separate, three-dimensional surfaces, characterized by their intersections with the x-z and y-z planes of this coordinate system. These intersection curves are characterized by their average curvature in both planes and the angles that their vertex tangents in the y-z plane make with the y-axis (by symmetry, there is no tilt in the x-z plane intersections, i.e., the horizontal section).

1376

The image surfaces are determined by locating several representative points in the x-z and y-z intersections, as indicated in Fig. 10. This is accomplished by tracing sets of five parallel rays backward through the system from the exit pupil through the hologram, and into the image space, as follows: For a particular direction in the angular FOV, a bundle of five parallel rays is launched through the pupil. The intersection of these five rays with the pupil plane is the same for all directions in the FOV, and these five intersection points are indicated in Fig. 11. The x_p- y_p coordinates are normal to the optical axis, with the origin located at the intersection of the optical axis and the pupil plane. The central ray (number 5 in Fig. 11) is the chief ray. Rays 1 and 2 are in a horizontal section; rays 3 and 4 are in a vertical section, spaced from the center by about 1/50 of the pupil size. The horizontal (vertical) focal point is the point along the chief ray where rays 1 and 2 (3 and 4) are closest together. The separation between the two focal points is the astigmatism.

This process is repeated for several different directions in the angular field of view. Typical field directions in the vertical and horizontal sections are indicated in Fig. 10, and the corresponding horizontal focal points are indicated by circled points, while the vertical focal points are indicated by noncircled points. Taken together, these sets of focal points establish the image surfaces. The tilt angles Ω_h and Ω_v are determined by drawing vertex tangents in the y-z intersection, as indicated in Fig. 10. The four average curvatures are determined from the formula $R = w^2/2\Delta$, where R is the radius of curvature, w is the distance along the tangent, and Δ is the perpendicular distance of a point from the tangent.

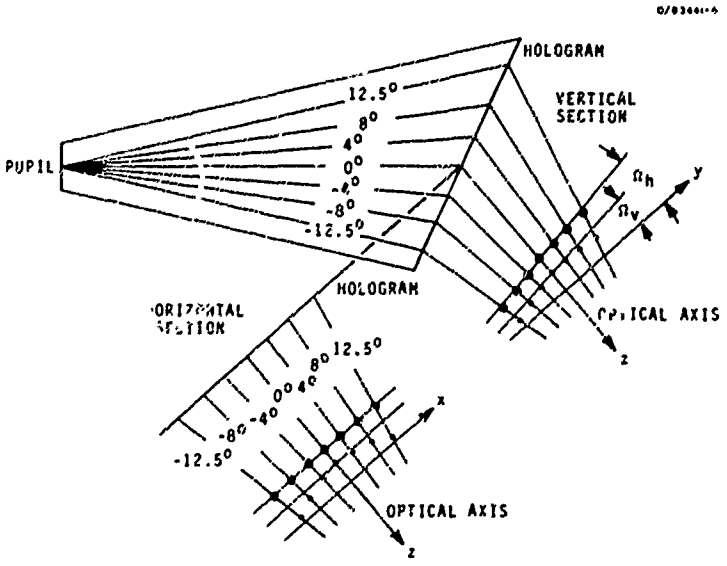

Fig. 10.
Vertical and horizontal sections of a transmission hologram HUD element, showing the paths of chief rays used to determine the focal surface characteristics.

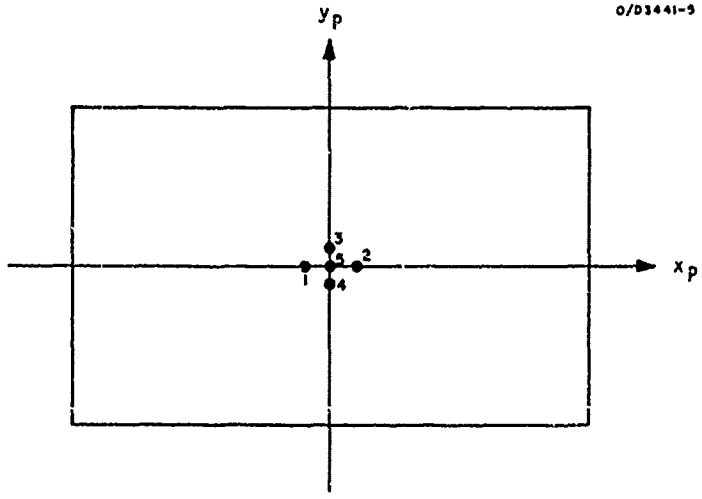

Fig. 11.
The exit pupil area, showing the intersection points of the five rays used to determine the focus points for any point in the angular field of view.

II. Parametric Analysis

B. Scope of the Parametric Study

5. OPTICAL EFFICIENCY ACROSS THE FIELD AND ACROSS THE PUPIL

The second major system characteristic to be considered is the optical (diffraction) efficiency of the hologram, which, for the basic continuous lens design, remains high for chief rays across the angular field of view, but tends to limit the exit pupil size, depending primarily on recording material film thickness.

The second step in the analysis of a particular configuration is to determine the optical efficiency of the hologram, which is assumed to be a thick, phase recording.[6] The characteristic of interest is the reduction of diffraction efficiency, relative to the maximum efficiency, as a function of position in the angular field and/or position in the system exit pupil. The cause of this efficiency drop is the deviation of ray directions from the directions used to construct the hologram, leading to a failure to satisfy the Bragg condition for maximum diffraction efficiency.[6]

The effect of the limited angular bandwidth of diffraction efficiency is that, for a given recording material film thickness, it is not possible to simultaneously achieve an arbitrarily large angular field of view and an arbitrarily large exit pupil. The continuous lens design approach, discussed in Section II-A, provides a uniform optical efficiency across the FOV at the center of the pupil; i.e., it is designed for a high chief ray efficiency. However, rays through the outer parts of the exit pupil will show a decrease in efficiency that is dependent on the geometrical configuration and on the thickness of the recording material. Furthermore, if modified construction wavefronts (e.g., astigmatic) are used, the chief ray efficiency may not remain high across the entire FOV, and the peak efficiency may not occur in the center of the exit pupil.

For both reflection and transmission configurations, the angular deviation of rays from the construction geometry that is allowed before the diffraction efficiency drops to zero is approximately $\Delta\theta = n\lambda/t \sin \phi/2$, where n is the average refractive index of the recording material λ is the operating wavelength, t is the thickness of the film of recording material and ϕ is the off-axis angle.[10] This expression provides estimates of the efficiency characteristics, but for quantitative information the theory of Kogelnik[6] must be applied in the ray tracing procedure.

The characteristic behavior of the optical efficiency is summarized in Table 6.

TABLE 6

Holographic HUD Optical Efficiency Characteristics

1. There is a tradeoff between angular FOV and system exit pupil.
2. The basic continuous lens approach provides maximum chief ray efficiency, with limited exit pupil size.
3. The efficiency characteristics are determined primarily by the recording material thickness and the system geometry.
4. Angular half-bandwidths are given approximately by the formula

$$\Delta\theta = \frac{n\lambda}{t \sin \frac{\phi}{2}}$$

T1377

II. Parametric Analysis

B. Scope of the Parametric Study

6. DISTORTION DERIVED FROM A NOMINAL FOCAL SURFACE

A measure of distortion is chosen which is equal to the horizontal-to-vertical magnification ratio of the ideal relay lens, which optimally compensates for the hologram lens distortion.

The third step in the analysis of a particular configuration is to characterize the amount of distortion in the intermediate image. For the parametric study, this requires a quantitative measure of distortion that can be easily interpreted and compared for different configurations. We first choose a nominal focal surface, based on the image-formation ray trace data, that best represents the intermediate image fields of the hologram lens. We then trace chief rays backward through the system, from a set of circular images at infinity, having different angular radii, and determine the points of intersection of these chief rays with the nominal intermediate image. For a given circular image, this set of intersection points will form an oval shape that is symmetric in the horizontal direction. An example of this shape is shown in Fig. 12. The measure of distortion is taken to be the ratio of the vertical dimensions of this oval shape, to the horizontal dimension of the oval, as a function of the radius of the circular image at infinity.

If there is no distortion, this ratio will be unity. If the vertical dimensions are the same in the positive and negative directions, but is not equal to the horizontal dimension, then there is anamorphic distortion, with the circle producing an elliptical intermediate image. If the positive vertical dimension is larger, for example, than the horizontal dimension, but the negative vertical dimension is smaller, then there is a keystone-type distortion, and the circle produces an egg-shaped intermediate image. There can be combinations of these types of distortion.

The importance of this form of intermediate image calculation is that if a relay lens is provided that produces this particular intermediate image from a circular input image, then that input image will be projected by the system as a circular image at infinity. In other words, the characteristic ratio determined in the above manner is the ratio of vertical to horizontal magnification of the ideal relay lens for that system. Therefore, although this measure of distortion is incomplete, it is easily interpreted and is of major importance in terms of system performance.

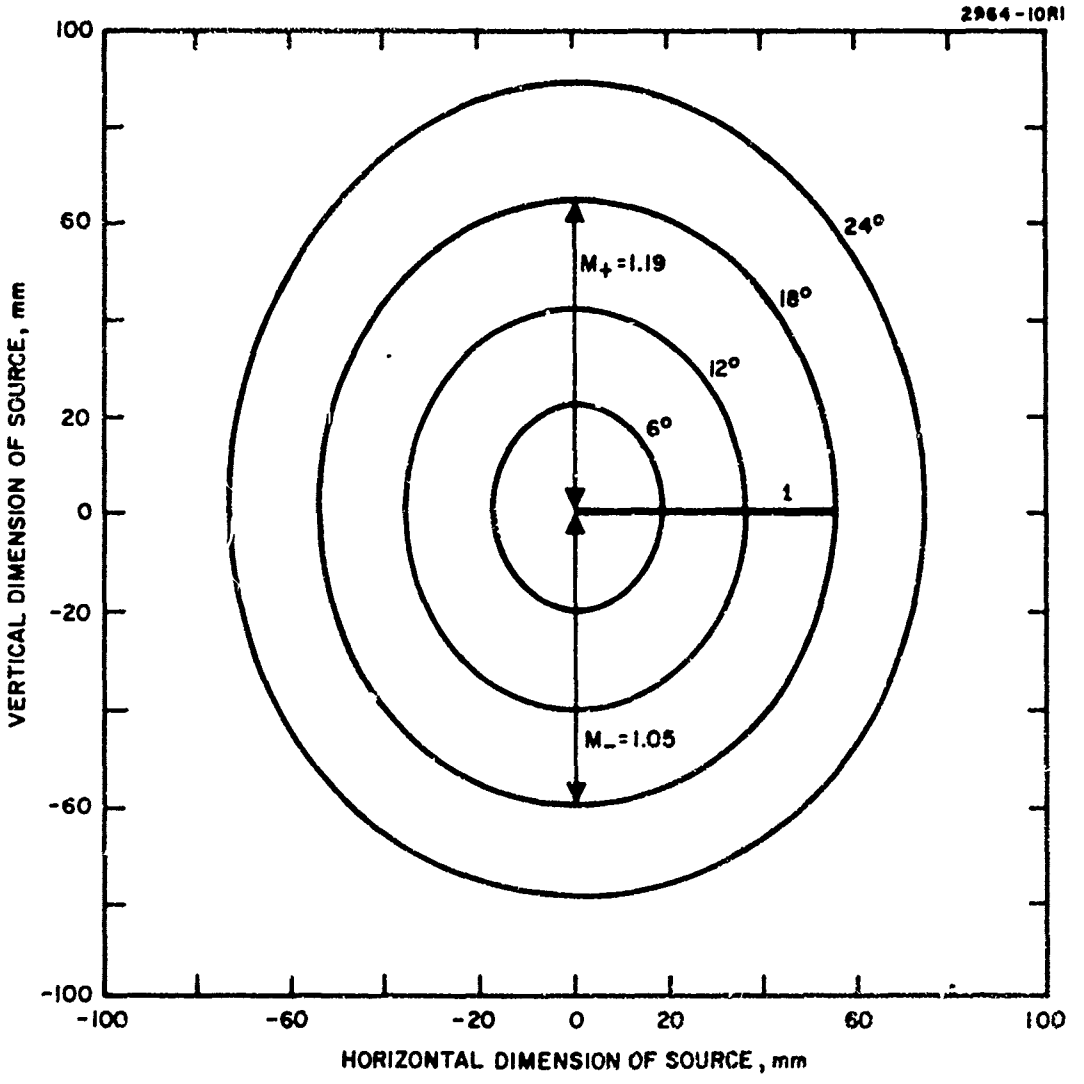

Fig. 12. An example of the distorted input to the holographic collimator required to provide circular images at infinity. Shown is the definition of the vertical to horizontal magnification ratio, which is a measure of the distortion.

II. Parametric Analysis

B. Scope of the Parametric Study

7. RAY INTERCEPT CURVES

Ray intercept curves, which plot ray intercepts with the image surface, relative to the chief ray intercept, as a function of ray position in the exit pupil, provide directly the type and size of aberrations for a particular configuration.

In order to compare the imaging characteristics of different configurations, we require an analysis technique that gives complete quantitative information about the image quality, but which can easily be interpreted in qualitative terms. In particular, for the systems of interest, we expect relatively large geometrical aberrations, with diffraction effects playing no significant role, and therefore, the analysis technique should be suitable for such systems.

In this situation, ray intercept curves[11] provide the required data in the form of deviations of the actual image from the small-pupil image, as a function of position within the exit pupil. We use the ray intercept curves in the way shown in Fig. 13. Having calculated the intermediate image fields, we choose a nominal focal surface and trace horizontal and vertical fans of parallel rays (each including the chief ray), from a particular point in the angular FOV, through the exit pupil, to be diffracted by the hologram, and intercept the nominal focal surface. We then make four plots of these image intercept coordinates (subscript i), relative to the chief ray intercept, as a function of the pupil coordinates (subscript p) shown in Fig. 13: x_i versus x_p, y_i versus x_p, x_i versus y_p and y_i versus y_p. In standard optical design terms, commonly used for rotationally symmetric optical systems,[11] for points in the angular FOV on the vertical axis, the vertical fan of rays is a tangential fan and the horizontal fan is a sagittal fan. For any other points in the angular FOV, this terminology is not applicable, due to the lack of rotational symmetry.

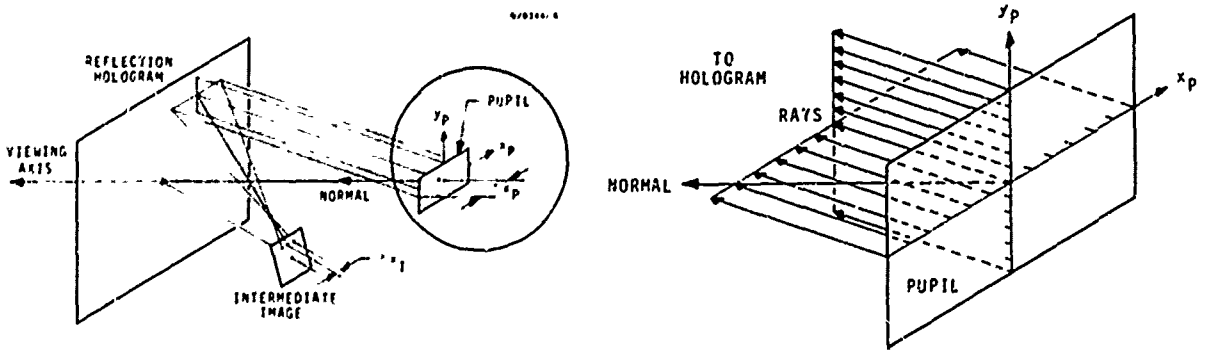

Fig. 13. Reflection HUD element schematic, showing ray fans used to calculate ray intercept curves.

For the purpose of comparing different configurations, we utilize these ray intercept curves for the axial point in the angular FOV. A typical ray intercept curve is shown in Fig. 14. The particular utility of the ray intercept curves is that the shape of the curve shows the type of aberrations that are pertinent for that point in the FOV and that choice of focal surface.[11] In particular, if the image quality is perfect, all rays meet at a point in the focal surface, and the ray intercept curves are straight, horizontal lines. (By definition, the ray intercept curves go through the origin, being relative to the chief ray.) For defocus, the curve forms a straight line; astigmatism produces straight lines at different angles; spherical aberration produces a curve that has odd symmetry; and coma produces a curve that has even symmetry. In our work, field curvature, which is essentially a defocus, is corrected as far as possible by the choice of focal surface, and chromatic aberration is ignored because of monochromatic operation.

For comparison terms, we assume that the design of the relay lens compensates for field curvature, defocus and astigmatism, these all being image location, or focus terms. Remaining are spherical aberration and coma, and these can be isolated by subtracting linear terms and then looking at the odd and even terms remaining. The ray intercept curves are also extremely useful for calculating collimation error and binocular disparity as will be shown in the next section.

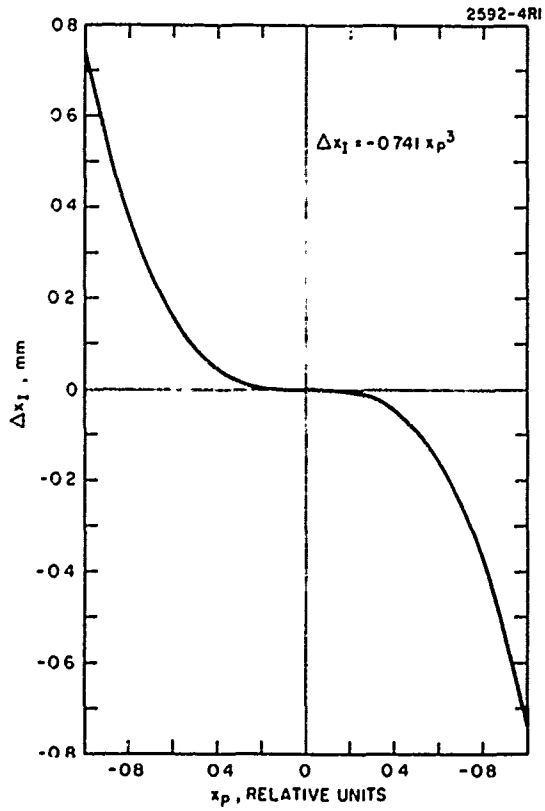

Fig. 14. A typical ray intercept curve.

II. Parametric Analysis

B. Scope of the Parametric Study

8. PUPIL ERRORS FROM RAY INTERCEPT CURVES

The two important system pupil errors are the collimation error and binocular disparity, and these can be defined and analyzed in terms of differential ray intercepts with the nominal focal surface.

For a HUD system, we require information on collimation error (CE) and binocular disparity (BD). The CE is the variation of image location, for a point input, as the viewer's eye moves about in the exit pupil, with reference to the image location observed at the center of the pupil. The BD is the difference in image location apparent to the viewer's two eyes; this generally changes with position of the eyes in the pupil. These errors are directly related to the pupil aberrations of the previous section.

If no aberrations are present, all parallel rays through the pupil converge to a point on the focal surface. Since both eyes will see the same image location at infinity, regardless of their position in the pupil, there is no CE or BD. With aberrations, two small, parallel ray bundles (corresponding to the two eyes) will intercept different points on the focal surface; conversely, rays from a single point on the focal surface will enter the two eyes in slightly different directions, producing different image locations at infinity.

We define the CE as the average image location seen by two eyes, relative to the image location seen by an eye centered in the pupil. The BD is defined as the difference in image location seen by the two eyes, with the horizontal component termed convergent if the eyes must cross to fuse the image, and divergent if the eyes turn out to fuse the image.

There is a one-to-one correspondence between the differential focal surface intercepts for two ray bundles from a single point at infinity, and the differential angle between two ray bundles from a single point on the focal surface. Therefore, we can use the ray intercept data to calculate the CE and BD, though in general this requires fans which do not include the chief ray.

The procedure for calculating the CE and BD, for a given point in the angular FOV and given horizontal positions of the eyes in the pupil, is to trace two vertical fans of rays going through the horizontal eye locations (for example, in Fig. 15, the right eye is on the y_p axis and the left eye is at the left edge of the pupil), and calculate the differential intercepts for each value of y_p. The differential intercepts calculated for a particular system example, using the ray fans of Fig. 15, are shown in Fig. 16, with the CE and BD errors indicated

for one eye location near the bottom of the pupil. The angular error is then the average (CE) or difference (BD) in the intercepts for the two eyes, divided by the local focal length, i.e., the distance from the intercept of the chief ray with the hologram surface to its intercept with the focal surface. We can then plot the horizontal and vertical components of both the CE and BD versus y_p, the vertical location of the eyes in the pupil. Note that this assumes the two eyes are always horizontally separated. This procedure can be repeated for other points in the FOV and/or horizontal eye locations. For comparison purposes, we choose the axial pont in the FOV, and the symmetric and left (Fig. 15) horizontal eye positions.

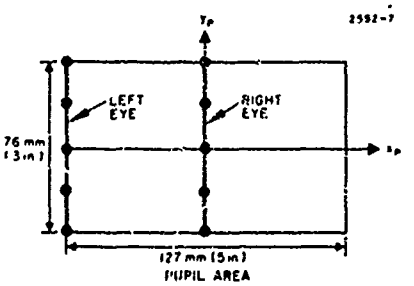

Fig. 15.
Pupil area and example of ray fans for calculating collimation error and binocular disparity.

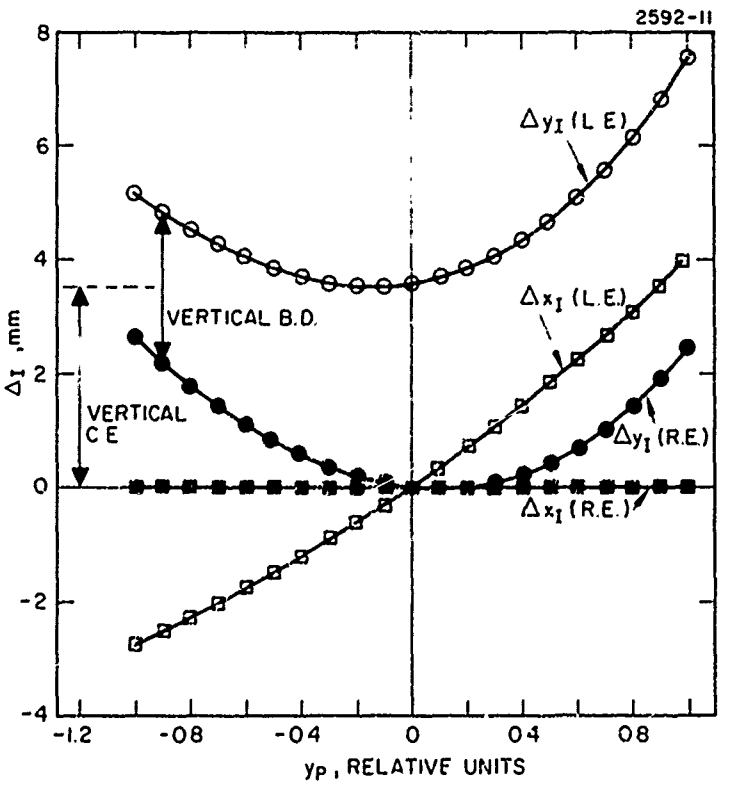

Fig. 16. Differential ray intercept curves for the error fans of Fig. 15 in a reflection continuous lens system.

II. Parametric Analysis

C. Results of the Study

1. FIELD TILTS AND CURVATURES

The tilts of the hologram focal surfaces are generally toward being parallel with the hologram surface, but are usually different for horizontal and vertical fans; the radii of curvature of these surfaces are different in horizontal and vertical sections, forming two intersecting spheroids.

A range of holographic HUD configurations was analyzed according to the methods discussed in Section II-B. The results of the first step of that analysis, i.e., the focal characteristics of the holographic elements, are summarized in Fig. 17 and Table 7. Figure 17 shows the vertical (y-z) section of the focal surfaces for system number 1 of Table 7. Table 7 lists the type of configuration, the off-axis angle ϕ and the asymmetry angle Ψ, as defined in Section II-B-1. In the specification of system type, an asterisk indicates that the focal surfaces were optimized for minimum astigmatism across the field, by varying the amount of astigmatism in the hologram construction beams. The construction beam astigmatism, i.e., the axial separation of the horizontal and vertical centers of curvature, is also listed in Table 7. The focal surface characteristics are provided in the last six columns of Table 7. Included are the tilt angles, Ω_h and Ω_v, of the vertical sections with respect to the optical axis, for horizontal and vertical ray fans, respectively, and the four average radii of curvature: R_{hh} and R_{hv}, the radii for the horizontal sections of the horizontal and vertical fan focal surfaces, respectively and R_{vh} and R_{vv}, the radii for the vertical sections of the horizontal and vertical fan focal surfaces, respectively.

A general characteristic of the results shown in Table 7 is that the focal surfaces are tilted in a direction toward being parallel with the hologram surface. This direction is such that the hologram local focal length variation is reduced, which reduces distortion and coma. Without minimization of astigmatism across the field, the field tilts for the horizontal and vertical fan focal surfaces are different. Optimization of astigmatism for reflection geometries requires large amounts of astigmatism in the construction beams, which nearly cancel but provide the relatively large amount of field tilt required to bring the focal surfaces together. The difference in tilt angles for the horizontal and vertical fan focal surfaces is much less for transmission geometries: for example, for $\phi = 40^\circ$ this difference is 20° for the reflection case and only 6° for the transmission case, both being symmetric, unoptimized systems.

Field curvature tends to be rather complex, but much more uniform for the systems that have minimized astigmatism. The general tendency for nonoptimized configurations is to have focal surfaces that are

spheroidal, having a different average curvature in the horizontal and vertical sections. Furthermore, the vertical section generally shows a larger radius of curvature for the horizontal fan focal surface, while the horizontal section is reversed, showing a larger radius of curvature for the vertical fan focal surface. This means that the focal surfaces tend to be "crossed" spheroids, with the larger radius of curvature of one being perpendicular to the larger radius of curvature of the other.

A positive radius of curvature can be easily matched by field curvature in the relay lens, but negative curvature (e.g., the PILT system) presents a relatively difficult design task.

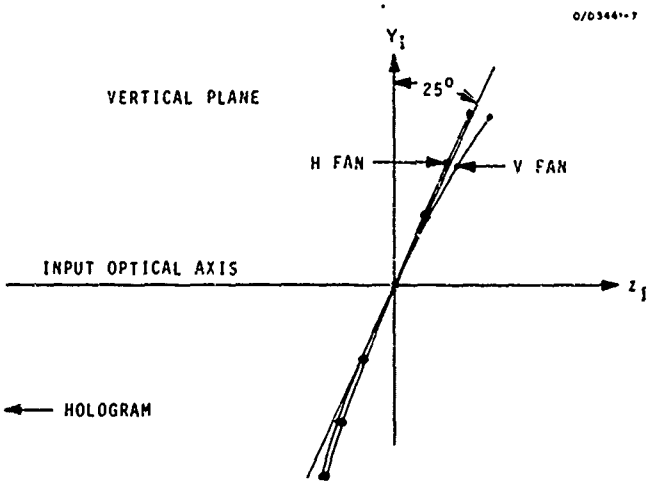

Fig. 17.
Vertical section of the focal surfaces for System No. 1. Solid points are vertical fan focal points, and circled points are horizontal fan focal points.

TABLE 7

Focal Characteristics of Holographic Lenses

System	Type	ϕ (deg)	ψ (deg)	Pupil Astigmatism (mm)	Source Astigmatism (mm)	Ω_h (deg)	Ω_v (deg)	R_{hh} (mm)	R_{hv} (mm)	R_{vv} (mm)	R_{vh} (mm)
1	R*	20	5	254	-238	25	25	800	1600	600	600
2	R*	30	5	294	-271	32	32	500	1600	600	600
3	R*	40	5	328	-289	38.5	38.5	540	1070	500	500
4	R*	50	4	337	-249	45.5	45.5	6400	1600	420	420
5	R*	60	3	335	-250	51	51	-1600	800	420	420
6	R	40	0	0	0	35.5	55	800	800	770	1350
7	T	30	0	0	0	12.5	7	460	1280	610	1600
7'	T*	30	0	0	0	15	15	3200	3200	3200	3200
8	T	40	0	0	0	17	11	460	1280	490	1810
8'	T*	40	0	2	-5	20	20	3200	3200	3000	3000
9	T	0	0	0	0	21.5	14.5	460	1280	590	1940
9'	T*	50	0	10	-32	25	25	860	2800	4400	6500
10	T	60	0	0	0	27	18	460	1280	660	2020
10'	T*	60	0	-7	25	30.5	30.5	1800	2400	1070	1300
11	PILT	—	—	0	0	0	0	-380	-1100	-380	-1100

T1378

II. Parametric Analysis

C. Results of the Study

2. OPTICAL EFFICIENCY

In order to maintain desirable optical efficiency characteristics in the holographic lens, the hologram should have minimum asymmetry and should be fabricated with point source construction beams, with one point source in the center of the exit pupil.

In section II-B-5 we discussed the trade-off between exit pupil size and angular FOV for a given recording material film thickness. We also described the reduced chief ray efficiency and the decentering of peak pupil efficiency that may occur when the pupil point source is shifted axially and/or the construction beams are made astigmatic, and we gave an equation that can be used to estimate the angular deviation of rays from the construction ray directions that reduces the efficiency to zero. This procedure can be used to quickly evaluate a particular configuration, but for quantitative efficiency behavior, Kogelnik's theory[6] is used in a raytrace calculation. A comparison of the estimate and actual raytrace results is given in Table 8. The estimate is accurate for the reflection configurations, but is systematically larger than the results from raytrace data for the transmission configurations by 10% to 20%.

Figure 18 shows typical pupil efficiency curves for systems with point source construction beams (no astigmatism), having one point source in the center of the pupil. There is little loss of efficiency across the horizontal pupil coordinate, but the loss of efficiency across the vertical pupil coordinate can be substantial for some points in the angular FOV (these curves are for a film thickness of 15 μm). For these cases, the chief ray efficiency remains high across the FOV, because the chief rays exactly follow the construction ray paths.

Figures 19 and 20 indicate the undesirable effect on efficiency caused by using strongly astigmatic construction beams to minimize astigmatism across the angular FOV. The chief ray efficiency is reduced at the edges of the FOV, as shown in Fig. 19, and the peak pupil efficiency can be shifted away from the center of the exit pupil, as shown in Fig. 20. It is, therefore, desirable to maintain approximately point source construction beams, and/or reduce dispersion (and therefore astigmatism) by utilizing a symmetric reflection configuration.

TABLE 8

Comparison of Estimated and Calculated Angular Widths

ϕ	θ, Degrees		
	Estimate	Reflection Raytrace	Transmission Raytrace
20	16.4	20	——
30	11.0	11	9.0
40	8.3	8	7.0
50	6.7	6.6	6.0
60	5.7	5.5	5.0

T1379

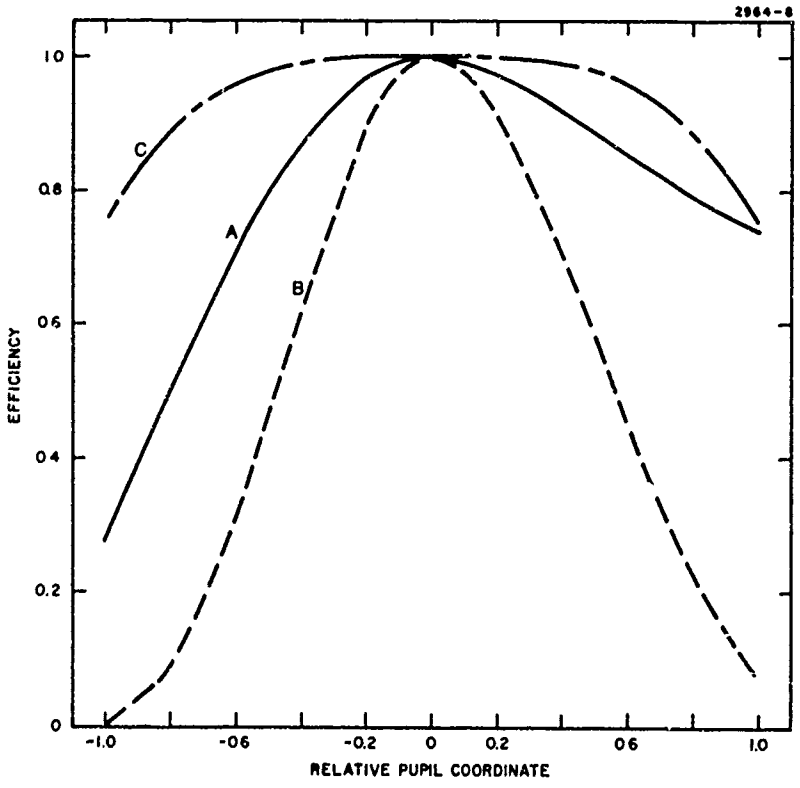

Fig. 18.
Representative optical efficiency across the pupil for symmetric transmission continuous lens systems with a film thickness of 15 μm. A is $\phi = 40^{\circ}$, $+12.5^{\circ}$ vertical field point, vertical pupil coordinate; B is $\phi = 40^{\circ}$, $+12.5^{\circ}$ horizontal field point, vertical pupil coordinate; C is $\phi = 50^{\circ}$, -12.5° vertical field point, horizontal pupil coordinate.

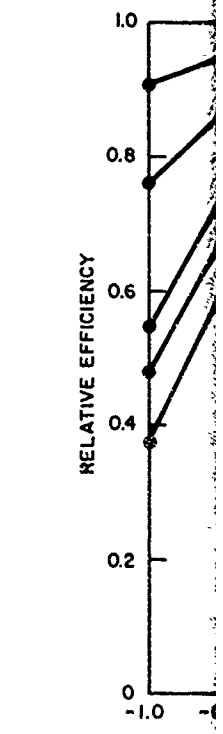

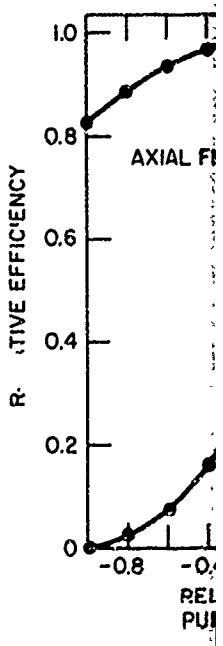

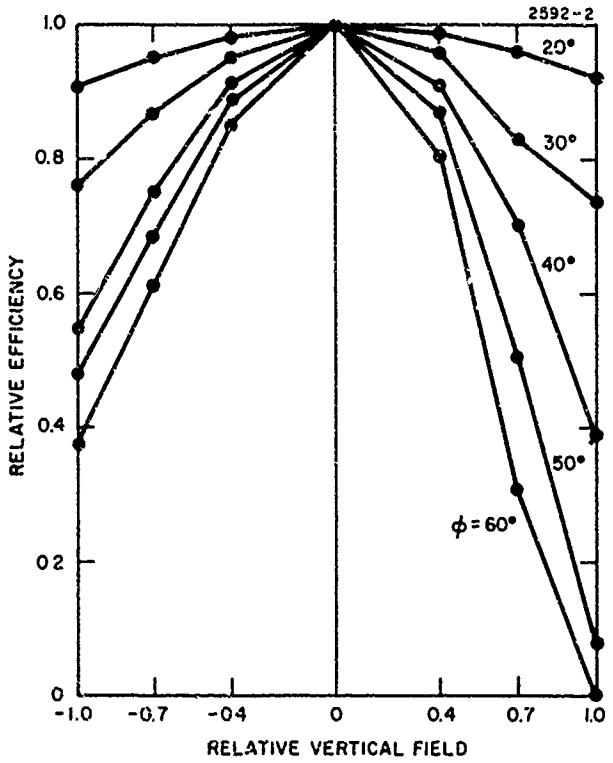

Fig. 19.
Chief ray optical efficiency versus the vertical field of view for several reflection continuous lens holographic HUC systems having astigmatism corrected across the field of view during hologram construction.[25]

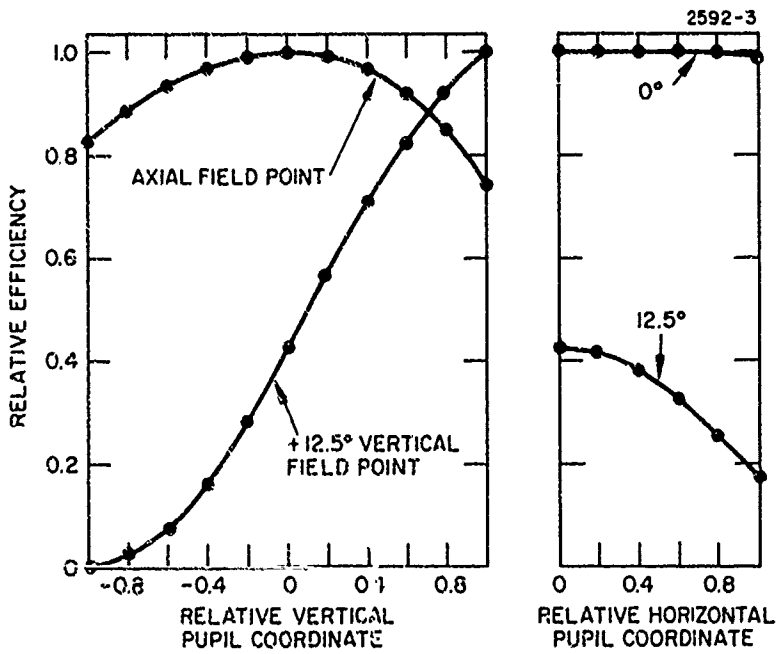

Fig. 20.
Relative optical efficiency across the pupil for vertical and horizontal fans for a reflection hologram with $\phi = 40^{\circ}$, $\psi = 5^{\circ}$ and astigmatism corrected during hologram construction.

II. Parametric Analysis

C. Results of the Study

3. DISTORTION

The relationship between intermediate image and field coordinates is more nearly linear for reflection systems than for transmission systems; the vertical/horizontal difference includes both anamorphic and keystone distortion, increasing with off-axis angle, mostly anamorphic in reflection systems and mostly keystone in transmission systems.

In considering the question of distortion in the holographic lens image, there are two important aspects. The first is linearity of the relationship between a coordinate on the intermediate image surface and the corresponding coordinate in the angular FOV, and the second is the difference between the horizontal and vertical directions.

For the reflection systems studied, the vertical field angle varied linearly with the vertical intermediate image coordinates within less than 1%. For the transmission systems, the deviation from coordinate linearity is greater and is a function of the off-axis angle ϕ, varying from 2.7% at $\phi = 30^{\circ}$ to 16.7% at $\phi = 60^{\circ}$. These results are for systems with astigmatism minimized across the FOV, so that a well-defined, single intermediate image surface can be defined.

The difference between horizontal and vertical directions was considered in Section II-B-6, and the ratio of vertical magnification to horizontal magnification, as a function of the vertical field angle, required from the relay lens to give zero difference, was chosen as a measure of the difference. This magnification ratio is plotted in Fig. 21 for several reflection geometries, and in Fig. 22 for several transmission geometries. In both figures, the amount of distortion increases with the off-axis angle. From Fig. 21, we see that the reflection continuous lens produces mostly anamorphic distortion, with some keystone. For the $\phi = 40^{\circ}$ reflection system, the distortion departs from simple anamorphic by less than 3%. From Fig. 21, we see that the transmission continuous lens produces mostly keystone distortion, with some anamorphic. For the $\phi = 50^{\circ}$ case, there is about 10% anamorphic distortion.

In general, therefore, the relay lens must be anamorphic and the object and intermediate image must be tilted to compensate for keystone distortion. Compensation for the coordinate nonlinearity must, in general, be accomplished in the scanner drive electronics, rather than in the relay lens.

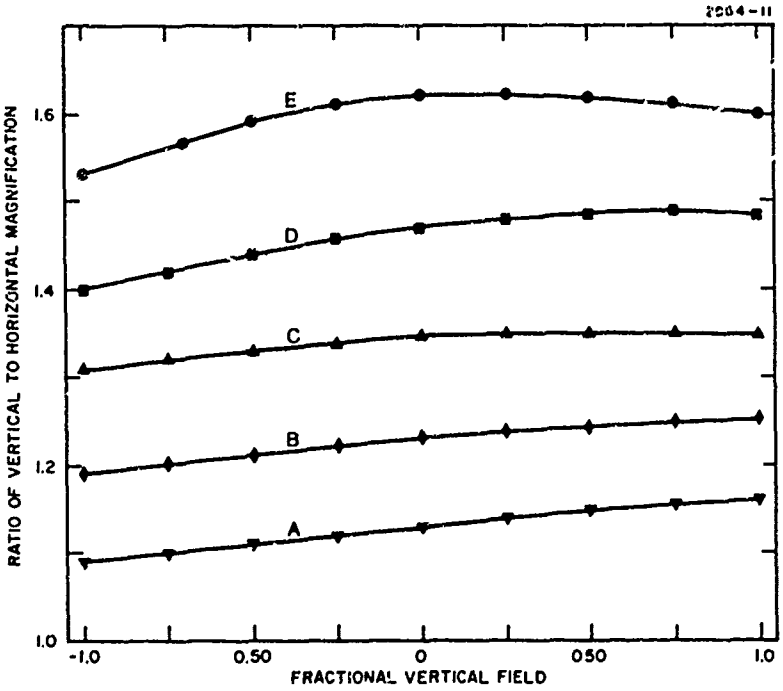

Fig. 21. The ratio of vertical to horizontal relay lens magnification required to provide an undistorted image, over the 25° vertical field, for several reflection continuous lens systems. A is $\phi = 20^{\circ}$ B is $\phi = 30^{\circ}$; C is $\phi = 40^{\circ}$; D is $\phi = 50^{\circ}$; E is $\phi = 60^{\circ}$.

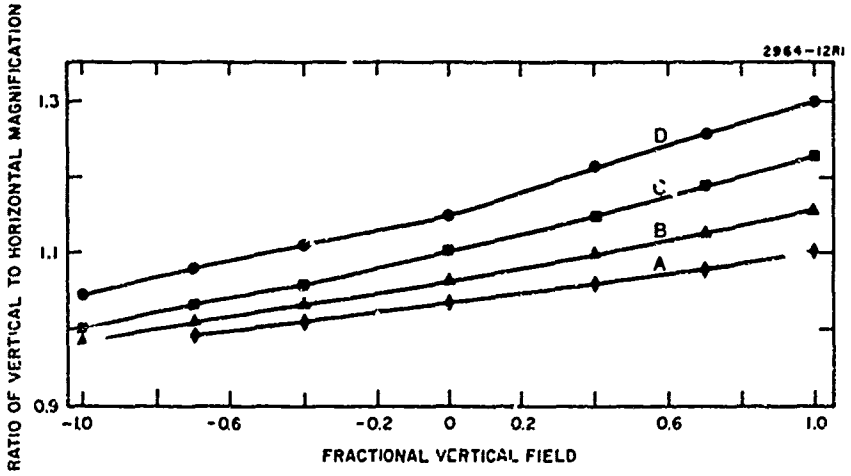

Fig. 22. The ratio of vertical to horizontal relay lens magnification required to give an undistorted image, versus the 25° vertical field, for several symmetric transmission continuous lens systems. A is $\phi = 30^{\circ}$; B is $\phi = 40^{\circ}$; C is $\phi = 50^{\circ}$; D is $\phi = 60^{\circ}$.

II. Parametric Analysis

C. Results of the Study

4. TYPICAL ABERRATIONS

The ray intercept curves typically show a combination of coma and spherical aberration, with coma dominating; the aberration magnitude is approximately in the ratio of 1:2 for transmission and reflection systems, and 1:4 for pseudo-inline and reflection systems.

The pupil errors are obtained by using ray intercept curves, as discussed in Section II-B-7. An example of typical pupil errors is shown in Fig. 23 for the particular case of the axial field point in a reflection continuous lens system with $\phi = 40^{o}$, having astigmatism minimized across the FOV. Figures 23(a) and 23(b) show the ray intercept curves for a ray fan corresponding to the sagittal fan in a rotationally-symmetric optical system. Figure 23(c) shows the ray intercept curve for a ray fan corresponding to the tangential fan in a rotationally-symmetric system. As discussed in Section II-B-7, these fan types do not, in general, apply to the nonrotationally-symmetric holographic HUD systems; however, the ray intercept curves can still be interpreted in terms of the characteristic aberrations. In general, both in-plane and out-of-plane intercept curves are required for both horizontal and vertical ray fans.

The horizontal differential intercept for the horizontal ray fan is plotted in Fig. 23(a) and shows only spherical aberration. The vertical differential intercept for the same fan is shown in Fig. 23(b), which gives only coma, but over three times larger than the spherical aberration. Figure 23(c) gives the vertical differential intercept for the vertical ray fan (in this instance, a tangential-type fan), and this curve shows both coma and spherical aberration, with the coma dominating by a factor of about 10.

Other systems and/or other field points produce similar results, i.e., a combination of coma and spherical aberration, with coma dominant. In general there are linear components, from astigmatism and/or field curvature, but these are easily correctable focus errors for the purposes of this analysis. The magnitude of the aberrations (especially coma) is generally about two times smaller for transmission systems than for reflection systems, and about four times smaller for the pseudo-inline transmission system than for reflection systems.

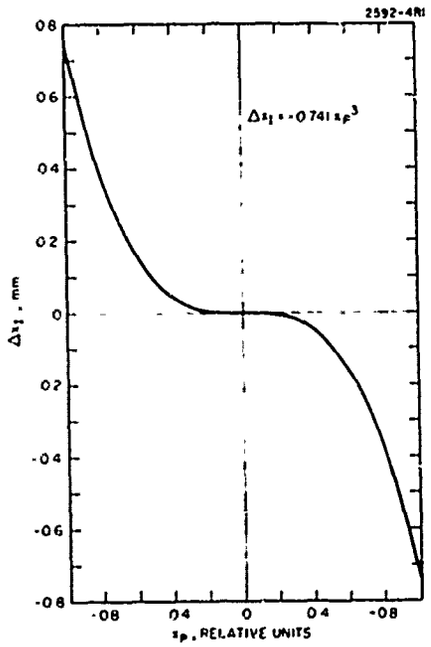

(a)

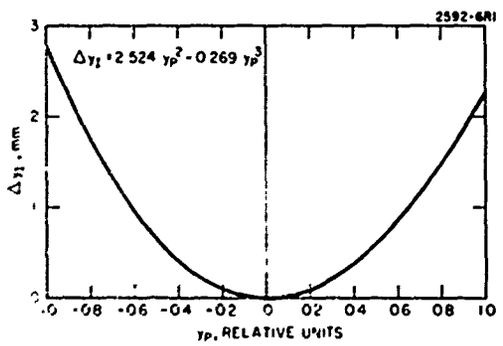

(b)

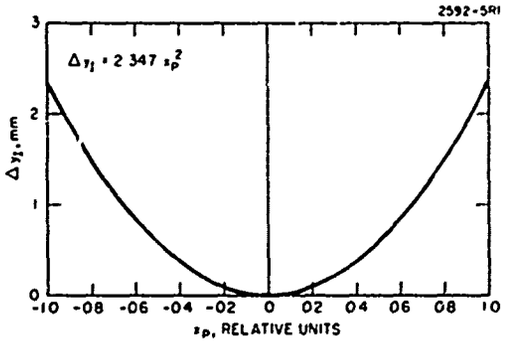

(c)

Fig. 23. Typical ray intercept curves for a holographic HUD lens; (a) horizontal intercepts of a horizontal ray fan, showing spherical aberration; (b) vertical intercepts of a horizontal ray fan, showing coma; (c) vertical intercepts of a vertical ray fan, showing coma and a relatively small amount of spherical aberration.

II. Parametric Analysis

C. Results of the Study

5. BINOCULAR DISPARITY AND COLLIMATION ERROR

Binocular disparity and collimation error increase with off-axis angle, are about two times larger in reflection systems than in transmission systems, and are in all cases large enough to require correcting elements in the final system.

The binocular disparity and collimation error were studied for several systems, using the techniques discussed in Section II-B-8. Typical results are shown in Figs. 24 and 25 for the left eye horizontally located at the left of the 5-in. wide pupil, and the right eye horizontally located at the center of the pupil, as a function of the vertical location of the eyes. This is called the "Eyes to Left" case. A second case, studied for this comparison, is the "Eyes Centered" case, where the eyes have the same horizontal spacing of 2.5 in. but are symmetrically located in the horizontal pupil dimension at ±1.25 in. from the pupil center. In all cases the axial field point was analyzed.

TABLE 9

Maximum Binocular Disparity and Collimation Error

System			Errors With Eyes Centered (mrad)				Errors With Eyes to Left (mrad)			
System Number	System Type	ϕ (deg.)	HBD[1]	VBD[2]	HCE[3]	VCE[4]	HBD[1]	VBD[2]	HCE[3]	VCE[4]
1	R	20	6.2	0	0	5.6	2.4	6.1	1.2	7.1
2	R	30	6.9	0	0	7.3	9.2	9.3	4.6	9.8
3	R	40	9.8	0	0	9.9	10.4	13.3	5.2	13.0
4	R	50	11.8	0	0	18.5	16.2	22.5	8.1	24.0
5	R	60	15.6	0	0	25.0	21.2	31.2	10.6	32.9
6	R	30	10.2	0	0	13.2	12.8	11.9	6.4	16.2
7	T	30	3.5	0	0	3.4	5.1	3.4	2.6	4.3
8	T	40	4.4	0	0	4.6	6.0	4.3	3.0	5.6
8'	T	40	6.7	0	0	6.8	9.5	6.7	4.7	8.5
9	T	50	5.4	0	0	5.5	7.0	5.4	3.5	7.2
10	T	60	6.4	0	0	7.4	8.2	6.8	4.1	9.1
11	PILT	--	1.1	0	0	0.7	2.7	1.2	1.3	2.9

Note 1: HBD = Horizontal Binocular Disparity
Note 2: VBD = Vertical Binocular Disparity
Note 3: HCE = Horizontal Collimation Error
Note 4: VCE = Vertical Collimation Error

T1380

Table 9 gives the maximum pupil errors in milliradians for a range of systems. The system number and type designations are the same as in Table 7 of Section II-C-1. The error sizes are closely associated with the amount of coma in the system. For the transmission systems, the errors are two to three times less than for corresponding reflection systems. An interesting tendency is for the errors to be slightly reduced when a reflection system has astigmatism minimized across the FOV by using astigmatic construction beams, while the errors are significantly increased by the minimization process in a transmission system. In all but the pseudo-inline transmission system, the errors are significantly larger than specified, and therefore correcting elements are required.

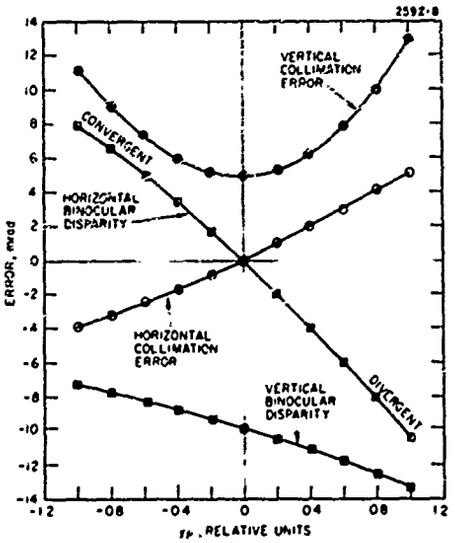

Fig. 24.
Vertical and horizontal components of collimation error and binocular disparity versus vertical eye position in the pupil, for a reflection holographic HUD lens with $\phi = 40^{\circ}$.

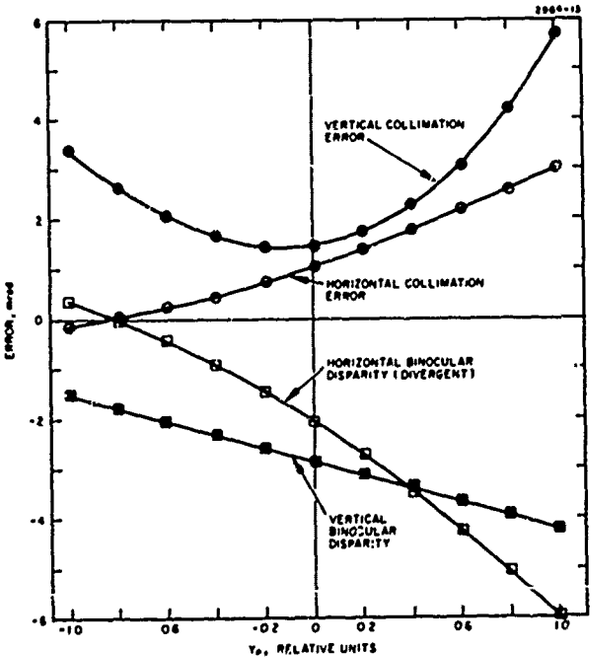

Fig. 25.
Vertical and horizontal components of collimation error and binocular disparity versus vertical eye position in the pupil, for a symmetric transmission continuous lens system with $\phi = 40^{\circ}$.

II. Parametric Analysis

C. Results of the Study

6. VARIATION OF COMA

Although transmission systems have from 1.5 to 2.5 times less coma than reflection systems with the same off-axis angle, their coma variation across the FOV is larger; therefore, it may be easier to correct the reflection systems by using a tilted plate in the relay lens.

We have seen that the binocular disparity and collimation error observed in the holographic lens imaging process derive primarily from coma introduced by the continuous lens hologram. Therefore, if the relay lens is able to compensate for this coma, the desired performance can be obtained. In fact, a tilted plate produces coma in a nonparallel light cone.[12] Since the amount of coma introduced in this way will be approximately constant over the FOV, we can estimate the degree of correction available by examining the variation of coma at different points in the angular FOV.

The amount of axial coma in reflection systems with minimized astigmatism, as a function of the off-axis angle ϕ, is shown in Fig. 26. The variation across the vertical field is substantial and is shown in Fig. 27 for the particular case $\phi = 40^{\circ}$. The variation across the horizontal field is small, and will therefore not be considered. The dashed line in Fig. 27 indicates the amount of coma that would be removed by the correcting relay lens. The residual coma is about ± 0.3 mm, or about 0.8 mrad for a focal length of 360 mm. Thus, a 40° reflection system with specified performance appears possible, pending further analysis.

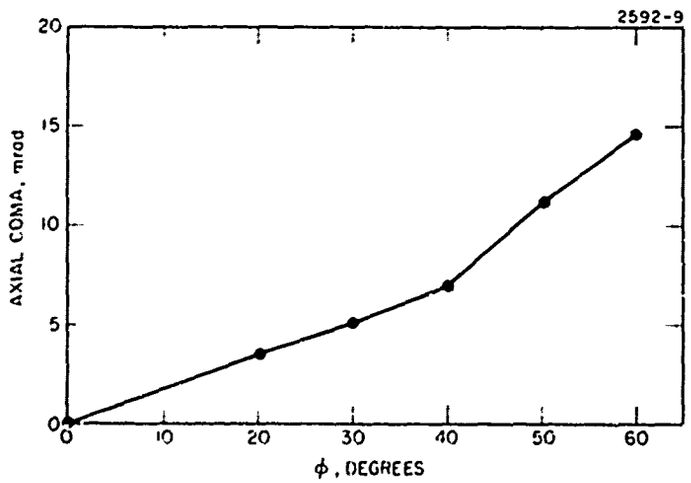

Fig. 26.
Axial coma for reflection continuous lens systems with astigmatism corrected across the field during hologram construction, as a function of off-axis angle.

The amount of coma for transmission systems is indicated in Fig. 28, for systems with and without minimization of astigmatism. In Fig. 28, the solid data point gives the average amount of coma, and the vertical bars indicate the variation of the amount of coma for different points in the vertical FOV. Note that systems with minimized astigmatism have more coma, and a larger variation across the vertical FOV, than unoptimized systems. These results indicate that, although the transmission systems have from 1.5 to 2.5 times less coma than the reflection systems with the same off-axis angle, it may be more difficult to correct the transmission systems, because of the larger variation across the FOV.

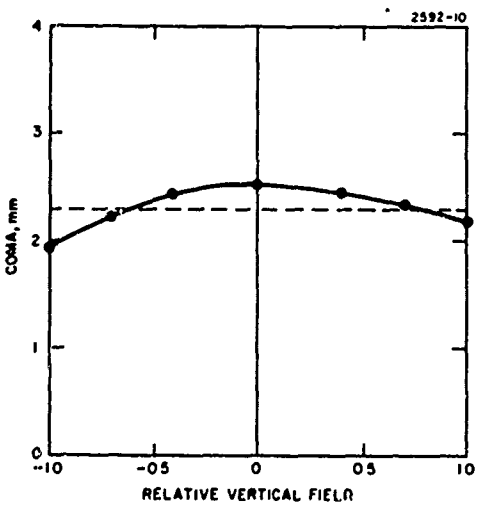

Fig. 27.
Variation of coma across the 25° vertical field for a reflection continuous lens system with $\phi = 40^{\circ}$ and $\psi = 5^{\circ}$. The dashed line indicates the amount of coma subtracted by the correcting relay lens.

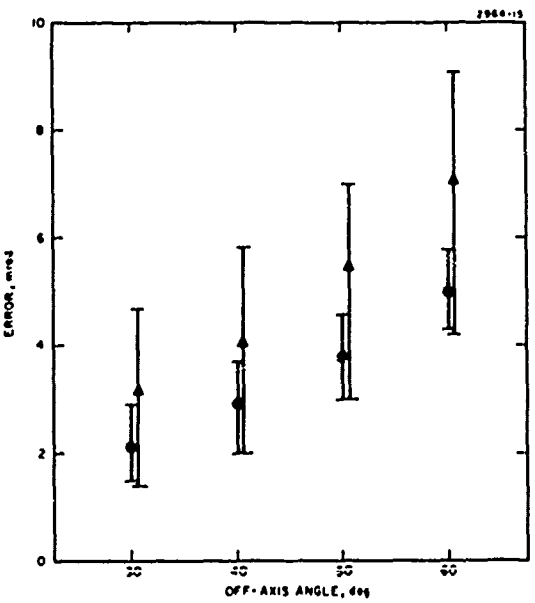

Fig. 28.
Variation of coma (vertical bars) for symmetric transmission continuous lens systems as a function of off-axis angle. Round points — without astigmatism correction during hologram construction; triangular points — with astigmatism correction.

II. Parametric Analysis

C. Results of the Study

7. SUMMARY AND CONCLUSIONS

Based on an overall consideration of the results of the parametric analysis study, and on the current state-of-the-art of hologram lens design and fabrication technology, we recommend a transmission configuration for the next phase of technology development; specifically, a symmetric transmission configuration with an off-axis angle of 50^{o} for the preliminary system design.

We made a detailed, parametric study of continuous lens type holographic optical elements that could be used in a HUD system. In particular, we studied transmission and reflection holograms that would provide both the collimating function and the combining function.

The holographic HUD lenses demonstrate a rather complex focal surface structure, which in general has astigmatism, tilts and field curvature. Astigmatic construction beams can be used to modify the tilts and the astigmatism across the angular FOV, but problems in maintaining desirable optical efficiency characteristics will, in general, require some correction of astigmatism in the relay lens and the choice of an asymmetrical configuration to modify the field tilts. Field curvature in the focal surfaces can be compensated in the relay lens by generating an intermediate image that conforms to the focal surfaces. Although not considered in this study, the curvature of the hologram substrate can also be used to control the image characteristics.

The unidirectional relationship between an intermediate image coordinate and the corresponding field angle is more nearly linear for the reflection systems than for the transmission systems. However, there are vertical/horizontal differences whose compensation in general requires an anamorphic relay lens, with tilted object/image surfaces. These complex distortions tend to be simpler in the reflection systems, but easier to correct in the transmission systems.

The analysis of pupil errors, using the ray intercept curve approach, shows that the major aberration is coma (discounting focus errors). The magnitude of the coma produces binocular disparity and collimation errors that are several times larger than the system goals. An average amount of coma can be compensated by tilted surfaces in the relay lens, so that the pupil errors can be greatly reduced, provided that a suitable set of focal surfaces can be designed such that the variation of coma across the FOV is limited.

Except for the variation of coma across the angular FOV, in systems with astigmatism minimized across the angular FOV, the overall image quality and efficiency characteristics are better for transmission systems than for corresponding reflection systems. Since the transmission systems also provide a simpler cockpit configuration and are easier to fabricate in practice, we recommend a transmission system for the next stage of technology development. In particular, the symmetric transmission continuous lens is chosen for the preliminary system design. The final choice of configuration for the system should be made only after further technology development and assessment of the complex design requirements, which involves many tradeoffs and includes human factors as well as purely technical considerations.

The general conclusion is that either a reflection or a transmission geometry could be designed that would meet the system specifications, provided that a thorough unified design procedure is followed, utilizing ordinary, refractive optical elements both in the hologram construction beams and in a complex, correcting relay lens.

III. Preliminary System Design

1. PARAXIAL RELATIONSHIPS

Fundamental system requirements for uniform brightness across the FOV, limited length, and exit pupil size restrict the practical range of hologram focal length to 11.25 in. < f_H < 14.4 in.; equivalently, the basic relay lens magnification is restricted to the range 1.25 < m < 1.6.

In this section we develop the basic relationships that control the use of a relay lens to produce an intermediate image of the scanner diffusing screen. These relationships are based on the wide-field, continuous lens design approach of Section II-A-5 and the simple lens equation, i.e., paraxial optics;[13] they determine the basic characteristics of the relay lens (focal length and aperture size) and the length of the system.

The system to be considered is illustrated in Fig. 29, which indicates the cone of light coming from the axial object point, through the relay lens to the intermediate image and on to the transmission hologram, and finally collimated by the hologram and sent through the system exit pupil. From the geometry of this cone of light, it is evident that the aperture size of the relay lens determines the size of the system exit pupil. Of course, this relay lens optical system could be folded with mirrors without changing its function or basic configuration.

In order to maintain image brightness across the angular FOV, the relay lens exit pupil must be located at the image of the system exit pupil, formed by the hologram. Since one of the hologram construction point sources is located at the center of the system exit pupil, 25 in. from the hologram, the relay lens exit pupil (or aperture, for the thin lens indicated in Fig. 29) must be located at the position of the other hologram construction point source. The distance of the relay lens from the hologram, Q, is, therefore, the distance d_2 of Section II-A-5, and is related to the hologram focal length f_H, by $1/Q = 1/f_H - 1/25$ (distances expressed in inches). Therefore, once the hologram focal length is chosen, the position of the relay lens is established.

The basic magnification of the relay lens is determined by the hologram focal length and the system focal length of 9 in. by the equation $m = f_H/9$ (see Section II-A-5). With the magnification and intermediate image location relative to the relay lens known, the relay lens focal length is given by the lens equation as $f_R = (Q - f_H)/(m + 1)$. For a maximum exit pupil dimension of 5 in. the relay lens aperture (exit pupil diameter) is determined from Fig. 29 by similar triangles to be

$$f_R 5(m + 1)/(9m) \qquad (4)$$

so that the relay lens f/no. is $9m/5(m + 1)$. The length of the system from the hologram to the input source is obtained by adding the relay lens object distance to the distance Q:

$$L = Q + (1 + 1/m)\, f_R \qquad (5)$$

This assumes a thin lens; with a thick lens, the distance L is increased by the distance between the principal planes of the lens.

The three important quantities that are tied together by these paraxial relationships are the hologram focal length (equivalent to the basic relay lens magnification), the relay lens f/no. and the length measure L. In Fig. 30, the f/no. and length are plotted as functions of the hologram focal length. Restrictions on acceptable ranges of f/no. and length determine the limits of allowable magnification (hologram focal length). Relay lens design feasibility requires that the f/no. be larger than about 1.0, giving $m > 1.25$. Length is restricted by practical cockpit configurations, and if $L < 46$ in., $m < 1.6$. Therefore, $1.25 < m < 1.6$ (or 11.25 in. $< f_H <$ 14.4 in.).

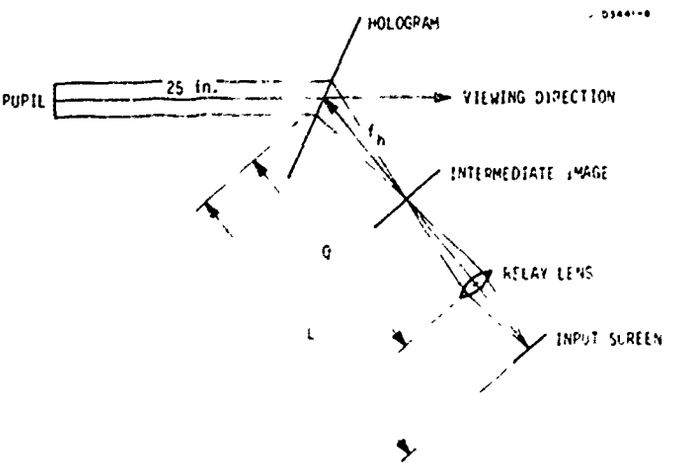

Fig. 29.
Vertical section of a HUD system.

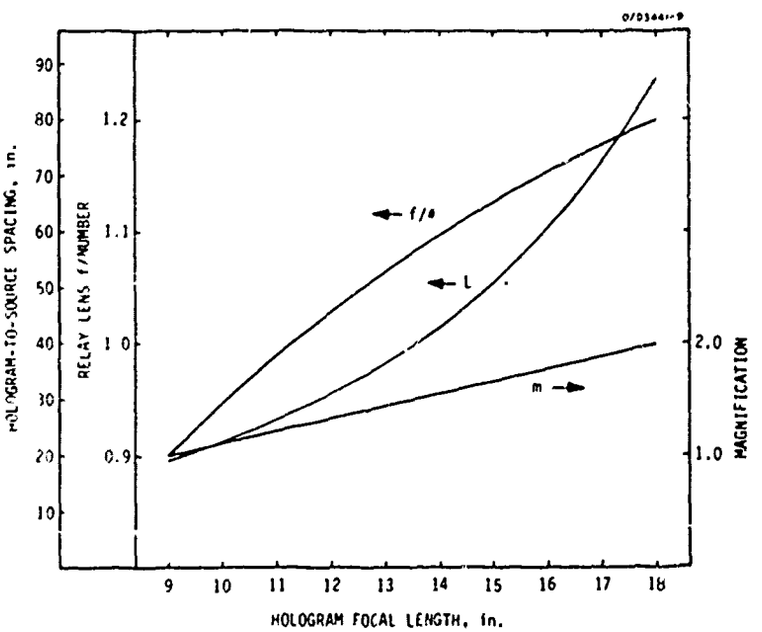

Fig. 30.
Variation of system parameters with hologram focal length.

III. Preliminary System Design

2. TILTED IMAGE PLANES

Tilted object/image planes are used in the HUD system to match the hologram distortion and intermediate image characteristics; in order to calculate the degree of matching achieved, we provide several paraxial imaging relationships for the tilted object/image situation.

The distortion and intermediate image characteristics of the hologram (see Sections II-B-4 and II-C-1, and Sections II-B-6 and II-C-3) require the use of tilted object and image in the relay lens optical system, as illustrated in Fig. 31. In this section we provide the paraxial relationships that describe this situation.

The relay lens optical system from Fig. 31 is redrawn in Fig. 32 with the necessary geometry for the calculation. A thin lens is shown, but the paraxial object/image relationships are unchanged for a thick lens. In Fig. 32, the object height, tilted by an angle Ω, is y_o, and the corresponding image height, tilted by an angle Ψ, is y_i. The height in the front and back focal planes is y and y', respectively. The spacing of the object from the front focal plane is x, and the spacing of the image from the back focal plane is -x'. The distances x and -x' are shown in Fig. 32 for the axial object and image points. The relay lens focal length is f_R. (Note that the use of the angles Ω and Ψ is different than for previous discussions of the hologram characteristics).

The basic paraxial lens imaging equation is[13]

$$xx' = -f_R^2 \quad . \tag{6}$$

The tilt angles are related by

$$\tan \Psi = m_o \tan \Omega, \tag{7}$$

where m_o is the axial magnification. The untilted image height is related to the untilted object height by

$$y' = my \quad , \tag{8}$$

where m is the magnification, given by

$$m = f_R/x = -x'/f_R \quad . \tag{9}$$

This equation, combined with the geometry of Fig. 31(b) then gives

$$-x' = f_R^2/(x_o + y_o \sin \Omega) \quad , \tag{10}$$

where x_o is the axial object spacing from the front focal plane. We can then use $m = -x'/f_R$ to obtain

$$y' = my = my_o \cos \Omega, \tag{11}$$

and finally get the tilted image height from

$$y_i = \sqrt{(-x')^2 + (y')^2} \quad . \tag{12}$$

These relationships can now be used to calculate the degree of distortion compensation in a particular relay lens/hologram configuration.

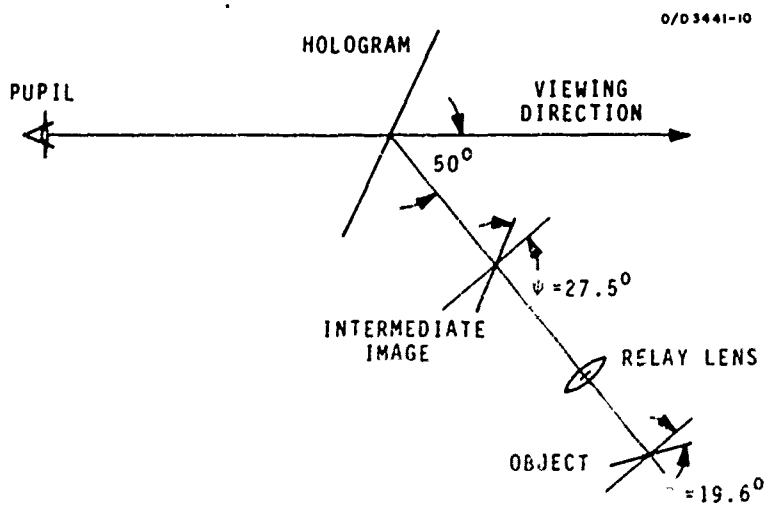

Fig. 31. Vertical section of a HUD system, showing typical tilted object/image geometry in the relay lens optical system.

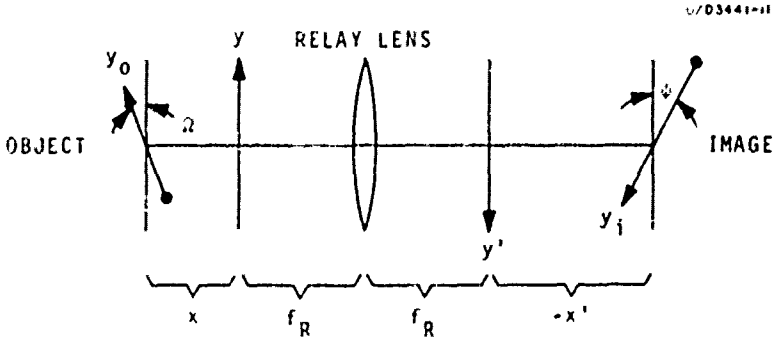

Fig. 32. Vertical section of a typical relay lens optical system, showing the coordinates used for paraxial calculations.

III. Preliminary System Design

3. APPROACH TO RELAY LENS DESIGN

The paraxial relay lens is designed, using the basic paraxial relationships, to match the intermediate image tilt angle and the axial vertical-to-horizontal magnification ratio of the hologram.

In order to apply the paraxial imaging relationships of the last section to a specific HUD system, we must provide an approach to relay lens design that takes into account the difference between the horizontal and vertical imaging characteristics of the hologram, which were described in Sections II-B-6 and II-C-3. As an input, we are given the intermediate image tilt angle and distortion information in the form of the vertical-to-horizontal magnification ratio desired in the relay lens, R. Then, using the paraxial relationships of Section III-1, we first set the horizontal relay lens magnification m_h from the equation

$$m_h = f_H/9 \, . \tag{13}$$

Then, the relay lens horizontal focal length is determined by the equation

$$f_{Rh} = \frac{Q - f_H}{m_h + 1} \, . \tag{14}$$

In the vertical plane, the axial magnification is determined by eq. (13) and the axial vertical-to-horizontal magnification ratio R_o from the distortion data:

$$m_{vo} = R_o m_h \, . \tag{15}$$

The relay lens vertical focal length f_{Rv}, must be determined from a thick relay lens design, because a thin lens cannot have different magnification/focal length combinations in the horizontal and vertical sections, and still have a single location. A detailed study of the thick lens characteristics is beyond the scope of this study; a good approximation is that the spacing between the principal planes remains constant, but the location is shifted, so that the object-to-image spacing is the same in both directions. Then the vertical focal length is

$$f_{Rv} = f_{Rh} \frac{2 + m_h + 1/m_h}{2 + m_{vo} + 1/m_{vo}} \, . \tag{16}$$

Finally, the object (scanner diffusing screen) tilt angle Ω is determined from the intermediate image tilt angle Ψ by

$$\tan \Omega = \frac{\tan \Psi}{m_{vo}} \quad . \tag{17}$$

The paraxial relay lens optical system is now completely specified, and we can proceed to calculate the overall distortion characteristics of the HUD system. This approach to relay lens design can be extended in a straightforward way to include situations where there is astigmatism and two different tilt angles in the intermediate image.

III. Preliminary System Design

4. PARAXIAL CALCULATION OF DISTORTION COMPENSATION

The degree of compensation of distortion can be calculated for a particular configuration; for a 50° off-axis angle, symmetric, transmission hologram, excellent distortion compensation is achieved for a hologram focal length of about 13.5 in.

The relay lens is designed to provide an intermediate image that is in focus, i.e., lies on the hologram focal surface (neglecting higher order effects such as field curvature, which can be provided in the detailed relay lens design). Furthermore, there is no anamorphic distortion in the center of the FOV. The remaining paraxial question to be answered is then to what extent the overall system distortion is minimized, as a function of location in the FOV. This question can be answered by calculating the vertical-to-horizontal magnification ratio of the relay lens, and then comparing this ratio with that required to compensate the distortion introduced by the hologram. This calculation must be made for a specific system.

In Section II-C-7, we chose a transmission hologram HUD configuration with an off-axis angle $\phi = 50^{\circ}$ for the specific preliminary system design. The magnification ratio required for undistorted imagery in a $\phi = 50^{\circ}$, transmission hologram with a focal length $f_H = 14.4$ in. was shown as curve C in Fig. 22 (Section II-C-3). This data is reproduced as the solid curve in Fig. 32(a).

Similar data can be obtained for the corresponding relay lens by obtaining the actual intermediate image height for a particular point in the vertical FOV, from the hologram focal surface information. With this, the paraxial tilted object/image relationships of Section III-2 are used to calculate the corresponding tilted object height and, therefore, the vertical magnification at this particular point. Finally, this relay lens vertical magnification is divided by the (constant) horizontal relay lens magnification to obtain the magnification ratio at this vertical FOV. The resulting ratios are plotted as the circled data points in Fig. 33(a). These curves show that the appropriate relay lens for the $f_H = 14.4$ in. ($m_h = 1.60$) system slightly undercorrects for the keystone distortion introduced by the hologram.

Similar calculations for a HUD system with $f_H = 11.7$ in. ($m_h = 1.30$) provide the results plotted in Fig. 33(b). In this case, the appropriate relay lens substantially overcompensates for the hologram's keystone distortion. It is apparent that the keystone distortion is essentially exactly compensated for some hologram focal length in the range 11.7 in. $< f_H <$ 14.4 in. ($1.3 < m_h < 1.6$). In fact, the minimum distortion case is probably very close to $m_h = 1.5$ ($f_H = 13.5$ in.) This particular case is therefore suggested for the next phase of development.

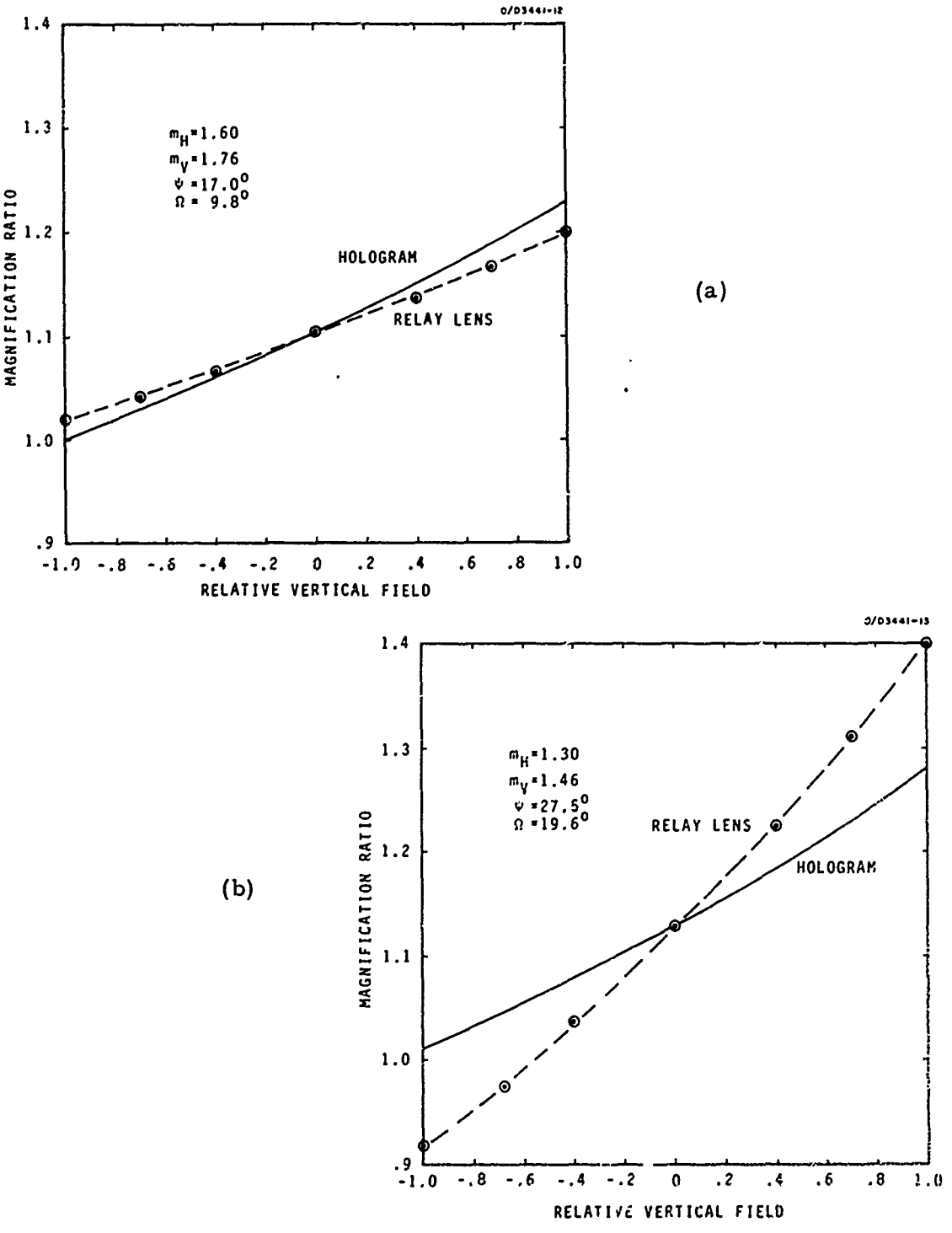

Fig. 33. Vertical-to-horizontal magnification ratios for $\phi = 50^{\circ}$, transmission HUD systems as a function of relative vertical field angle (total field of view is 25°). The solid lines show the ratios required to achieve circular images at infinity for circular inputs. Circled data points show the ratios provided by the particular relay lens systems. (a) Hologram focal length is 14.4 in., (b) hologram focal length is 11.7 in.

III. Preliminary System Design

5. RECOMMENDED SYSTEM

The recommended system, using a 50° off-axis, symmetric transmission holographic HUD element, offers many advantages for the next phase of system and technology development, regardless of what configuration is chosen for the final system.

Based on the results of the parametric study and preliminary system design work, we have recommended a symmetric, transmission hologram, with an off-axis angle of 50°, for the next stage of system and technology development. There are several advantages for this system, primarily related to the fact that hologram optics technology, in general, and particularly the use of large aperture elements, is in an early stage of development. The major advantages of the recommended system are: feasibility, relative ease of fabrication, and relatively simple design.

The recommended system offers the best configuration for the use of a correcting relay lens. The hologram is easier to fabricate because the requirements for large area fringe stability and large area material thickness uniformity are relatively low, compared to reflection holograms. The distortion characteristics are relatively easy to correct and the aberrations are low enough to pose minimal design problems.

There is one apparent systems difficulty with the recommended configuration: the presence of strong dispersion in the element leads to considerable light spreading, producing spectral flares that are visually uncomfortable and distracting. These flares are caused by light (e.g., sunlight) diffracted by the hologram. Even though the Bragg condition is strongly violated and the diffraction is relatively very weak, the flares can be a problem with strong illumination sources.

It is not clear at this point, because of this problem of dispersion, whether or not the recommended, or a modified, transmission configuration will be usable in an aircraft environment. It is clear that even more advanced design and fabrication technology will be required to achieve an alternate system. Hughes Aircraft Company is very interested in developing this technology, and is currently engaged in answering these questions, using Company funding. It is believed that the experience of advanced development by NADC of the recommended (transmission) system will provide extensive insight into the considerations involved with any configuration, as well as the design tools and carry-over technology that are a major requirement for successful development of the final system. The experience, equipment, and technology provided by the next stage of development will apply to whatever configuration is ultimately chosen, because of the similarity in imaging characteristics.

CHARACTERISTICS OF THE RECOMMENDED SYSTEM

- Hologram configuration . . . . . Symmetric transmission, 50° off-axis angle.

- System optical parameters
  Hologram focal length . . . . . 13.5 in.

  Relay lens basic focal length. . . 6.3 in.

  Relay lens f/no. 1.1

  Unfolded length. . . . . 40 in.

- Equipment, system design effort, and hologram fabrication techniques are applicable to any final configuration.

IV. Red-Sensitive Recording Materials Development

1. CHOICE OF A HOLOGRAM RECORDING MATERIAL

Dye sensitized dichromated gelatin was selected as the best hologram recording material, and after optimization, collectively it has the highest diffraction efficiency, largest index modulation, and best red light sensitivity of any holographic material known.

The HUD holographic lens system requires a holographic recording material that can satisfy the criteria imposed by the optical design. At the beginning of this program we made a survey of all holographic materials and assessed their properties to identify potential materials candidates. Table 10 shows the major requirements and compares holographic materials characteristics. We also considered the qualities of:

- permanence
- resolution
- environmental endurance
- optical quality
- lack of noise.

Our conclusion was that the gelatin systems offer the best compromise in characteristics, and we concentrated on the optimization of dye-sensitized dichromated gelatin (DSDCG). The last two entries in Table 10 show the properties of DSDCG at the beginning of the present program and at the end of the program following materials optimization. It is evident that DSDCG's properties have been considerably improved and that DSDCG is still the best material to use in the Hologram Lens System (HLS).

Optical cement[14] was dropped from consideration because it cannot generate the required index modulation and because it requires excessively large exposures. We also conducted some research on bleached silver emulsions and were able to eliminate the image instability problem due to printout;[15] however, scatter levels are still high enough to disqualify this material from application to the HLS.

TABLE 10

Phase Holographic Materials and Properties

Material Type	Index Modulation	Diffraction Efficiency (%)	Typical Exposure (mJ/cm^2)	Sensitivity at 632.8 nm wavelength
HLS Requirements:	> 0.0127	> 80	< 200	Yes
1. Photopolymers				
a. Ba Acrylate	0.01	45	0.6	Yes
b. Optical Cement	0.0055	98	8200	Yes
c. Dye Sensitized Photoresist	---	10	10000	Yes
2. Direct Optical Effect Materials				
a. Lithium Niobate	0.00004	40	10^5	---
b. Arsenic Sulfur Glass	---	18	9000	---
3. Gelatin Systems				
a. Bleached Silver Halide Emulsions	0.033	75	0.11	Yes
b. Dye-Alcohol Sensitized Gelatin	---	---	---	Yes
c. Dichromated Gelatin	0.027	> 90	30	No
d. Dye Sensitized Dichromated Gelatin (beginning of program)	0.020	> 59	2000	Yes
e. Dye Sensitized Dichromated Gelatin (end of program)	0.022	> 85	600	Yes

T1381

IV. Red-Sensitive Recording Materials Development

2. RELIEF AND VOLUME IMAGES IN DICHROMATED GELATIN

Dichromated gelatin has been investigated for several decades, but since the holographic image is a film volume effect, the early studies are not directly applicable.

Dichromated gelatin (DCG) has been used for numerous photolithographic processes and color printing methods since its discovery in 1830.[16] The dichromate ion, when irradiated with blue or green light, becomes susceptible to reduction in certain colloid films, such as gelatin. The reduction products cross-link individual colloid molecules, thereby changing their physical and chemical properties. The essential mechanism of image formation in the early reproduction processes is shown in Fig. 34. The gelatin film areas, that are not illuminated with actinic radiation, remain water-soluble and are washed away subsequent to exposure.[17] Exposed film areas are insolubilized by the photochemical reaction and remain on the substrate material. This type of relief image has been used to record two-dimensional holographic images,[18] but the diffraction efficiency of these gratings is generally restricted to less than 33.9%.[19]

DCG is also capable of recording three-dimensional phase images,[20] and this mechanism is schematically shown in Fig. 35. Prior to exposure the film is crosslinked to the extent that it will not dissolve in the unexposed areas during the development steps. Following exposure, the film is first swelled with water and then dehydrated in an alcohol, such as 2-propanol. This treatment results in differences of index of refraction between the exposed and unexposed portions of the film. Such a dielectric grating can produce diffraction efficiencies approaching the theoretical 100% maximum.[19]

Within the past century a considerable amount of empirical knowledge has been accumulated on the formation of relief images in DCG.[21] However, this technology is not directly applicable to phase image formation, since the mechanisms of image formation are quite different in the two- and three-dimensional holographic gratings. Confirming this belief, in our DSDCG optimization work we found few realizable film response improvement ideas in previous literature.

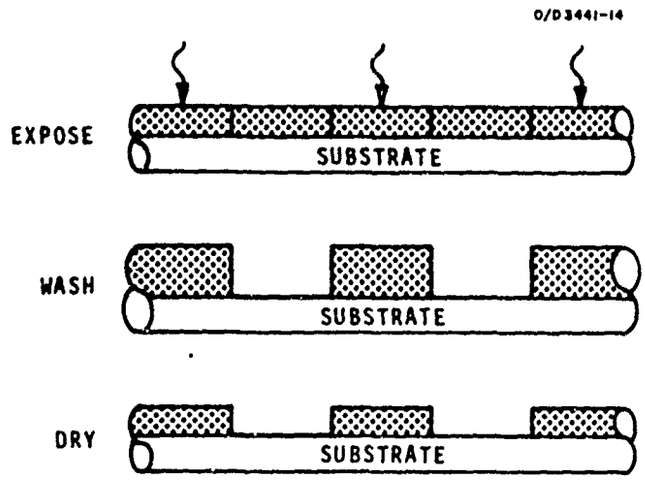

Fig. 34. Schematic illustration of the old, etching process with soft dichromated gelatin.

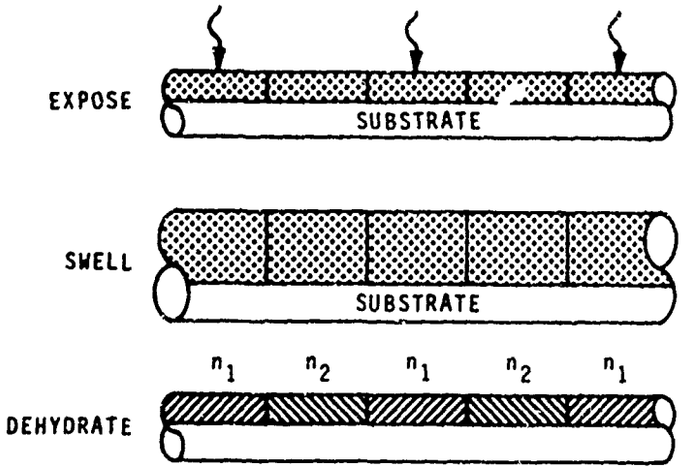

Fig. 35. Schematic illustration of the process of forming phase images in hardened dichromated gelatin.

IV. Red-Sensitive Recording Materials Development

3. DYE-SENSITIZED DICHROMATED GELATIN

The spectral response of dichromated gelatin can be made panchromatic by the addition of photoreducible dyes.

The practical spectral sensitivity for DCG is limited to wavelength less than 550.0 nm.[22] If, however, a photoreducible dye is incorporated into a dichromated gelatin film, the spectral sensitivity becomes panchromatic. Both relief images[23-25] and holographic volume phase gratings[26] have been recorded in DSDCG. Figure 36 shows the relative absorption spectra of the dichromate ion and two spectrally sensitizing dyes. The methylene green dye has two broad absorption bands that permit effective sensitization in the 500 to 690 nm wavelength range.

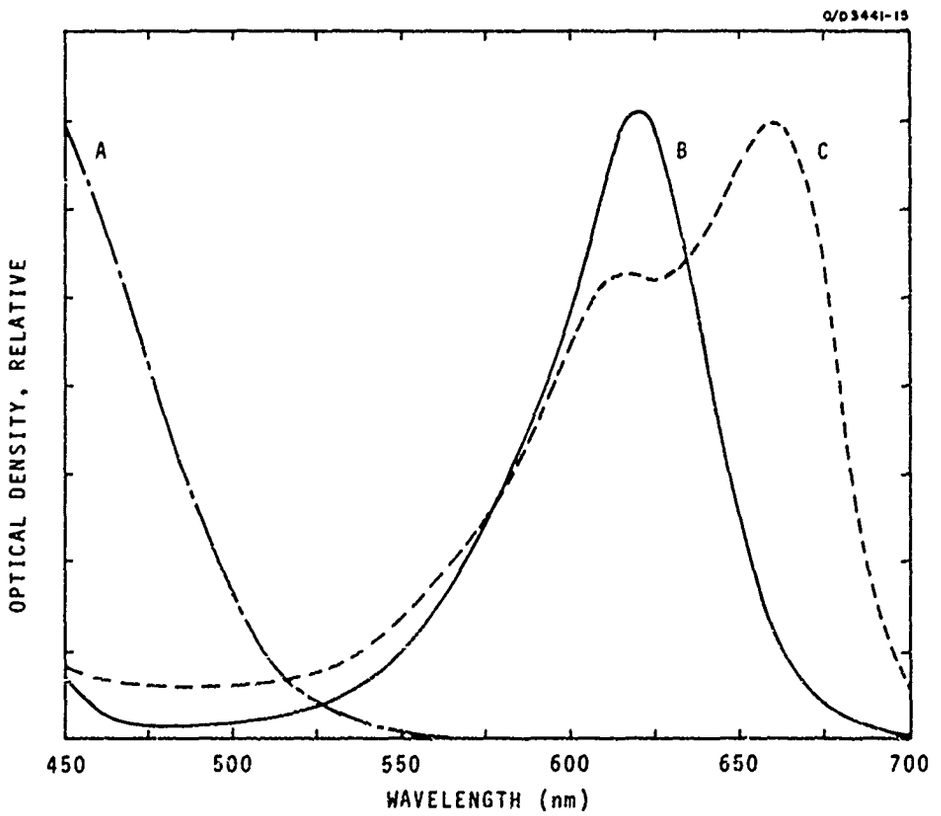

Fig. 36. Relative absorption spectra of A - dichromate ion, B - guinea green dye, and C - methylene green dye.

The photochemical mechanism by which DCG becomes crosslinked is poorly understood,[27] and the image formation mechanism of DSDCG appears to be even more complex. Figure 37 shows the basic postulated chemical mechanism whereby a dye absorbs an actinic photon and is photoreduced by a reducing agent.[28] The reduced dye then reduces the dichromate from a valence of 6 to 3, and crosslinks are formed by the lower valence chromium compound between individual gelatin molecules. This chemical system must be stable in the dark, so that neither the dye nor the reducing agent can be oxidized by dichromate without light activation.

The mechanism by which a strong phase image is formed in the film is also a controversial issue. Some investigators feel that cracks are formed in the gelatin,[20] while others believe that a chemical complex is formed around the crosslinks by the alcohol in the developing solution.[27] We believe that both theories are partially correct, each applying to some extent, depending on the condition of the film and development technique.

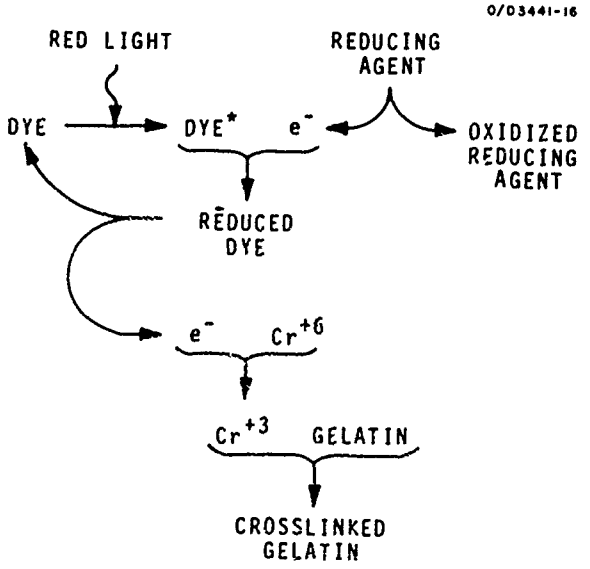

Fig. 37.
Postulated chemical mechanism for the photoreduction of chromium VI.

IV. Red-Sensitive Recording Materials Development

4. SPECTRALLY SENSITIZING DYES FOR DSDCG

Our survey of many dyes revealed that the thiazine and triphenylmethane dyes are the best spectral sensitizers for DSDCG.

Previous literature on DSDCG reveals that suggested sensitizing dyes are from the xanthene, thiazine, and triphenylmethane dye families.[22-26] To determine whether other dye types are spectral sensitizers and to find which dyes form the most sensitive film layers, we examined over 120 dyes for the DSDCG system.

For a dye to act as a red light sensitizer for DCG, it must possess the following properties:

- Water solubility
- Red light absorption
- Photoreducibility
- Compatability with the dichromate ion

Since it is difficult to tell on an a priori basis whether a dye possesses the above characteristics, we first qualitatively examined the dyes for water solubility and red light absorption. Those dyes that possessed both of these characteristics were then incorporated into the dichromate sensitizing solution and tested for red light sensitivity.

Table 11 shows all of the dyes that we found capable of forming phase images in DSDCG. The dyes have been arranged in decreasing order of film sensitivity, subjectively determined by the diffraction efficiency resulting from Ronchi ruling image exposures.

The dyes showing good sensitivity generally belong to either the thiazine or triphenylmethane dye families, confirming the findings of previous investigators. The xanthene dyes were not effective photosensitizers at 632.8 nm since they typically do not exhibit red light absorption.

In the category of dyes showing marginal sensitivity, there may be some dyes that can harden gelatin without the presence of dichromate. Such hardening dyes have been previously reported,[29] but since their sensitivity was found to be so low, they were not further considered for the present application.

TABLE 11

Sensitizing Dyes for Red Sensitive Dichromated Gelatin.
The dyes are listed in a decreasing order of film sensitivity.

	Dye Name	Manufacturer*
A.	Dyes Showing Good Sensitivity	
1)	Azure B	A
2)	Azure A	ALD.
3)	Methylene Green	A
4)	Azure C	A
5)	Toluidine Blue 0	E
6)	Basic Black KMPA	GD
7)	Guinea Green	MCB
8)	Crystal Violet	MCB
9)	Acid Fast Violet BG Concentrate	A
10)	Malachite Green	MCB
11)	Light Green SF Yellowish	MCB
12)	Brilliant Green	MCB
B.	Dyes Showing Fair Sensitivity	
1)	Methyl Violet 2B	MCB
2)	Alphazurine 2G (Patent Blue V)	A
3)	Aniline Blue	MCB
4)	Acid Blue 3	MCB
5)	New Methylene Blue N	B
6)	3', 3''-Dichlorophenolsulfonephthalein Na salt	E
C.	Dyes Showing Marginal Sensitivity	
1)	FD&C Blue No. 2	A
2)	Methylene Blue	MCB
3)	3', 3''-Diethyl-9-methylthiacarbocyanine iodide	E
4)	New Solid Green 3B	MCB
5)	Nigrosine ESB Extra (Acid Black 2)	GD
6)	Ahcoquinone Brilliant Cyanine Green 5GX	ICI
7)	D&C Black No. 1 (Naphthol Blue Black)	A
8)	Indigotetrasulfonic acid, K salt	ALD
9)	Acid Blue (Acid Blue 48)	HS
10)	Calcocid Ink Blue R	ACC
11)	Helvetia Blue Extra High Concentrate	GC
12)	Cryptocyanine	B

A = Allied Chemical Co.	GC = Geigy Chemical Corp.
ALD = Aldrich Chemical Co.	GD = General Dyestuff Co.
ACC = American Cyanamid Co.	HS = Holland — Suco Color Co.
B = J.T. Baker Chemical Co.	ICI = ICI Organics, Inc.
E = Eastman Organic Chemicals	MCB = Matheson Coleman and Bell

T1383

IV. Red-Sensitive Recording Materials Development

5. CHOICE OF A SPECTRALLY SENSITIZING DYE

The selection of a spectral sensitizer for DCG is constrained by both the dye-dichromate solubility product and the dye quantum efficiency.

To choose the best sensitizing dye for DSDCG, we measured the relative quantum efficiencies for the dyes by assessing the amount of light absorbed in a sensitized film and comparing this value to the resulting index modulation in the developed plate. Table 12 shows the relative quantum efficiencies of the most sensitive dyes tested.

A complicating factor is that many of the dyes precipitate in dichromate solution, and this precipitation follows a solubility product relationship.[30] The low solubility products for the five most efficient dyes preclude their use in DSDCG, because in the dichromate concentrations normally employed (~0.2 to 0.7 M), only very small dye concentrations can be used, and the sensitized layer can absorb only a small fraction of the actinic radiation.

It is possible, however, to use a mixture of dyes: first employing the most efficient dye to its maximum dichromate concentration; then adding the next most efficient dye, and so on until the desired film absorption is reached. The dyes listed in Table 12 belong to either the thiazine or triphenylmethane dye families, and the chemical structures of dyes within a family are very similar, usually differing by only a few functional groups. Therefore, the maximum solubility products are not attainable if mixtures of dyes from the same family are used. For example, in a 1 molar ammonium dichromate solution, 1.2×10^{-6} molar azure B dye can be dissolved, but if azure A is added, dye precipitation will begin before its concentration rises to 2.0×10^{-6} molar because of the presence of azure B.

We found that the most sensitive film could be obtained by taking the dye whose quantum efficiency multiplied by its solubility product is the largest number. This dye is methylene green of the thiazine family. Then we added the most efficient triphenylmethane dye (guinea green) to achieve the desired light absorption in the film.

TABLE 12

Most Sensitive Spectrally Sensitizing Dyes for Dichromated Gelatin

Dye Name	Relative Quantum Efficiency*	Dichromate Solubility Product**
1) Azure B	100	1.2×10^{-6}
2) Azure A	99	2.0×10^{-6}
3) Methylene Green	93	3.2×10^{-6}
4) Azure C	83	2.1×10^{-6}
5) Toluidine Blue 0	74	2.7×10^{-6}
6) Basic Black KMPA	62	
7) Guinea Green	56	$> 10^{-4}$
8) Crystal Violet	54	3.3×10^{-6}
9) Acid Fast Violet BG Conc.	48	$> 10^{-4}$
10) Malachite Green	48	1.5×10^{-5}
11) Light Green SF Yellowish	42	$> 10^{-4}$
12) Brilliant Green	26	1.9×10^{-5}

*Relative quantum efficiency was measured as the amount of index modulation produced after development as a function of light absorbed in the film.

**[dye] $[(NH4)_2\ Cr_2O_7]$, moles^2/liter^2 at the point of dye precipitation from solution.

T1382

IV. Red-Sensitive Recording Materials Development

6. IMPROVEMENT OF DYE SOLUBILITY IN DICHROMATE SOLUTION

Methylene green dye is the best spectral sensitizer for DSDCG, but only if it is added in solid form to the sensitizing solution.

As indicated in the previous section, it would be desirable to improve the solubility of the efficient thiazine dyes in dichromate solution. We explored a variety of methods for solubility improvements: (1) variation of pH in the sensitizing solution, (2) incorporation of the dye in the gelatin film before dichromate solution application, and (3) use of chelating agents, such as triethanolamine, in the sensitizing solution. No substantial improvement in film light absorption was observed with these methods.

Some increase in the solubility product can be achieved by adding a surfactant to the sensitizing solution, as shown in Fig. 38. This approximate twofold increase in the solubility product, however, is not adequate for using methylene green solution in the DSDCG system.

A notable exception to the apparent solubility product constant was discovered when dry methylene green dye was added to a solution of ammonium dichromate: they dye dissolved slowly but retained its color without forming a precipitate. Methylene green is the only thiazine dye that possesses this characteristic. Not only does this dye retain its color when added to a dichromate solution, it is also stable for long periods of time.

The sensitizing solution is prepared by adding enough dry methylene green dye to the dichromate solution to form a saturated dye solution. By filtration, undissolved dye is removed, and once prepared, the sensitizing solution is usable for several hours. Sensitization of 12 μm thick gelatin layers results in films that absorb about 63% of incident 632.8 nm light.

Figure 39 shows that methylene green and methylene blue are identical in structure, except for the nitro group attached in the 1-position on methylene green. We believe that this polar nitro group is responsible for methylene green's unique behavior and makes this dye the most effective spectral sensitizer for DSDCG if it is added to the sensitizing solution in the solid state.

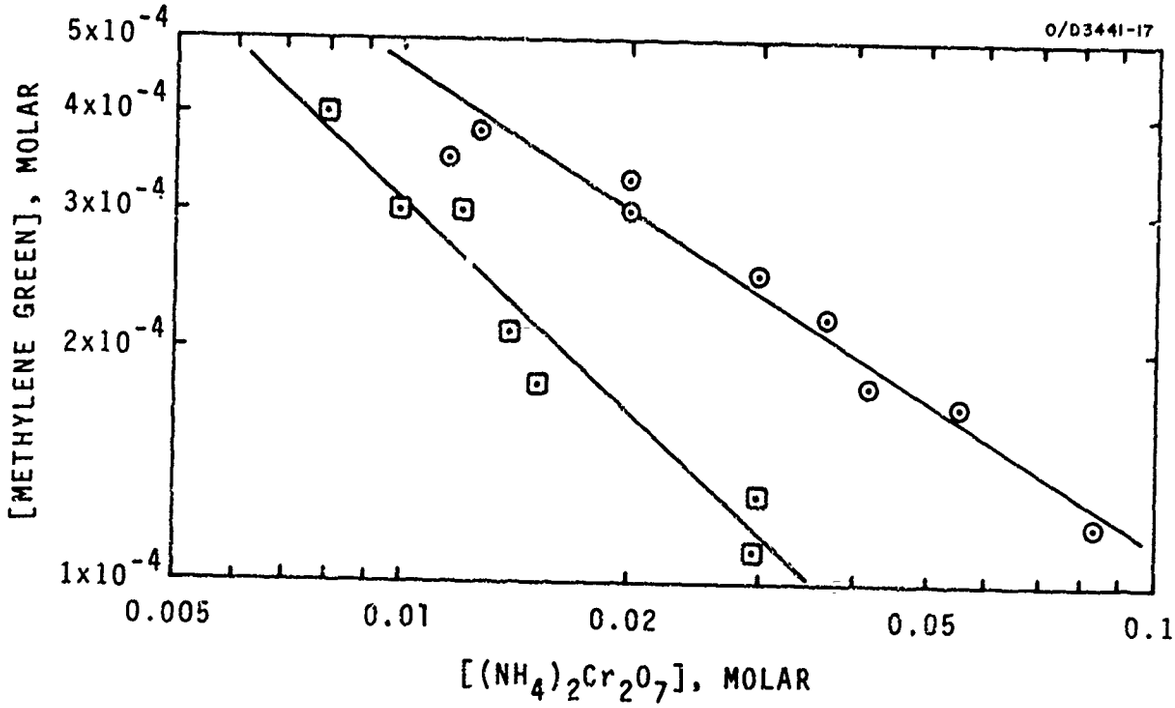

Fig. 38. Methylene green and ammonium dichromate concentrations at the point of dye precipitation. Circled data points — with 1 ml of Kodak Photo-Flo 200 per 100 ml of solution; boxed data points — without Photo-Flo.

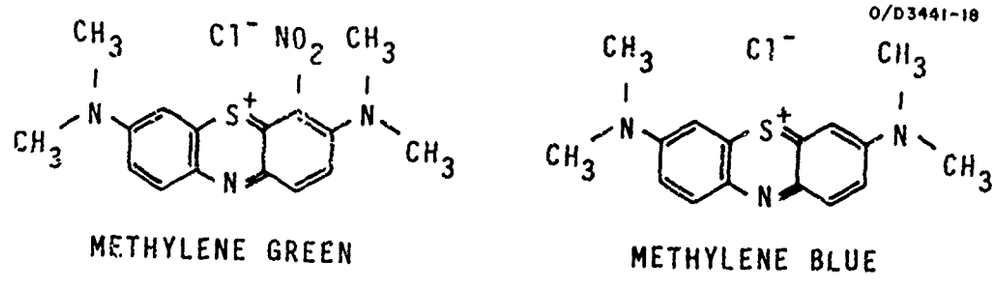

Fig. 39. Structure of two thiazene dyes used in DSDCG.

IV. Red-Sensitive Recording Materials Development

7. OPTIMIZATION OF SENSITIZING SOLUTION I

Film sensitivity is maximized when both ammonium dichromate and ammonium nitrate are used in high concentrations in the sensitizing solution.

The sensitivity of DCG films generally increases with the concentration of ammonium dichromate in the sensitizing solution.[22,31] As shown in Fig. 40, we found this also to be true in DSDCG. This implies that although the consecutive reaction rate equation may not have a simple form, the initial dichromate ion concentration does affect the rate law for this photochemical reaction.

The addition of small amounts of ammonium nitrate to DCG sensitizing solutions has been previously reported for improving film speed.[32] We found that large concentrations of NH_4NO_3 in the sensitizing solution can dramatically increase film speed. Figure 41 shows the sensitivity improvement derived from the use of NH_4NO_3 and NH_4 CNS. At high concentrations, NH_4NO_3 is a more effective film hypersensitizer than NH_4 CNS.

We believe that when NH_4NO_3 is added to the sensitizing solution, the nitrate ion forms a complex with the dichromate ion. This complex is relatively unstable,[33] and apparently it participates more effectively in the photochemical reaction than the dichromate ion by itself.

Since the film sensitivity improves with higher concentrations of both $(NH_4)_2 Cr_2O_7$ and NH_4NO_3, it may be reasoned that saturated solutions of both salts should be used. But, if the salt concentrations are too high, the salts will crystallize on the surface of the dry film, leaving it unsuitable for holographic exposures. We have found that a sensitizing solution containing 0.6 M $(NH_4) Cr_2O_7$ and 0.68 M NH_4NO_3 is a good compromise between film speed and optical quality of the dry film.

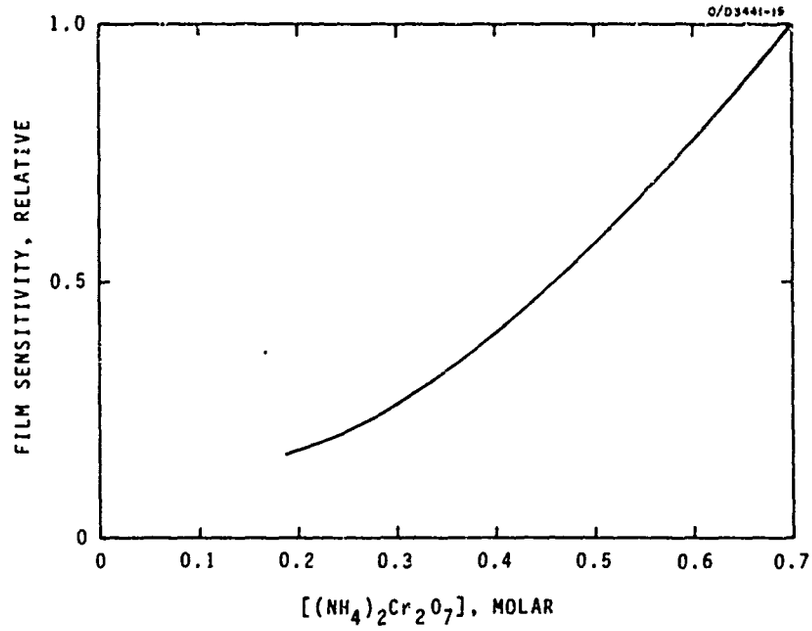

Fig. 40. Film sensitivity as a function of dichromate concentration in the sensitizing solution.

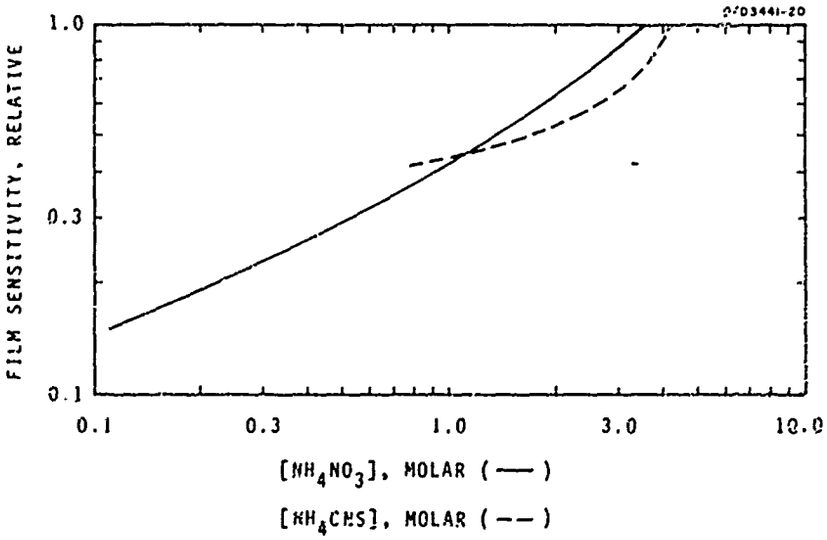

Fig. 41. Film sensitivity as a function of ammonium nitrate and ammonium thiocyanate concentrations in the sensitizing solution.

IV. Red-Sensitive Recording Materials Development

8. OPTIMIZATION OF SENSITIZING SOLUTION II

We explored several previously reported methods for DCG film sensitivity improvement, but DSDCG sensitivity augmentation was not realized.

The pH of the sensitizing solution is known to affect DCG film speed because of the equilibrial dependence of the acid chromate ion on hydrogen ion concentration. The acid chromate ion is believed to be the active light absorbing and crosslinking species in DCG films.[21] Our experiments, however, showed that the pH of the sensitizing solution was not an important factor in the pH range from 1 to 11 in DSDCG. Ammonium dichromate has a pH of about 5 in the concentration range of 0.01 to 1.2 molar, and no pH adjustment appears to be necessary in the sensitizing solutions.

The use of reducing agents in the sensitizing solution for DCG has been suggested by several previous investigators.[24,28,34] We tried various concentrations of pyridine, pyridine hydrochloride, hydroquinone, terephthalic acid, phloroglucinol, thiourea, and resorcinol in the sensitizing solution, but none of these substances showed measurable sensitivity improvement in DSDCG. It appears that a sufficient reducing agent is present on the gelatin functional groups to reduce the photoexcited dye, and additional reducing species are not required. Since the carboxyl functional group on gelatin is believed to be the primary crosslink site,[33] it is possible that as dichromate oxidizes gelatin, it also locally forms its crosslink attachments.

Numerous attempts have been made to increase DCG film sensitivity by the addition of soluble inorganic substances to the sensitizing solution.[21] Review literature reveals that the sensitivity improvement claims are often contradictory and controversial.[35]. Nevertheless, we tried to duplicate some of these previous methods:

- The use of soluble rare earth salts[36,37] that precipitate at a pH slightly above the pH of the sensitizing solution has been reported.[38] We employed lanthanum sulfate, neodymium chloride, and yttrium oxide, but no improvement in sensitivity was observed.

- Soluble nickel, copper, cobalt, and manganese salts[39-41] also failed to improve sensitivity.

- Phosphoric acid and sodium dihydrogen phosphate have also been suggested[42, 43] but no sensitivity improvement was gained.

- Magnesium chloride[42] did improve sensitivity, but it left the film highly scattering.

From these results we conclude that although these inorganic salts may improve the sensitivity of DCG, sensitivity improvement in DSDCG is not realizable without destroying the transparency of the gelatin film.

IV. Red-Sensitive Recording Materials Development

9. OPTIMIZATION OF DRYING TIME

The best drying time for the most sensitive DSDCG was empirically determined to be 15 minutes.

The optimum drying time to achieve maximum film sensitivity is a function of several different parameters, the most important of which are film moisture content and rate of the dark reaction.[21]

A gelatin layer derives its integrity from the equilibrium of two opposing forces: hydrolysis and molecular association. In a fully swollen gelatin layer hydrolysis is the dominant factor, and it forces individual gelatin molecules apart, breaking associative hydrogen bonds. In this gelatin state, cross-linking becomes difficult due to the physical separation of crosslink sites and the inability of relatively small crosslinking complexes to bridge this gap. Hence, it is not surprising that fully swollen DSDCG films show low light sensitivity. Figure 42 offers supporting evidence to this theory: if it can be assumed that the rate of dye fading in a sensitized film is a measure of the extent of the crosslinking reaction, the graph shows only a slight reaction in the first six minutes of exposure. As the film dries, the reaction rate approaches steady state after six minutes. On the other hand, completely dehydrated layers also show low sensitivity, since the crosslinks formed by reduced dichromate are ionic in nature[33] and the ionic state of gelatin is, in turn, dependent upon its moisture content. It is, therefore, necessary to adjust the moisture content of DSDCG films.

In our materials optimization work we used a controlled environment drying apparatus. Laminar flow air was directed over the sensitized plates and was kept at 40% relative humidity by a constant humidity chemical ($CaCl_2 \cdot 6H_2O$).

The second important factor that determines film sensitivity is the rate of the dark reaction. This reaction is the crosslinking of gelatin without the benefit of actinic radiation. If a sensitized plate is dried for a long time, it will become fully hardened by the dark reaction and will be unable to record an image. The length of time a plate may be dried before the dark reaction hardens the plate is dependent on the sensitivity of the film: increased sensitivity is concommitant with a faster dark reaction. Long drying time and film sensitivity appear to be mutually exclusive.[44]

Since the determination of optimum drying time cannot be done analytically, we determined the best drying time by exposing several plates of a particular composition after various drying times. Figure 43 shows curves for two different sensitization solution compositions. Note that the material in curve (B) is more sensitive and has a faster dark reaction, and therefore less drying time is required for it to reach the sensitivity peak.

For fabricating the large HUD holograms, we anticipate 12 to 18 minute drying times following sensitization. This relatively short drying time for the large 18 by 18 in. plates obviates the necessity for multiplate drying chambers and long preparation times for plate exposure.

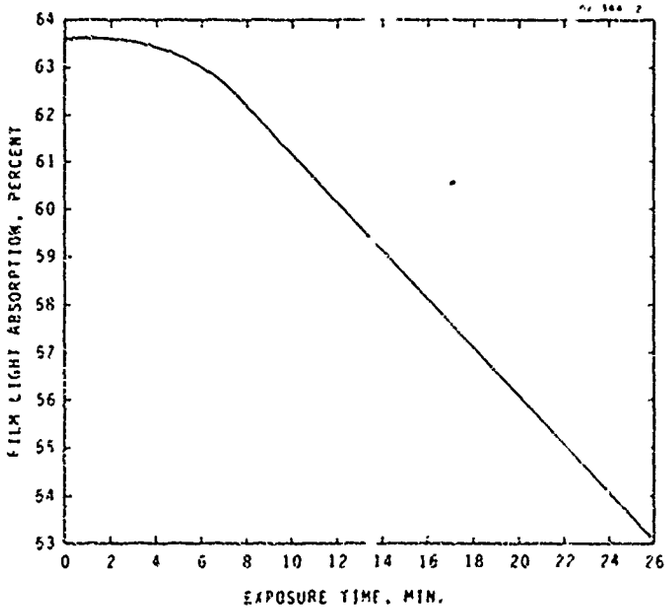

Fig. 42.
Film light absorption as a function of exposure time, with 1.28 mW/cm^2 incident light intensity at 632.8 nm wavelength. The plate was sensitized at time zero.

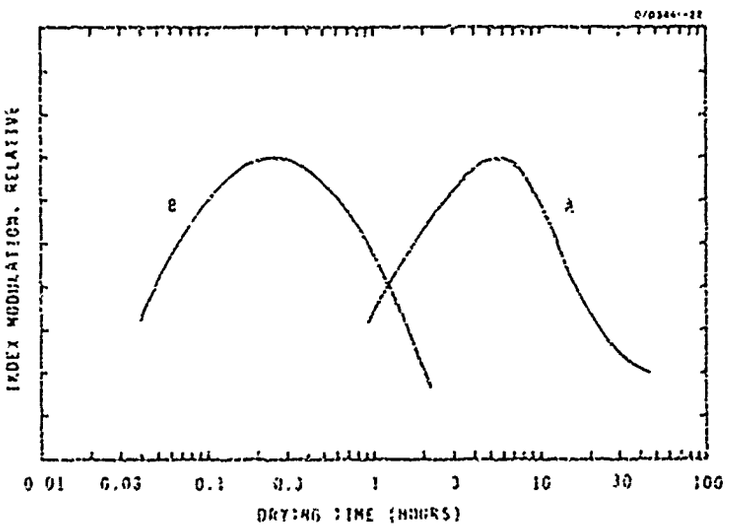

Fig. 43.
Comparison of film response as a function of drying time. A - DSDCG sensitized with acid fast violet dye; B - DSDCG sensitized with methylene green dye and ammonium nitrate.

IV. Red-Sensitive Recording Material Development

10. OPTIMIZATION OF POST-EXPOSURE PROCESSING

We have found a development procedure that produces high efficiency, low noise holograms and is adaptable to large plate processing.

In the exploration of development techniques we strived not only to achieve maximum diffraction efficiency and low noise, but also to develop a process by which the large HUD (18 x 18 in.) plates could be conveniently processed.

After exploring a large number of development techniques, we found that the best development method consists of the following steps:

a. Triethanolamine, 3M, 22°C, 1 minute

b. 50% water-50% 2-propanol solution, 50°C, 2 minutes

c. 50% water-50% 2-propanol solution, 50°C, 2 minutes

d. 100% 2-propanol, 22°C, 2 minutes

e. Dry nitrogen, 5 minutes.

However, it became apparent that this development technique would be hard to implement on the large HLS plates for two reasons. First, 3 molar triethanolamine (TEA) is a rather viscous solution, and to uniformly remove this solution's run-off, the samples had to be vigorously agitated in the second development solution. Since the same agitation rate is not practicable for 18 x 18 in. plates, we reduced the viscosity of the first development solution by making the TEA concentration 1 molar. Second, the alcohol concentration increase in successive development steps are relatively abrupt and also require vigorous agitation. We substituted other alcohol solutions into the process to make the transition from TEA to 100% 2-propanol more gradual, thus preventing nonuniform plate development.[45] This modified and optimized development consists of the following steps:

a. TEA, 1M, 1 minute

b. 25% 2-propanol solution, 2 minutes

c. 50% 2-propanol solution, 2 minutes

d. 75% 2-propanol solution, 2 minutes

e. 100% 2-propanol solution, 2 minutes

f. Dry nitrogen, 5 minutes.

The use of TEA in the first developing solution appears to have several distinct advantages over conventional water baths.[46] First, TEA acts as a film swelling promoter, producing increased thickness gelatin layers than water alone. The very rapid film swelling may be caused by the simultaneous action of swelling (i.e., TEA) and hardening (i.e., dichromate) agents in the gelatin layer.[47] Second, the swelling is very rapid, obviating the need for long washing times and large quantities of water. Third, the TEA solution removes unreacted dichromate and a large portion of the dye from the gelatin layer. The remaining dye diffuses out in the subsequent alcohol solutions.

It should be pointed out that this particular development procedure is matched only for our particular prehardening and sensitization procedures. In fact, variation in any of the film preparation steps may necessitate development reoptimization.

Following development, a cover glass must be sealed over the hologram to prevent its destruction by high humidity or abrasion. We used a pressure sensitive adhesive, Loctite 404, which worked satisfactorily for the small plates. A different clear adhesive will have to be used for the large HLS holograms, and several acceptable adhesives are well known for this purpose.[48]

IV. Red-Sensitive Recording Material Development

11. DSDCG EXPOSURE CHARACTERISTICS

The sensitivity of DSDCG has been substantially improved through processing parameter optimization, and the required exposure has been reduced to 600 mJ/cm^2.

Using the optimized sensitizing solution, drying time, and development procedure, we tested the sensitivity of the material for first order diffraction efficiency response as a function of exposure energy. Figure 44 shows that diffraction efficiencies exceeding 80% can be obtained with 600 mJ/cm^2 exposures, while maintaining scattering noise levels below 5%. The incident interrogation beam was corrected for front and back surface reflections since the HUD hologram will have antireflection coatings. A beam phase control system was not implemented for these exposures, and we believe that when such a system is made operable for the large HLS holograms, high diffraction efficiencies will be attainable with less exposure.

Since the sensitizing dye, methylene green, has a broad absorption band in the red spectral region, we anticipate that the krypton laser exposure at 647.1 nm will require about as much energy as He-He laser exposures at 632.8 nm, i.e. 600 mJ/cm^2 or less.

In our materials evaluation study we used a Spectra Physics Model 125 He-Ne 50 mW laser, spatially filtered through a 10X microscope objective and 12.5 μm pinhole, and collimated by a 30 cm focal length lens, as shown in Fig. 45. A single optical element (a Fresnel mirror) was used to create the object and reference beams. The sample plate holder was attached to the Fresnel mirror platform, and the exposing beams formed symmetrical angles with the perpendicular to the plate normal, resulting in a spatial frequency of about 600 cycles/mm.

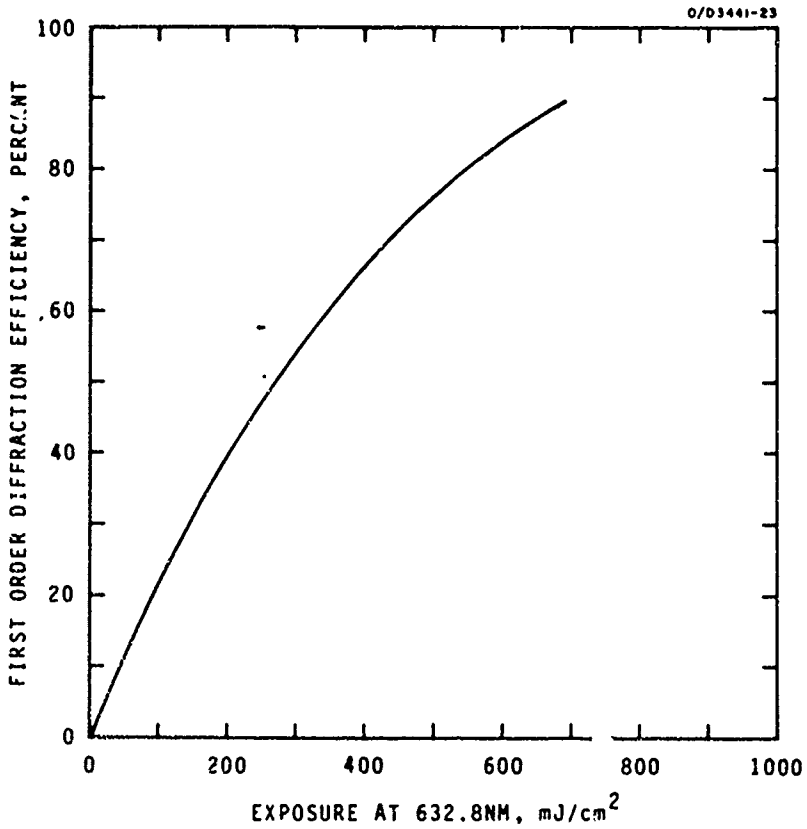

Fig. 44. First order diffraction efficiency as a function of exposure energy for DSDCG sensitized with methylene green, ammonium dichromate and ammonium nitrate.

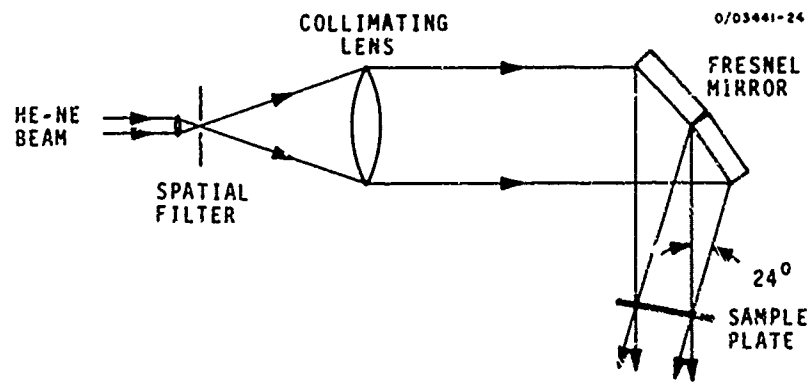

Fig. 45. Exposure apparatus used for hologram materials tests.

IV. Red-Sensitive Recording Material Development

12. LARGE HOLOGRAM RECORDING PROCEDURES

The optimized processing specifications for fabricating the HLS have been determined, and they have been specifically adapted for large hologram preparation.

The various facets of the optimization work have been assembled into an integrated system, and the anticipated large HUD hologram preparation procedure is enumerated in Table 13. The preparation of a large area, uniform gelatin layer film involves considerable technology and know-how. Although we are capable of fabricating uniform gelatin layers by dip-coating and doctor-blading on small plates, we anticipate the coating difficulty to increase proportionally with plate area. Hence, Kodak 649F plates were selected for the hologram material because they exhibit good uniformity and are available in large sizes. Also, once the silver halide is removed from the emulsion thickness, the dry film thickness decreases to about 12 μm. This thickness, coupled with an index modulation of 0.022, will give diffraction efficiencies over 90%.

The relatively long fixing time ensures that all of the silver halide is removed from the gelatin layer and gives the film sufficient hardening and rigidity to prevent scattering noise formation in the development steps.

Since the fixing solution contains sodium thiosulfate (hypo), and since sodium thiosulfate is a reducing agent for ammonium dichromate, we use a long duration wash following the fixing step (2). Only 0.003% of the hypo should remain in the emulsion after a 20 minute wash.[49]

To ensure a uniform drying rate and a rapidly moving drying boundary, a rubber squeegee (similar to a windshield wiper) is used to remove excess liquid from the gelatin film in steps (4), (6), and (11).

The hardening agent used in Kodak Rapid Fixer is probably an aldehyde-type compound and may take up to three weeks to achieve full hardening in the gelatin film.[50] To prevent the film from changing hardness during storage, we accelerate the process by baking the dry plates (Step 7) and drive the hardening reaction to completion.

Although relatively small (2 x 3 in.) sample plates were used to develop this hologram fabrication procedure, we feel that no serious difficulties will be encountered when the transition is made to the large HUD holograms.

TABLE 13

Processing Specifications for Fabricating Holographic Lens

Starting material: Kodak 649F
Spectroscopic Plates, 18 x 18 in.

Step	Time	Temperature (°C)
1. Apply Kodak Rapid Fixer (with hardener), mild agitation.	15 min	22
2. Deionized water wash	20 min	22
3. Kodak Photo Flo 200 diluted with dionized water 1:200 volume ratio.	30 sec	22
4. Squeegee gelatin surface	—	—
5. Dust-free air dry, 40% RH	overnite	22
6. Repeat steps (1) to (5)		
7. Bake in air atmosphere	2 hrs	150
8. Store in 40% RH air		
9. Prepare sensitizing solution:		
a. Make solution containing — 0.60 M $(NH_4)_2 Cr_2O_7$ 0.68 M $NH_4 NO_3$		
b. Add dry methylene green dye to form saturated dye solution		
c. Stir solution vigorously (dye dissolves reluctantly)	2 min	
d. Filter through fast filter paper (e.g., Whatman No. 541)		
10. Sensitize plates by immersing in sensitizing solution with mild agitation (in the dark)	6 min	22
11. Squeegee gelatin surface (in the dark)		
12. Wipe solution from glass side (in the dark)		
13. Dry plates in gently flowing 40% RH air (in the dark)	15 min	22
14. Expose plates to interfering 632.8 nm laser beams to 600 mJ/cm^2		
15. Develop with agitation in:		
a. 1M triethanolamine	1 min	22
b. 25% 2-propanol: 75% H_2O solution	2 min	22
c. 50% 2-propanol: 50% H_2O solution	2 min	22
d. 75% 2-propanol: 25% H_2O solution	2 min	22
e. 100% 2-propanol	2 min	22
f. Dry in dry nitrogen	5 to 15 min	22
16. Seal on cover glass for environmental protection		

V. Experimental Study of a Holographic HUD Lens

1. SPECIFICATION OF THE EXPERIMENTAL HOLOGRAM

The experimental hologram lens is a symmetric transmission continuous lens, approximately one-half size, with an off-axis angle of 40° and a focal length of 15.5 in.

An experimental demonstration and study of a holographic HUD lens was accomplished, using a symmetric transmission continuous lens configuration similar to the configuration that was recommended for the next stage of development. The experimental hologram has a 40° off-axis angle. Table 14 compares the characteristics of the experimental hologram and the full scale hologram. The experimental hologram is approximately half the size required to provide a full 25° FOV from anywhere within the 3 in. high by 5 in. wide exit pupil area. However, with a tilt of 20°, the experimental lens does provide 18° FOV at the center of the exit pupil, for an eye relief of 25 in. Figure 46 shows scaled horizontal and vertical sections that indicate the relative size and orientation of the experimental and recommended hologram lenses.

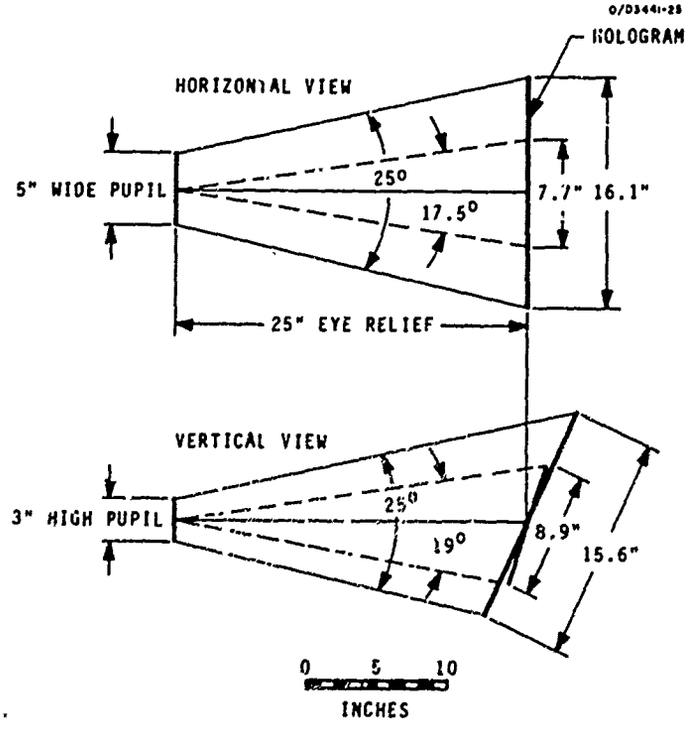

Fig. 46.
Horizontal and vertical sections of the pupil and hologram, showing the size of the experimental hologram and the full scale hologram size required to observe the 25° field of view from anywhere within the 3 in. by 5 in. pupil area.

TABLE 14

Comparison of Characteristics of the Experimental and Full-Size Hologram

Characteristic	Experimental Hologram	Full-Size Hologram
Approach	Symmetric Transmission Continuous Lens	Symmetric Transmission Continuous Lens
Off Axis Angle	40°	50°
Holcgram Tilt Angle	20°	25°
Hologram Size	7.7 in. x 8.9 in.	15.6 in. x 16.1 in.
Hologram Focal Length	15.5 in.	13.5 in.
Pupil Size	3 in. High by 5 in. Wide	3 in. High by 5 in. Wide
Eye Relief	25 in.	25 in.
Field of View	~18° Circular at the Center of the Pupil	25° Circular, full pupil
Construction	632.8 nm HeNe Laser	647.1 Krypton Ion Laser
Material	Bleached Silver Halide	Dye-Sensitized Dichromated Gelatin

T1384

V. Experimental Study of a Holographic HUD Lens

2. CONSTRUCTION OF THE EXPERIMENTAL HOLOGRAM

An optical system including a 14 in. diam, spherical mirror was built up on a vibration isolated table, along with a He-Ne laser, to provide the required hologram construction beams.

Construction of the experimental hologram required a beam from a point source located at the center of the exit pupil, 25 in. away from the hologram, and a beam from point source on an axis deviating from the pupil beam axis by 40° and spaced to provide a desirable focal length. Obtaining a desirable focal length requires that one of these beams be converging and the other diverging. In our construction apparatus, the converging beam is provided by an off-axis spherical mirror, used with aberration correction optics.

Figure 47 is a schematic layout of the construction beams, and Fig. 48 shows the major features of the construction apparatus. The construction optics consist of one beam splitter, two spatial filters, five plane mirrors and one spherical mirror. The hologram bisects the 40° angle formed by the construction beam axes.

A point source 60 in. away from the 14.4 in. diam, 60 in. radius, spherical mirror is imaged by the mirror to form the converging construction beam. Astigmatism in this beam was minimized by reducing the tilt angle of the spherical mirror to 25°. At this angle, there is 6.1 in. of astigmatism, which is corrected with a negative cylindrical

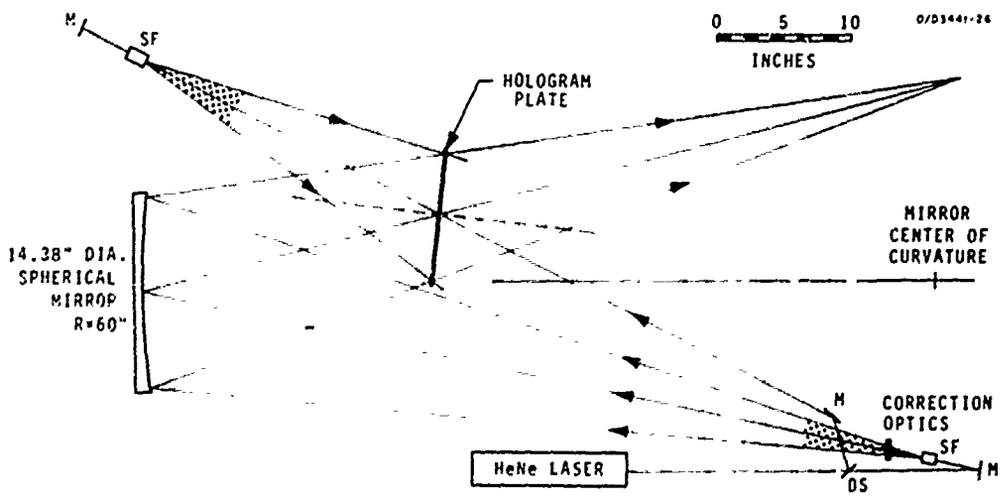

Fig. 47. Schematic of the experimental hologram construction apparatus, showing the construction beam configuration.

lens near the original point source. The corrected beam converges to a point 63.9 in. away from the mirror surface, and 40.9 in. from the hologram. The focal length is thus determined by $1/f = 1/25 + 1/40.9 = 1/15.5$.

The hologram is recorded on a 6-μm thick, silver halide emulsion (Kodak type 120 plates, 8 in. x 10 in.), using 632.8 nm, HeNe laser light. The path lengths of the two construction beams from the beam splitter to the center of the hologram were matched. The optical system was mounted on a 3 ft by 6 ft granite slab table, with pneumatic mounts used to isolate the table from floor vibrations, and shielding around the apparatus to minimize atmospheric disturbances. The resulting amplitude holograms were bleached, using the bromine vapor bleach process developed on this program, to provide high quality, high efficiency, phase holograms.

Fig. 48. View of the major components of the experimental hologram construction apparatus.

V. Experimental Study of a Holographic HUD Lens

3. APPROACH TO ANALYZING THE EXPERIMENTAL HOLOGRAM

Analysis of the experimental hologram was accomplished by comparing theoretical and experimental ray trace data on the system and image quality characteristics.

Experimental analysis of the experimental hologram is done through a series of ray traces performed both mathematically and experimentally. The theoretical analysis is achieved with a computer program which traces designated rays through a mathematical model of the hologram lens. Experimental analysis traces small ray bundles through the hologram lens, similar to the computer program. These beams are observed at the intermediate image plane. Ray intercept curves are derived from both experimental and analytical data, to be used to evaluate the hologram lens. Of primary interest in this analysis are:

a. Astigmatism and intermediate image plane determination

b. Chief ray efficiency and efficiency across the pupil

c. Distortion

d. Pupil errors.

The instrumentation used to make experimental measurements is shown in Fig. 49. When located in the pupil plane, the beam positioner allowed both x_p and y_p motion to locate the ray bundle, a 632.8 nm laser beam, at various positions in the pupil area. Also adjustable are the vertical and horizontal field angles, θ_x and θ_y, at which the ray is directed toward the hologram from the pupil. The laser beam can also be recollimated to make the necessary experimental measurements required to evaluate astigmatism and determine the image plane tilt. Figure 50 shows the geometry and coordinate axes used to make experimental measurements. Notice in Fig. 49 that the system is physically lying on its side with the y-axis parallel to the table and the x-axis perpendicular to the table top. A sheet of graph paper at the image plane is used to determine ray intercepts for the distortion and pupil errors measurements.

Fig. 49. View of the experimental hologram evaluation apparatus. (Top of facing page)

Fig. 50. Perspective drawing of the HUD coordinate systems and their geometrical relationships. (Bottom of facing page).

MIDSIP

3441-28

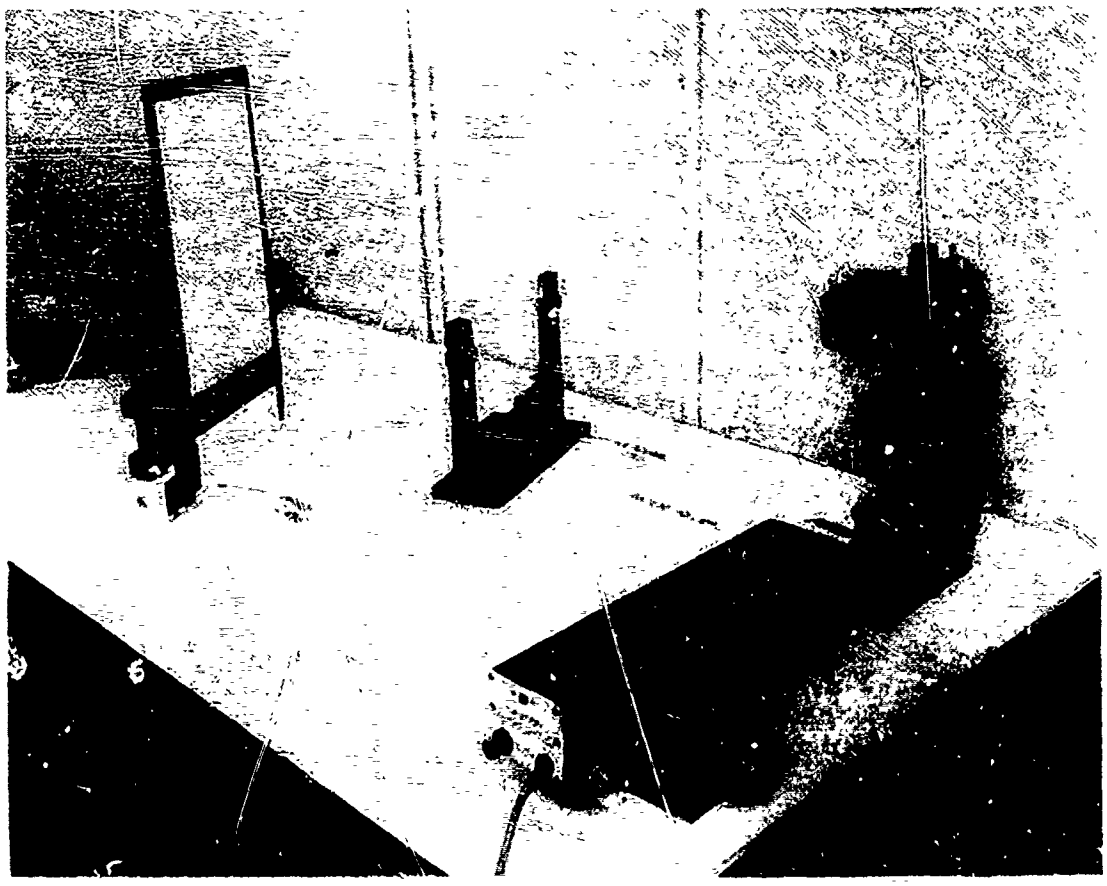

O/03441-29

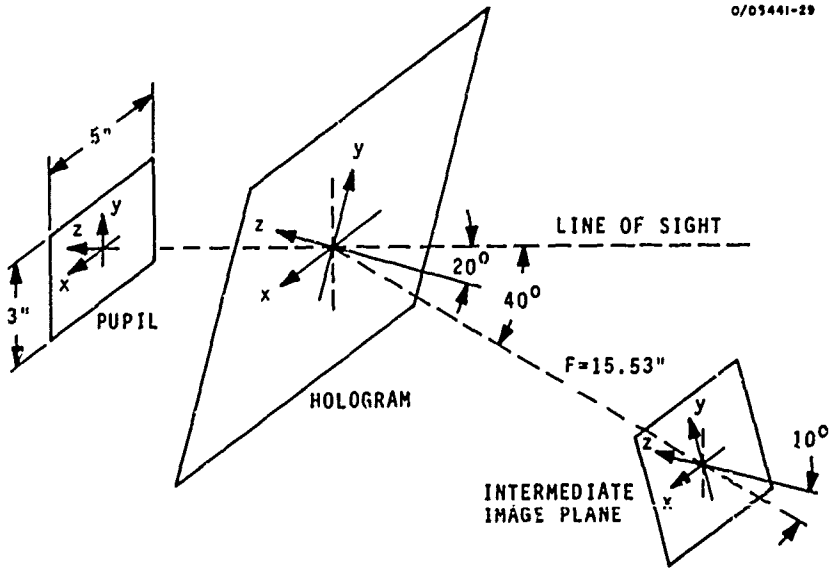

V. Experimental Study of a Holographic HUD Lens

4. IMAGE PLANE DETERMINATION

Computed and measured focal surface characteristics agree on focal length, astigmatism versus field and tilt angles.

The image surface of the relay lens optical system is curved and rotated through some angle relative to the plane of the hologram to match the focal surface of the hologram lens. In this section we compare the theoretical and experimental focal surfaces.

In order to determine the focal surface, chief rays are projected from the center of the pupil, at varying horizontal and vertical field angles, through the optical system. Vertical and horizontal focus locations are determined by using 5-mm long vertical and horizontal bundles of collimated rays from the pupil. A convenient set of coordinates in which to plot the focus points has a z-axis located on the optical axis at the focus of the hologram. Figure 51 shows an exaggerated view of the rays traced at a negative vertical field point.

Figure 52 shows plots of horizontal and vertical focus obtained experimentally and theoretically. The experimental data uphold the theoretical predictions very well. The focal length of the hologram measured experimentally was 15.5 in. corresponding to a calculated 15.53 in. Axial astigmatism is zero as expected. Astigmatism in the horizontal field is near zero. In the vertical field, astigmatism increases to 0.6 in. at -9° and 0.25 in. at $+9^{\circ}$. The horizontal and vertical focus locations indicate two distinct curved focal surfaces. Straight line approximations are used to obtain horizontal and vertical focus planes. An average between these two planes is then taken to determine the intermediate image plane location. From Fig. 52, the experimental intermediate image plane must be rotated 10.5°, confirming the theoretical value of 10°. The size of the intermediate image plane is

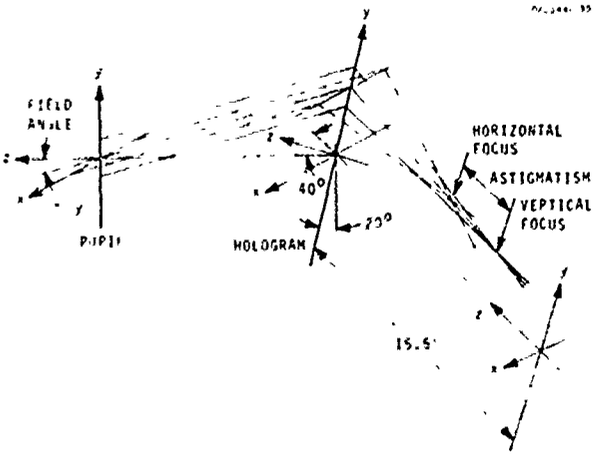

Fig. 51.
Perspective drawing of the ray tracing procedure used to claculate and measure focal points for a negative vertical field angle.

approximately 5 in. high by 5 in. wide. Figure 53 shows the basic geometry of the experimental transmission heads-up display optical system.

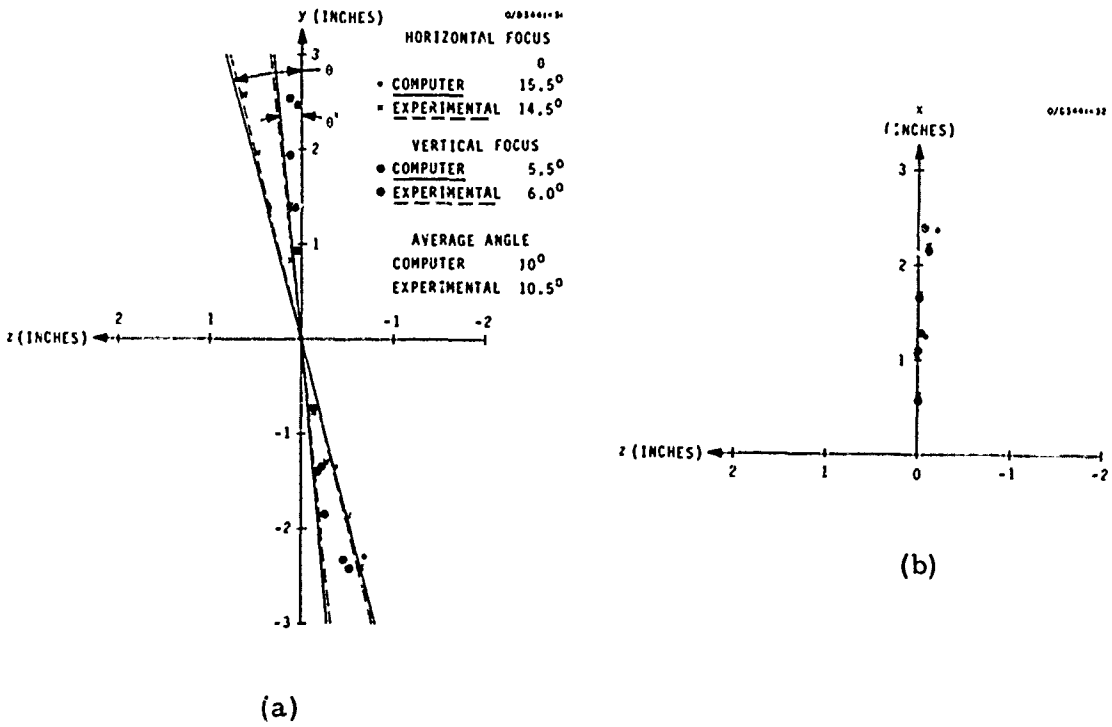

Fig. 52. Comparison of calculated and measured focal surfaces. (a) Points in the vertical section; (b) points in the horizontal section.

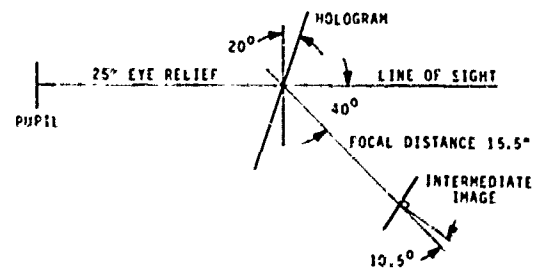

Fig. 53.
Vertical section, showing the experimentally determined intermediate image plane, relative to the system configuration, including the focal length of 15.5 in. and the tilt angle of 10.5°.

V. Experimental Study of a Holographic HUD Lens

5. OPTICAL EFFICIENCY

Deviations between predicted and observed efficiency are accounted for by a systematic loss of fringe stability during recording; this will be avoided during full scale hologram recording.

Optical efficiency as a function of the field location is measured by projecting chief rays from the pupil at varying horizontal and vertical field angles, and measuring the amount of diffracted power at the intermediate image plane. A United Detector Technology power meter calibrated for 632.8 nm was used to measure the diffracted power. In the symmetric transmission geometry, the chief ray efficiency should be high across the field. Figure 54 shows experimental measurements of relative chief ray efficiency versus the fractional vertical and horizontal field. Experimental data show efficiency fluctuations across both the horizontal and vertical field.

Efficiency across the pupil is determined by measuring the diffracted power as a ray is projected at zero field angle from various locations on the x_p and y_p axes of the 3 in. high by 5 in. wide pupil. Diffracted power is again measured at the intermediate image plane. Relative efficiency is plotted versus fractional horizontal and vertical pupil coordinates in Fig. 55. There is a significant deviation between the calculated and measured efficiencies over most of the horizontal pupil dimension and at the top 1/8 of the vertical pupil dimension. These deviations correlate strongly with the deviations in chief ray efficiency.

The deviations together indicate a systematic loss of efficiency in going from the lower right to upper left areas of the hologram, as viewed from the pupil. Probable causes for the efficiency degradation are, first, phase instability during exposure of the hologram due to path length differences of the two construction beam across the exposed hologram, and second, disturbances due to air motions and floor vibrations during exposure. A fringe monitoring and stabilizing system will alleviate this problem during exposure of the full-scale hologram.

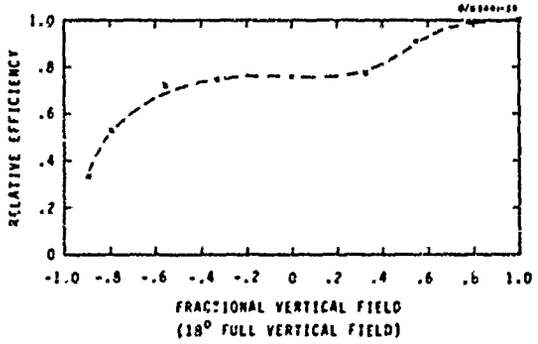

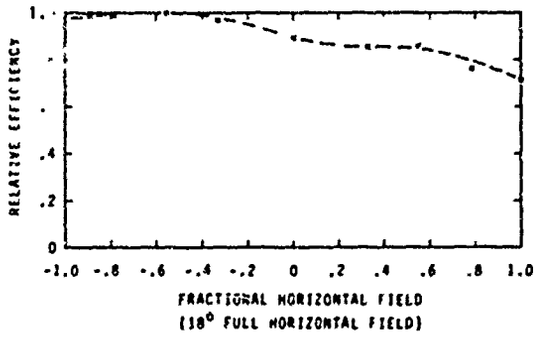

Fig. 54.
Observed chief ray relative efficiency.

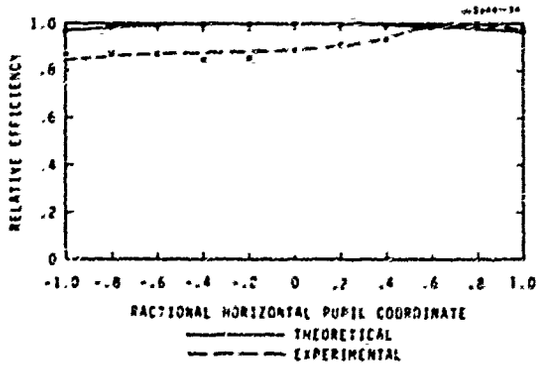

Fig. 55.
Comparison of calculated and observed pupil efficiency for the axial image point.

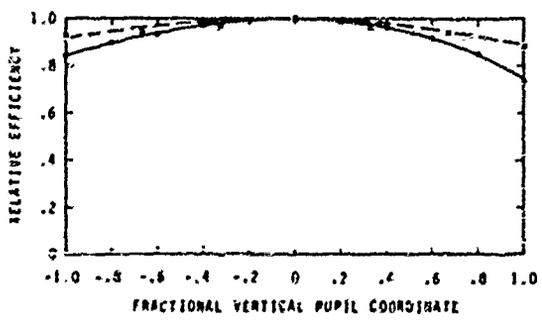

V. Experimental Study of a Holographic HUD Lens

6. DISTORTION

The calculated and measured distortion characteristics of the experimental hologram are the same, within experimental error, being 1.5% anamorphic and 5% keystone, calculated, and 2.5% anamorphic and 4.95% keystone, measured.

Ray tracing of rays for circular images subtending various angles at infinity, to determine the corresponding image at the intermediate image plane, gives a description of the distortion introduced by the hologram lens. A useful and convenient measure of distortion is the ratio of vertical to horizontal magnification for circular images subtending various angles at infinity, as discussed in Sections II-B-6 and II-C-3. Figure 56 illustrates ray traces of a circular image subtending an angle 2θ at infinity. The ratio of the vertical intercept, y_I, to the horizontal intercept, x_I, for corresponding vertical and horizontal field angle θ is called the magnification ratio. By varying θ and obtaining the corresponding vertical and horizontal intercepts at the image plane, a plot of the magnification ratio versus vertical field angle is obtained. A distortion-free hologram would produce a circular distribution at the intermediate image plane for a circular image at infinity. In the vertical to horizontal magnification ratio versus vertical field angle plot, this corresponds to a magnification ratio of one across the full vertical field, i.e., a horizontal line at a value of unity.

Figure 57 is a plot of vertical to horizontal magnification ratio, measured and calculated, versus the vertical field, for the experimental hologram lens. Because of symmetry in the experimental configuration about the vertical axis, the magnitude of horizontal magnification for a positive and negative horizontal field angle is equal. Both experimental and theoretical data show that the hologram lens introduces both keystone and anamorphic distortion. A measure of keystone is the rate at which magnification ratio varies across the vertical field, i.e., the magnitude of the slope of the distortion plot. The 4.95% keystone distortion introduced by the hologram distorts rectangular images at the source to trapezoids at infinity. Constant magnification ratio across the vertical field, other than one, indicates anamorphic distortion. A measure of anamorphic distortion is the magnification ratio at zero vertical field. The experimental hologram lens introduces 2.5% anamorphic distortion. If we consider a point at the center of the image plane as the limit of a circular image approaching zero radius, the image of the point at infinity flares out vertically 1.025 times the horizontal dimension.

Anamorphic distortion can be corrected with an anamorphic relay lens, and keystone distortion can be at least approximately corrected by tilting the image plane (see Section IV).

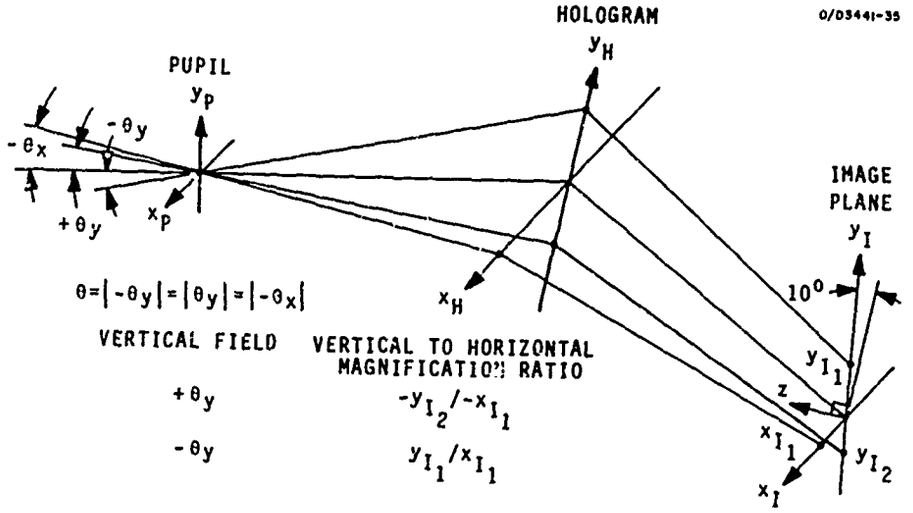

Fig. 56. Perspective drawing of the three rays used to determine the vertical-to-horizontal magnification ratio for a circular image at infinity subtending 2θ degrees.

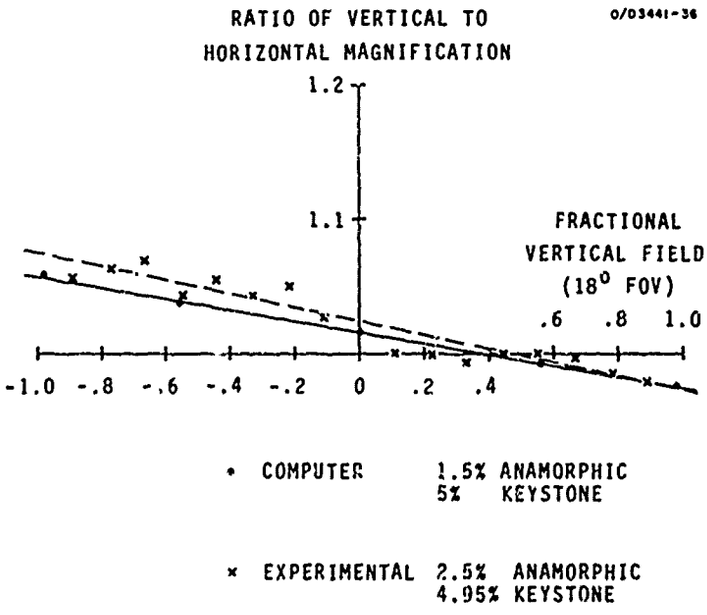

Fig. 57. Comparison of calculated and observed magnification ratios.

V. Experimental Study of a Holographic HUD Lens

7. DETERMINATION OF PUPIL ERRORS FROM RAY INTERCEPTS

The pupil errors of interest, collimation error and binocular disparity, are conveniently defined in terms of ray intercepts, and were calculated and measured for the axial field point and two different horizontal eye locations, as functions of vertical eye position.

Pupil errors, i.e., collimation error and binocular disparity, are calculated by generating ray intercept curves. These curves are plots of intercepts at the image plane, relative to the chief ray intercept, of rays from infinity versus the position at which the rays pass through the pupil. The pupil errors for two eyes horizontally separated by 2.5 in. are calculated by tracing two vertical fans separated by 2.5 in.

Figure 58 is an exaggerated view of two such rays. The collimation error and binocular disparity are defined in the enlarged view of the intercept region. By tracing the two vertical fans, i.e., varying y_p, ray intercept curves of x_I and y_I for the left and right eye versus the y_p location of the pupil are obtained. Since the pupil errors can be directly calculated from the ray intercept curves, pupil errors at various pupil heights can be obtained.

Pupil errors were investigated for two eyes separated by 2.5 in. at relative pupil coordinates $x_p = 0$ and $x_p = -1.0$ and at $x_p = 0.5$ and $x_p = -0.5$, for the axial field point. The full pupil size is 5 in. wide by 3 in. high. Both theoretical and experimental ray intercept curves are shown in the next two sections, for the two cases studied. Many intercept values measured experimentally were on the order of a fraction of a millimeter. With the experimental difficulty of this measurement, an exact mapping of experimental data onto theoretical curves was not expected.

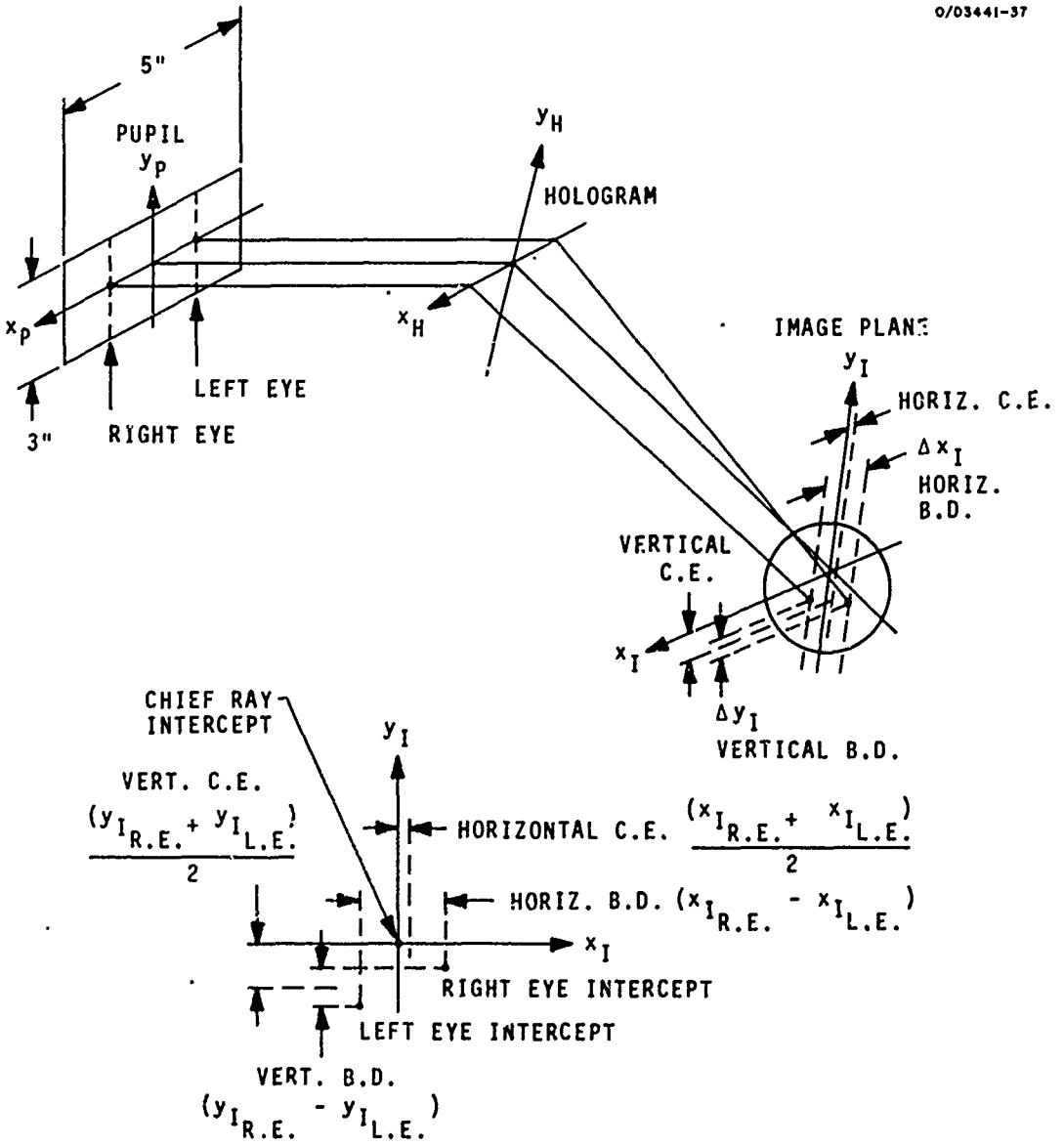

Fig. 58. Perspective drawing of the two rays used to determine the pupil errors, and the definitions of the errors in terms of the intercepts.

V. Experimental Study of a Holographic HUD Lens

8. PUPIL ERRORS FOR THE SYMMETRIC EYE LOCATION

For the right eye located at $x_p = 0.5$ and the left eye located at $x_p = -0.5$, maximum pupil errors of -3.41 mrad vertical collimation error and -3.4 mrad horizontal binocular disparity occur at $y_p = 1.0$.

For the case where the left eye is at $x_p = -0.5$ and the right eye is at $x_p = 0.5$ (relative coordinates), as shown in Fig. 59, theoretical and experimental ray intercept curves were generated. These curves are shown in Fig. 60. Theoretical data show no horizontal collimation error nor vertical binocular disparity. Experimental measurements confirm the zero horizontal collimation error, but indicate a small amount of vertical binocular disparity. Both theoretical and experimental results show minimum vertical collimation error and horizontal binocular disparity at a relative vertical eye location of $y_p = 0.1$. Pupil errors increase as the pupil height deviates from $y_p = 0.1$, becoming about 1.3 mm or 3.4 mrad at $y_p = 1.0$. General agreement between theory and experiment is excellent.

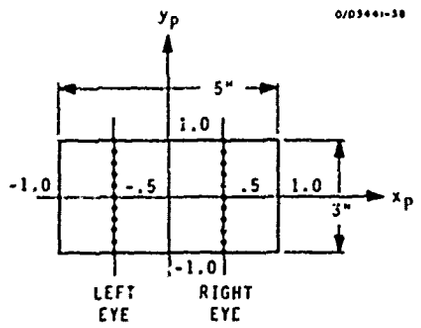

Fig. 59.
The pupil area, showing the symmetrical horizontal eye locations.

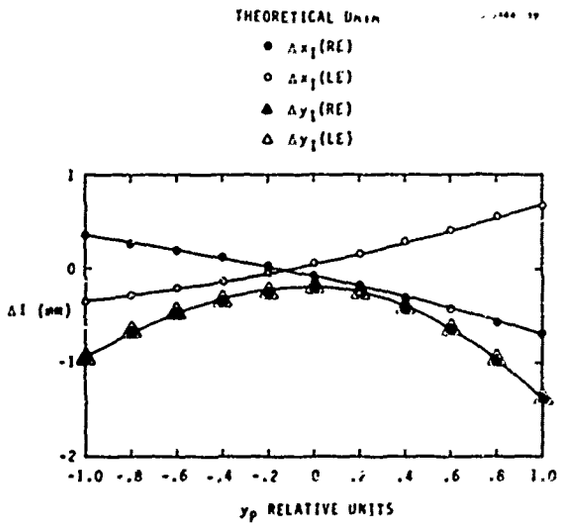

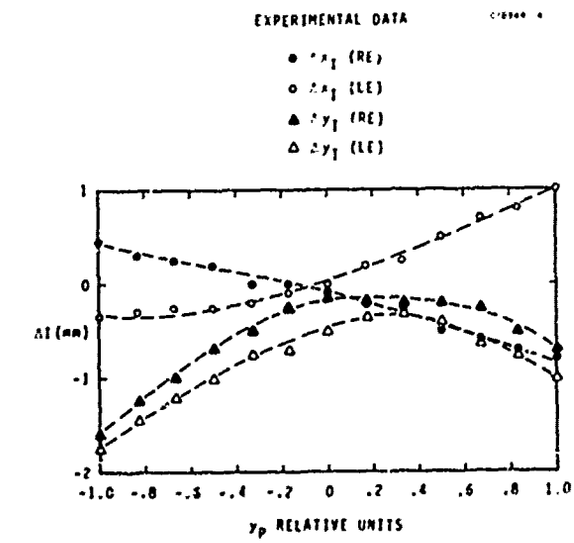

Fig. 60.
Ray intercept components as functions of the relative vertical eye position for the symmetrical horizontal eye locations shown in Fig. 59. Top: calculated results; bottom: observed results.

V. Experimental Study of a Holograhic HUD Lens

9. PUPIL ERRORS FOR AN EXTREME EYE LOCATION

As the eyes move to the edge of the pupil, the horizontal collimation error and the vertical binocular disparity increase, reaching a maximum of about 5 mrad (uncorrected) for the experimental hologram lens.

Next consider an extreme eye location, shown in Fig. 61, where the left eye is at the edge of the pupil x = -1.0 and the right eye at $x_p = 0$. The ray intercept curves for this case are shown in Fig. 62 and again show excellent agreement between theory and experiment.

Horizontal and vertical binocular disparity increase as the eyes approach the top of the 3 in. high pupil. At $y_p = 1.0$ relative coordinates, i.e., the eyes at the top of the pupil, horizontal binocular disparity is -1.75 mm or -4.49 mrad, and vertical binocular disparity is +1.25 mm or 3.14 mrad. There is a general increase in horizontal collimation error toward the top of the pupil. Vertical collimation error is minimum when the eyes are located at $y_p = 0$.

Comparing the two cases, as the pupils move toward the side of the 3 in. by 5 in. pupil, there is an increase in horizontal collimation error with little change in horizontal disparity. However, vertical binocular disparity increases with little change in vertical collimation error. The maximum pupil errors encountered in the experimental HUD system are 5 mrad without any relay lens correction.

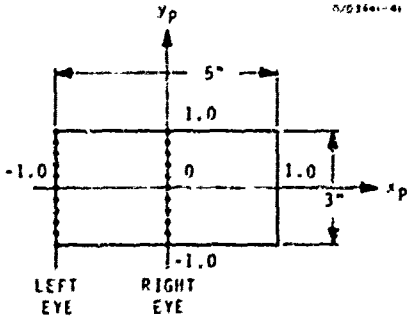

Fig. 61.
Pupil area, showing an extreme horizontal eye location.

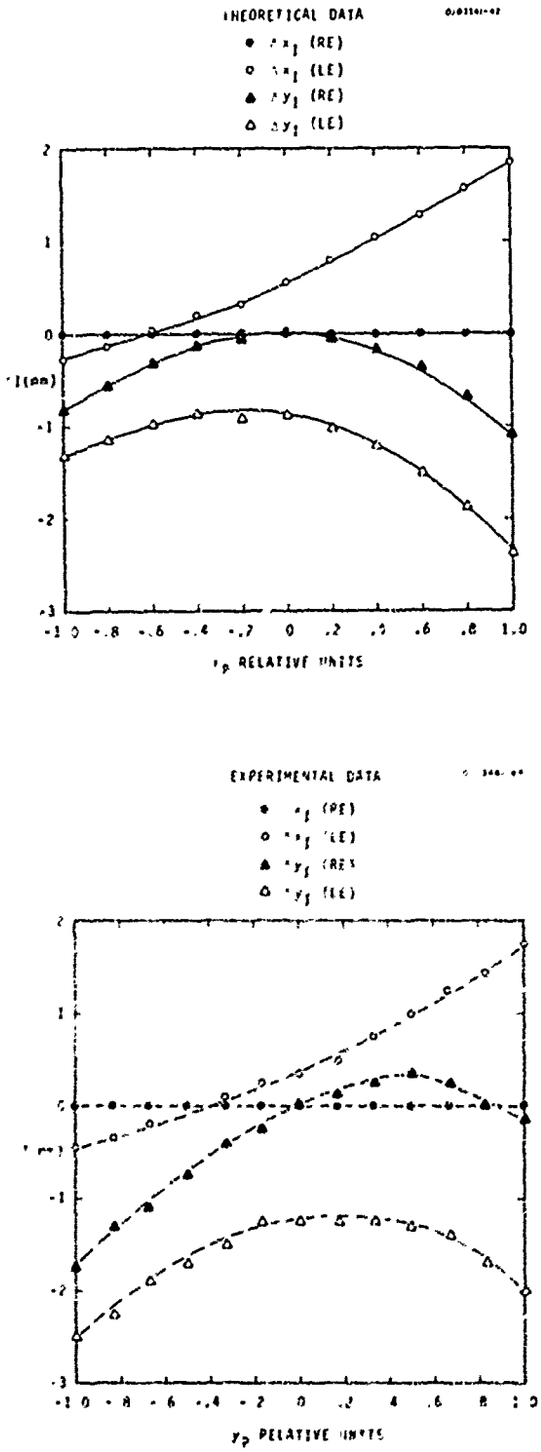

Fig. 62.
Ray intercept components as functions of the relative vertical eye position, for the extreme horizontal eye location shown in Fig. 61. Top: calculated results; bottom: observed results.

V. Experimental Study of a Holographic HUD Lens

10. CONCLUSIONS ON DEMONSTRATOR PERFORMANCE

The experimental hologram, which confirmed our analysis techniques, was incorporated in a HUD demonstrator that shows excellent image quality.

The experimental hologram was incorporated in a HUD demonstrator, which has been delivered to NADC. This demonstrator, shown in Fig. 63, establishes the size of the full-scale hologram, the location of the intermediate image plane and the location of the exit pupil, as well as providing an example of holographic HUD imagery.

With the experimental hologram lens HUD system, the efficiency across the pupil is reasonably uniform. Distortions in the system are small, primarily keystone in nature. For axial field points, the worst case pupil errors are in the order of 5 mrad. When the eyes are centered in the 3 in. high by 5 in. wide pupil, the pupil errors fall to less than 1 mrad. The resultant image at infinity in the HUD system is quite good even without correction by a relay lens, and can be seen in Fig. 64.

All experimental data correlated very closely to the predicted performance of the experimental hologram lens. The design of the full size HUD system represents a complex task. However, the performance of the design can be readily predicted with computer analysis.

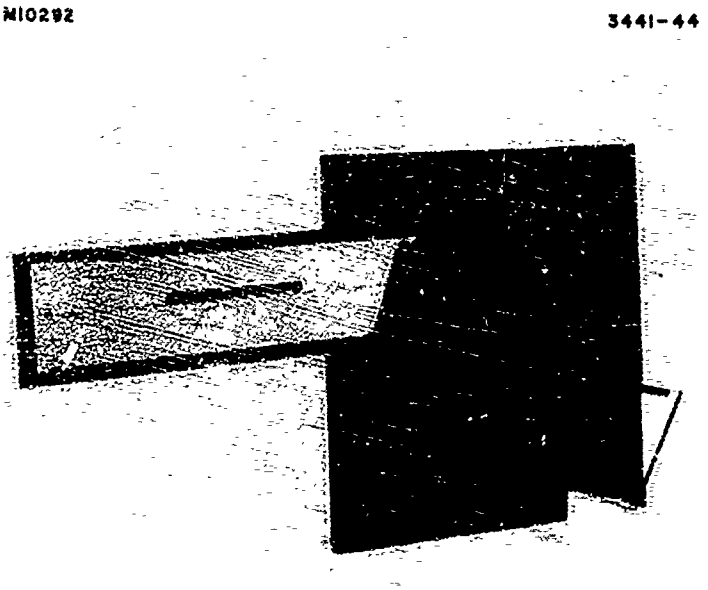

Fig. 63.
The holographic HUD demonstrator.

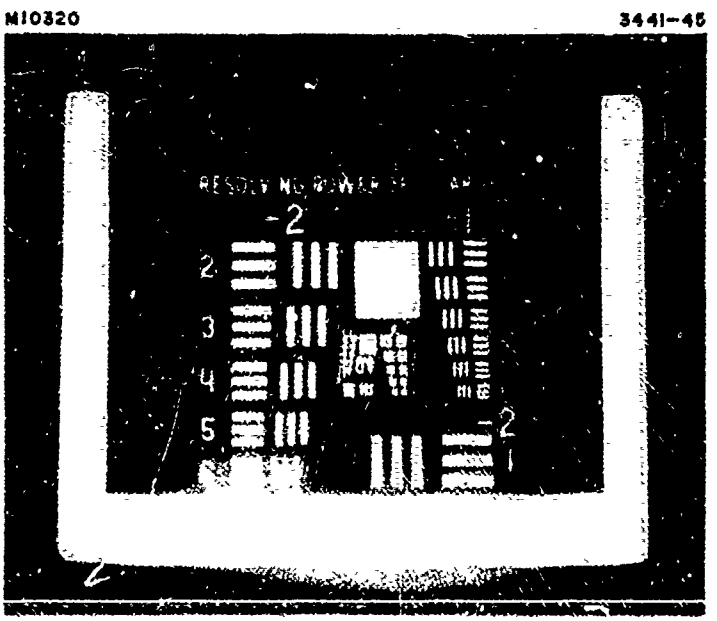

Fig. 64.
Image of a resolution chart, projected by the holographic HUD demonstrator, as viewed by a camera focused at infinity and located at the center of the exit pupil.

REFERENCES

1. Technical Proposal, "Holographic Lens for Pilots' Head-Up Display," 72M-3163/C9006 (January 1973).

2. D.G. McCauley, C.E. Simpson, and W.J. Murbach, Appl. Optics 12, 232 (February 1973).

3. G.E. Moss, "Wide-Angle Holographic Lens for a Display System," J. Opt. Soc. Am. 64, 552A (April 1974).

4. Contract F33615-73-C-4110, from the Aerospace Medical Research Laboratory, Wright-Patterson AFB, "Holographic Visor Helmet Mounted Display," Final Report not yet available.

5. U.S. Air Force Contract F33615-72-C-2140. See Technical Report AFAL TR-73-215 by E.W. Opittek (July 1973).

6. H. Kogelnik, Bell Syst. Tech. J. H8, 2909 (November 1969).

7. E.B. Champagne, J. Opt. Soc. Am. 57, 51 (1967).

8. "Specification for Hologram Lens System," Naval Air Development Center, Air Vehicle Technology Department (20 November 1972).

9. J.N. Latta, Appl. Opt. 10, 2698, December 1971; J.N. Latta, Appl. Opt. 10, 599 and 609, March 1971; and J.N. Latta, Appl. Opt. 11, 1686, August, 1972.

10. R.J. Collier, C. B. Burckhardt, and L.H. Lin, Optical Holography (Academic Press, New York, 1971).

11. W.J. Smith, Modern Optical Engineering (McGraw-Hill, New York, 1966), p. 68.

12. Ibid, p. 84.

13. Ibid, Chapter 2.

14. V. Files, Appl. Phys. Lett. 19, 11, p. 451-452, (December 1971).

15. A. Graube, J. Opt. Soc. Am. 64, 563A (April 1974).

16. J. Kosar, Light Sensitive Systems (John Wiley & Sons, 1965), p. 46.

17. A.C. Hardy and F.H. Perrin, J. Franklin Inst. 205, 197-219 (1928).

18. D. Meyerhofer, Appl. Opt. 10, 416 (1971).

19. J.C. Urbach, "Advances in Hologram Recording Materials," Developments in Holography, S.P.I.E. Seminar Proceedings 25, p. 17-41, April 14-15, 1971.

20. T.A. Shankoff, Appl. Opt. 7, 2102 (October 1968).

21. J. Kosar, Light Sensitive Systems (John Wiley and Sons, 1965), Chapter 2.

22. D.H. Close and A. Graube, Final Report, Contract F33615-73-C-5137, Air Force Materials Laboratory.

23. G.O.'t Hooft, Z. Wiss, Phot. 25, 394 (1928).

24. G.K. Oster and G. Oster, U.S. Pat. No. 3,074,794 (1963).

25. Y.K. Kerutskite, L.M. Ryabova, B.A. Shashlov, and V.I. Sheberstov, Zh. Nauchnoi i Prikladnoi Fotografii i Kinematografii 8, 303, (August 1963).

26. A. Graube, Opt. Commun. 8, No. 3, 251-253, (July 1973).

27. D. Meyerhofer, RCA Review 33, 110-130, (March 1972).

28. G.K. Oster and G. Oster, J. Am. Chem. Soc. 81, 5543 (1959).

29. A.A. Meisling, Dansk Fotografish Tidssk. 38, 65,73 (1916).

30. F. Daniels and R.A. Alberty, Physical Chemistry (John Wiley and Sons, New York, 1962), Chapter 15.

31. D.G. McCauley, C.E. Simpson, and W.J. Murbach, Appl. Opt. 12, 232 (1973).

32. R. John, U.S. Patent No. 1,875,292 (1932).

33. C.E.K. Mees and T.H. James, The Theory of the Photographic Process (Macmillan Co., New York, 1966), Chapter 3.

34. A. Zechnall, Uber die Empfindlichkeitssteigerung von Lightempfindlichen Bichromat-Fischleim-Schichten, Diss., Darmstadt 1932.

35. K. Jacobsohn and E. Wagner, Atetier Phot. 37, 98-100 (1938).

36. F.J. Tritton, Modern Lithographer and Offset Printer 25, 178-180 (1929).

37. F.W. Sharp, U.S. Patent No. 1,994,289 (1935).

38. H.T.S. Britton, J. Chem. Soc. 127, 2142-2147 (1925).

39. E. Valenta, Photographische Korrespondenz 51, 329-330 (1914).

40. J.M. Eder, Photographische Korrespondenz 51, 326-328 (1914).

41. E. Valenta and J.M. Eder, Procede 20, 132-133 (1919).

42. W.H. Wadhams, A. Ziehm, H.A. Sandermann, and P. Woithe, British Patent No 228,377 (1925).

43. W. Weissenberger, Photographische Korrespondenz 25, 463-467 (1888).

44. A.C. Hardy and F.H. Perrin, J. Franklin Inst. 205, 197-219 (1928).

45. G.L. Fillmore and R.F. Tyman, J. Opt. Soc. of Am. 61, 199-203 (1971).

46. R.G. Brandes, E.E. Francois, and T.A. Shankoff, Appl. Opt. 8, 2346 (1969).

47. E. Tojo, K. Nagao, T. Miura, and S. Nagatomo, Photographic Gelatin, R.J. Cox, ed. (Academic Press, Inc., London, 1972), p. 49.

48. Hughes Aircraft Company, Technical Proposal, HAC Ref. No. 72-27-17550/C8918 (1972), pp. 2-34.

49. L.F.A. Mason, Photographic Processing Chemistry (The Focal Press, London and New York, 1966), pp. 197-203.

50. G.F. Duffin, Photographic Emulsion Chemistry (The Focal Press, London and New York, 1966), pp. 158-163.